ANNALS OF PHYSICS 133, 79–153 (1981)

Neutrino-Excitation of Baryon Resonances and Single Pion Production

DIETER REIN AND LALIT M. SEHGAL

III Physikalisches Institut, Technische Hochschule, Aachen, West Germany

Received October 31, 1980

This is an attempt to describe all existing data on neutrino production of single pions in the resonance region up to $W = 2$ GeV in terms of the relativistic quark model of Feynman, Kislinger and Ravndal (FKR). We considered single pion production to be mediated by all interfering resonances below 2 GeV. A simple noninterfering, nonresonant background of isospin $\frac{1}{2}$ was added. It improved agreement with experiment, particularly in the ratio of isospin amplitudes in charged current reactions, at the expense of one additional constant. All total cross sections, cross section ratios and W-distributions are well reproduced at low and high energies, with charged and neutral currents (supposing the Salam–Weinberg theory with $\sin^2\theta_w \approx \frac{1}{4}$ to be correct), and for neutrinos and antineutrinos, giving predictions where data are lacking. New predictions have been made for complex angular distributions in $\mathcal{N}\pi$ channels exhibiting strong interference between neighbouring resonances. These are sensitive (for 1.1 GeV $\lesssim W \lesssim$ 1.5 GeV) to the sign of the Roper resonance $P_{11}(1450)$ which is controversial in photoproduction experiments.

1. INTRODUCTION

There is now growing conviction that for many low and moderate energy phenomena a nucleon can be treated as a bound state of three constituent quarks whose excitations are the resonances seen in the pion–nucleon system. One of the basic tasks of hadron dynamics is to produce a model that explains the energy levels of this system, the hadronic widths of the resonances, and the matrix elements describing the transitions between the ground state and the excited levels, induced by weak or electromagnetic currents.

In this context, the process of single pion production by electrons and neutrinos acquires special significance, since the various resonances seen in the $\pi\mathcal{N}$ system should be present in the invariant mass spectra of these reactions. Thus a model that specifies the matrix elements for resonance excitation can be subjected to tests in a multitude of reaction channels. The use of neutrinos as probes offers the advantage that one can measure the response of the 3-quark system to both vector and axial vector currents, and exploit the large variety of single pion production processes (14 in all!) that are accessible to neutrino and antineutrino beams, counting both charged and neutral current reactions. In the case of the neutral current channels,

0003-4916/81/050079-75$05.00/0

one can also carry out an inverse analysis, in which the model, tested and calibrated with the aid of charged current reactions, helps in determining the properties of the neutral current.

This paper is devoted to a systematic analysis of all existing data on neutrino-production of pions, treating the final state as essentially a superposition of resonances. The model used is the harmonic oscillator quark model in the relativistic formulation proposed by Feynman, Kislinger, and Ravndal [1]. This model has been applied with considerable success to photoproduction of nucleon resonances [2] (among other things, it predicts correctly the relative signs of various resonance amplitudes in 15 out of 16 cases), and its application to charged current neutrino-production has been discussed by Ravndal [3]. We have extended this work by including practically all known resonances [4, 5] in the region $W < 2$ GeV, and have applied the model to both neutral and charged currents. A new feature is the detailed consideration given to the effects of overlapping resonances. A large amount of data, both from the low energy and high energy laboratories, is brought into confrontation with the predictions of this model.

In Section 2, we recapitulate the kinematics of neutrino-production of pions, and discuss three aspects of the process, in order of increasing complexity: (i) the cross section for a single isolated resonance, (ii) the invariant mass distribution in the presence of several overlapping resonances, and (iii) the angular distribution of the pion in the pion nucleon center of mass frame, again including the effects of resonance interference. In Section 3, we discuss the dynamics of this process in the FKR model, and obtain all the transition matrix elements of interest. The results and the comparison with experiment are described in Section 4. The concluding section contains a critical assessment of the model, and its comparison with some other approaches [6–13]. An Appendix displays in some detail the density matrix formalism for interfering resonances which should be used for analysing the pion angular distribution.

2. Kinematics

2.1. *Neutrino Production of Isolated Resonances*

Let us first recall the neutrino excitation of a single nonstrange nucleon resonance by either charged or neutral weak currents. The process to be investigated is

$$\nu + \mathcal{N} \to l + \mathcal{N}^*, \tag{2.1}$$

where $\mathcal{N}^*$ denotes the nucleon resonance and the lepton l is either charged or neutral. Thus we envisage a slightly more general situation than described by Ravndal [3], whose notation we essentially adopt. According to the effective current–current formulation of weak interactions the production matrix element is given by

$$T(\nu\mathcal{N} \to l\mathcal{N}^*) = \frac{G}{\sqrt{2}} [\bar{u}_l \gamma^\beta (1 - \gamma_5)\, u_\nu] \langle \mathcal{N}^* \mid J_\beta^+(0) \mid \mathcal{N} \rangle \tag{2.2}$$

with $G = G_F \cos\theta_c \approx G_F$ the weak coupling constant for strangeness conserving transitions. The hadronic current operator J_β^+ contains a vector and an axial vector part and may be written factoring out the resonance mass M as

$$J_\beta^+ = V_\beta - A_\beta = 2MF_\beta = 2M(F_\beta^V - F_\beta^A). \tag{2.3}$$

The leptonic current matrix element $\bar{u}_l\gamma^\beta(1-\gamma_5)\,u_\nu$ is interpreted as the virtual intermediate boson's polarization vector, which may be decomposed into three standard polarization vectors e_L^μ, e_R^μ, e_0^μ corresponding to left-handed, right-handed and scalar polarization. With the 3-momentum of the virtual boson along the z-axis the usual definition is

$$\begin{aligned} q^\mu &= (\nu, 0, 0, Q), \\ e_L^\mu &= \frac{1}{\sqrt{2}}(0, 1, -i, 0), \\ e_R^\mu &= \frac{1}{\sqrt{2}}(0, -1, -i, 0), \\ e_0^\mu &= (1, 0, 0, 0), \\ e_L^\mu e_{L\mu}^+ &= e_R^\mu e_{R\mu}^+ = -e_0^\mu e_{0\mu} = -1. \end{aligned} \tag{2.4}$$

This decomposition is not unique but depends on the frame of reference. In the leptonic Breit system, where the 3-momentum vectors of the leptons are antiparallel along the z-axis, the leptonic current matrix element is

$$\bar{u}_l\gamma^\mu(1-\gamma_5)\,u_\nu\,|_{\substack{\text{lepton}\\ \text{Breit frame}}} = -2\sqrt{2}\,\sqrt{-q^2}\,e_L^\mu = -2\sqrt{-q^2}\,(0, 1, -i, 0). \tag{2.5}$$

Boosting to the hadronic Breit system with the incoming nucleon and the outgoing resonance being aligned along the z-direction (whereas the lepton momenta aquire additional components in x-direction), one finds

$$\begin{aligned} \bar{u}_l\gamma^\mu(1-\gamma_5)\,u_\nu\,|_{\substack{\text{nucleon}\\ \text{Breit frame}}} = -\sqrt{2}\,\sqrt{-q^2}\,\{&(1-\cosh\xi)\,e_L^\mu \\ &+ (1-\cosh\xi)\,e_R^\mu + 2\sinh\xi e_0^\mu\}. \end{aligned} \tag{2.6}$$

The boost parameter ξ is expressed in terms of laboratory frame quantities according to

$$1 \pm \cosh\xi = \frac{Q \pm (E+E')}{Q}, \qquad \sinh\xi = \sqrt{\cosh^2\xi - 1}, \tag{2.7}$$

where the incident and final lepton energies are denoted by E and E', respectively, and Q is the modulus of the three momentum transfer in the Lab.

The most convenient frame of reference for practical purposes is, however, the

center of mass system of the outgoing hadrons, i.e., the resonance rest frame. It is furthermore well suited for calculating resonance excitation or decay processes with the aid of potential models for quarks, describing hadronic bound states in a simple and appealing way.

From the nucleonic Breit frame the resonance rest frame is reached again by a Lorentz-transformation in the direction of the momentum transfer. This leaves the transverse polarization vectors $e^{\mu}_{L,R}$ unchanged, converting only $e_0{}^{\mu}$ to

$$e_s{}^{\mu} = \frac{1}{\sqrt{-q^2}}(Q^*, 0, 0, \nu^*) \tag{2.8}$$

where starred quantities now refer to the resonance rest frame. They are connected to their corresponding quantities in the Lab frame through

$$\frac{Q^*}{Q} = \frac{m_{\mathcal{N}}}{M}, \qquad q^2 = \nu^2 - Q^2 = \nu^{*2} - Q^{*2}$$

$m_{\mathcal{N}}$ being the nucleon mass.

For abbreviation we use also

$$u = \frac{E + E' + Q}{2E} \qquad v = \frac{E + E' - Q}{2E} \tag{2.9}$$

finding

$$\bar{u}_l \gamma^{\mu}(1 - \gamma_5)\, u_{\nu}\,|_{\substack{\text{resonance}\\ \text{rest frame}}} = -2\sqrt{2}\, E \sqrt{\frac{-q^2}{Q^2}} \{u \cdot e_L{}^{\mu} - v \cdot e_R{}^{\mu} + \sqrt{2uv} \cdot e_s{}^{\mu}\}. \tag{2.10}$$

The full neutrino excitation matrix element then reads

$$T(\nu\mathcal{N} \to l\mathcal{N}^*) = -4GME \left\{ \sqrt{\frac{-q^2}{Q^2}} \langle \mathcal{N}^* \mid uF_- - vF_+ \mid \mathcal{N} \rangle + \frac{m_{\mathcal{N}}}{M} \sqrt{2uv}\, \langle \mathcal{N}^* \mid F_0 \mid \mathcal{N} \rangle \right\} \tag{2.11}$$

with

$$\begin{aligned} F_+ &= e^{\mu}{}_R F_{\mu} = \frac{-1}{\sqrt{2}}(F_x + iF_y), \\ F_- &= e^{\mu}{}_L F_{\mu} = \frac{1}{\sqrt{2}}(F_x - iF_y), \\ F_0 &= \sqrt{\frac{-q^2}{Q^{*2}}}\, e_s{}^{\mu} F_{\mu} = F_t + \frac{\nu^*}{Q^*} F_z . \end{aligned} \tag{2.12}$$

Although the whole matrix element is Lorentz-invariant the derivation shows that its hadronic parts $\langle \mathcal{N}^* \mid F_{\pm,0} \mid \mathcal{N} \rangle$ are to be evaluated in the resonance rest frame. That

is exactly the situation where the constituent quark model is considered to be applicable. But before entering dynamical models let us fully exploit the kinematics of resonance production by neutrinos and antineutrinos.

First we quote the production cross section of a single resonance with mass M and negligible width

$$\frac{d\sigma}{dq^2\,d\nu} = \frac{1}{32\pi m_{\mathcal{N}} E^2} \cdot \frac{1}{2} \cdot \sum_{\text{spins}} |\, T(\nu\mathcal{N} \to l\mathcal{N}^*)|^2\, \delta(W^2 - M^2). \tag{2.13}$$

The three terms of T referring to different helicities of the incident current add up incoherently resulting in

$$\frac{d\sigma}{dq^2\,d\nu} = \frac{G^2}{4\pi^2}\left(\frac{-q^2}{Q^2}\right)\kappa\{u^2\sigma_{\mathrm{L}} + v^2\sigma_{\mathrm{R}} + 2uv\sigma_s\}. \tag{2.14}$$

Here the partial cross sections for the absorption of an intermediate vector boson of virtual "mass" q^2 and positive, negative or zero helicity are given by

$$\sigma_{\substack{\mathrm{L}\\\mathrm{R}}}(q^2, W) = \frac{\pi}{\kappa} \cdot \frac{M}{m_{\mathcal{N}}} \cdot \frac{1}{2}\sum_{j_z} |\langle \mathcal{N}, j_z \mp 1 \mid F_{\mp} \mid \mathcal{N}^*, j_z\rangle|^2\, \delta(W - M), \tag{2.15a, b}$$

$$\sigma_s(q^2, W) = \frac{\pi}{\kappa} \cdot \frac{M}{m_{\mathcal{N}}}\left(\frac{Q^2}{-q^2}\right) \cdot \frac{m_{\mathcal{N}}^2}{M^2} \cdot \frac{1}{2}\sum_{j_z} |\langle \mathcal{N}, j_z \mid F_0 \mid \mathcal{N}^*, j_z\rangle|^2\, \delta(W - M) \tag{2.15c}$$

including a conventional kinematical factor

$$\kappa = \nu + \frac{q^2}{2m_{\mathcal{N}}} = \frac{M^2 - m_{\mathcal{N}}^2}{2m_{\mathcal{N}}}. \tag{2.16}$$

With the momentum transfer along the z-direction the matrix elements

$$f_{\pm|2j_z|} = \langle \mathcal{N}, j_z \pm 1 \mid F_{\pm} \mid \mathcal{N}^*, j_z\rangle, \tag{2.17a, b}$$

$$f_{0\pm} = \langle \mathcal{N}, \pm\tfrac{1}{2} \mid F_0 \mid \mathcal{N}^*, \pm\tfrac{1}{2}\rangle \tag{2.17c}$$

are just the helicity amplitudes for the *production* process. These are provided by the dynamical model.

For incident antineutrinos left- and right-handed current components are interchanged and the transition matrix element takes the form

$$\bar{T}(\bar{\nu}\mathcal{N} \to \bar{l}\mathcal{N}^*) = -4GME\left\{\sqrt{\frac{-q^2}{Q^2}}\,\langle \mathcal{N}^* \mid u\bar{F}_+ - v\bar{F}_- \mid \mathcal{N}\rangle - \frac{m_{\mathcal{N}}}{M}\,\langle \mathcal{N}^* \mid \bar{F}_0 \mid \mathcal{N}\rangle\right\}. \tag{2.18}$$

In the charged current case F and $\bar{F}$ differ by their isospin direction, for neutral currents they need not be distinguished. The antineutrino cross section is then given by

$$\frac{d\bar{\sigma}}{dq^2\,dv} = \frac{G^2}{4\pi^2}\left(\frac{-q^2}{Q^2}\right)\kappa\{u^2\bar{\sigma}_R + v^2\bar{\sigma}_L + 2uv\bar{\sigma}_s\}. \tag{2.19}$$

Having thus established the production cross sections for a single resonance in narrow width approximation we go over to resonances of finite width replacing the δ-function in the partial cross sections by a Breit–Wigner factor

$$\delta(W - M) \to \frac{1}{2\pi}\cdot\frac{\Gamma}{(W-M)^2 + \Gamma^2/4}. \tag{2.20}$$

For a first orientation we may take the total resonance width to be energy independent. Then the total cross sections are obtained by integrating (2.14) and (2.19) within the bounds

$$\begin{aligned} W_{\min} = m_{\mathcal{N}} + m_\pi \leqslant W \leqslant W_{\max} = s = 2m_{\mathcal{N}}E_\nu + m_{\mathcal{N}}^2, \\ |q^2|_{\min} = 0 \leqslant |q^2| \leqslant |q^2|_{\max} = \frac{(s - m_{\mathcal{N}}^2)(s - W^2)}{s}. \end{aligned} \tag{2.21}$$

2.2. *Interfering Resonances*

Our ultimate interest actually goes beyond neutrino excitation of single isolated resonances. In practice always several nearby resonances will overlap and even non-resonant background amplitudes of various quantum numbers may interfere to produce the measurable final state. So we now turn to a description of inelastic neutrino (antineutrino)–nucleon scattering where the final hadronic state is selected to consist of a nucleon accompanied by a single pion.

There are altogether 14 reactions of this kind, 6 of them being mediated by charged currents

$$\begin{aligned} \nu p &\to \mu^- p\pi^+ \quad \text{(a)} & \bar{\nu}n &\to \mu^+ n\pi^- \quad \text{(a')} \\ \nu n &\to \mu^- p\pi^0 \quad \text{(b)} & \bar{\nu}p &\to \mu^+ n\pi^0 \quad \text{(b')} \\ \nu n &\to \mu^- n\pi^+ \quad \text{(c)} & \bar{\nu}p &\to \mu^+ p\pi^- \quad \text{(c')} \end{aligned} \tag{2.22}$$

while the remaining 8 reaction channels are populated by neutral current interactions

$$\begin{aligned} \nu p &\to \nu p\pi^0 \quad \text{(a)} & \bar{\nu}p &\to \bar{\nu}p\pi^0 \quad \text{(a')} \\ \nu p &\to \nu n\pi^+ \quad \text{(b)} & \bar{\nu}p &\to \bar{\nu}n\pi^+ \quad \text{(b')} \\ \nu n &\to \nu n\pi^0 \quad \text{(c)} & \bar{\nu}n &\to \bar{\nu}n\pi^0 \quad \text{(c')} \\ \nu n &\to \nu p\pi^- \quad \text{(d)} & \bar{\nu}n &\to \bar{\nu}p\pi^- \quad \text{(d')} \end{aligned} \tag{2.23}$$

All these reaction amplitudes are expected to be dominated by nucleon resonances as long as the pion–nucleon invariant energy does not exceed about 2 GeV.

The formalism for describing single resonance production by neutrinos must consequently be extended to include several interfering resonances $\mathcal{N}_\gamma^*$ which, by simultaneous decay, feed the same final $\mathcal{N}\pi$-state at a fixed invariant energy W. So we have to deal with a sum of helicity amplitudes $f_{\pm 1}^{(\gamma)}$, $f_{\pm 3}^{(\gamma)}$, $f_{0\pm}^{(\gamma)}$ for single resonance production each of them being accompanied with the corresponding decay amplitude $\eta^{(\gamma)}$ into the $\mathcal{N}\pi$ state under consideration.

For the subsequent calculations we have taken into account all nucleon resonances of unambiguous classification up to 2 GeV according to the most recent $\pi\mathcal{N}$ partial wave analysis [4, 5]. Those are listed in Table 1.

(a) *Isospin Analysis of the Full $\mathcal{N}\pi$-Reaction Amplitude*

Calling A_3^{CC}, A_1^{CC} the reduced amplitudes for producing a $\mathcal{N}\pi$-final state with isospin $\frac{3}{2}$ ($\frac{1}{2}$) by a charged isovector current (CC), and A_3^{NC}, A_1^{NC} and S_1^{NC} the corresponding neutral current (NC) amplitudes originating from the isovector and isoscalar part, respectively, we find from isospin Clebsch–Gordan rules:

$$\text{Ampl}(\nu p \to \mu p\pi^+) = A^{CC}(p\pi^+) = \sqrt{2}\, A_3^{CC}, \tag{2.24a}$$

$$\text{Ampl}(\nu n \to \mu p\pi^0) = A^{CC}(p\pi^0) = \frac{2}{3}(A_3^{CC} - A_1^{CC}), \tag{2.24b}$$

$$\text{Ampl}(\nu n \to \mu n\pi^+) = A^{CC}(n\pi^+) = \frac{\sqrt{2}}{3}(A_3^{CC} + 2A_1^{CC}), \tag{2.24c}$$

$$\text{Ampl}(\nu p \to \nu p\pi^0) = A^{NC}(p\pi^0) = \frac{2}{3} A_3^{NC} + \frac{1}{3}(A_1^{NC} - \sqrt{3}\, S_1^{NC}), \tag{2.25a}$$

$$\text{Ampl}(\nu p \to \nu n\pi^+) = A^{NC}(n\pi^+) = \frac{\sqrt{2}}{3} A_3^{NC} - \frac{\sqrt{2}}{3}(A_1^{NC} - \sqrt{3}\, S_1^{NC}), \tag{2.25b}$$

$$\text{Ampl}(\nu n \to \nu n\pi^0) = A^{NC}(n\pi^0) = \frac{2}{3} A_3^{NC} + \frac{1}{3}(A_1^{NC} + \sqrt{3}\, S_1^{NC}), \tag{2.25c}$$

$$\text{Ampl}(\nu n \to \nu p\pi^-) = A^{NC}(p\pi^-) = \frac{\sqrt{2}}{3} A_3^{NC} - \frac{\sqrt{2}}{3}(A_1^{NC} + \sqrt{3}\, S_1^{NC}), \tag{2.25d}$$

where each of these relations refers to every helicity component separately. Now A_3^{CC}, A_3^{NC} are dominated by isospin $\frac{3}{2}$ resonances while A_1^{CC}, A_1^{NC} and S_1^{NC} are dominated by isospin $\frac{1}{2}$ resonances. Thus we may write for charged current amplitudes

$$\begin{aligned} \sqrt{2}\, A_3^{CC} &= \sqrt{3} \sum_{\substack{\text{all } I=\frac{3}{2} \\ \text{resonances}}} a^{CC}(\mathcal{N}_3^{*+}), \\ \tfrac{2}{3} A_1^{CC} &= \sqrt{\tfrac{1}{3}} \sum_{\substack{\text{all } I=\frac{1}{2} \\ \text{resonances}}} a^{CC}(\mathcal{N}_1^{*+}) \end{aligned} \tag{2.26}$$

TABLE I

Nucleon Resonances below 2 GeV/c² according to Ref. [4]

Resonance Symbol[a]	Central mass value M [MeV/c²]	Total with Γ_0[MeV]	Elasticity $x_E = \pi\mathcal{N}$ branching ratio	Quark-Model/ SU_6-assignment
$P_{33}(1234)$	1234	124	1	$^4(10)_{3/2}\,[56, 0^+]_0$
$P_{11}(1450)$	1450	370	0.65	$^2(8)_{1/2}\,[56, 0^+]_2$
$D_{13}(1525)$	1525	125	0.56	$^2(8)_{3/2}\,[70, 1^-]_1$
$S_{11}(1540)$	1540	270	0.45	$^2(8)_{1/2}\,[70, 1^-]_1$
$S_{31}(1620)$	1620	140	0.25	$^2(10)_{1/2}\,[70, 1^-]_1$
$S_{11}(1640)$	1640	140	0.60	$^4(8)_{1/2}\,[70, 1^-]_1$
$P_{33}(1640)$	1640	370	0.20	$^4(10)_{3/2}\,[56, 0^+]_2$
$D_{13}(1670)$	1670	80	0.10	$^4(8)_{3/2}\,[70, 1^-]_1$
$D_{15}(1680)$	1680	180	0.35	$^4(8)_{5/2}\,[70, 1^-]_1$
$F_{15}(1680)$	1680	120	0.62	$^2(8)_{5/2}\,[56, 2^+]_2$
$P_{11}(1710)$	1710	100	0.19	$^2(8)_{1/2}\,[70, 0^+]_2$
$D_{33}(1730)$	1730	300	0.12	$^2(10)_{3/2}\,[70, 1^-]_1$
$P_{13}(1740)$	1740	210	0.19	$^2(8)_{3/2}\,[56, 2^+]_2$
$P_{31}(1920)$	1920	300	0.19	$^4(10)_{1/2}\,[56, 2^+]_2$
$F_{35}(1920)$	1920	340	0.15	$^4(10)_{5/2}\,[56, 2^+]_2$
$F_{37}(1950)$	1950	340	0.40	$^4(10)_{7/2}\,[56, 2^+]_2$
$P_{33}(1960)$	1960	300	0.17	$^4(10)_{3/2}\,[56, 2^+]_2$
$F_{17}(1970)$	1970	325	0.06	$^4(8)_{7/2}\,[70, 2^+]_2$

[a] A resonance is specified by the $\pi\mathcal{N}$-partial wave from which it arises, the labels indicating isospin and spin : $L_{2I,\,2J}$ (mass).

and correspondingly in the neutral current case

$$\tfrac{2}{3}A_3^{\mathrm{NC}} = \sqrt{\tfrac{2}{3}} \sum_{\substack{\text{all } I=\frac{3}{2} \\ \text{resonances}}} a^{\mathrm{NC}}(\mathcal{N}_3^{*+}) = \sqrt{\tfrac{2}{3}} \sum_{\substack{\text{all } I=\frac{3}{2} \\ \text{resonances}}} a^{\mathrm{NC}}(\mathcal{N}_3^{*0}), \quad (2.27a)$$

$$\tfrac{1}{3}(A_1^{\mathrm{NC}} - \sqrt{3}\,S_1^{\mathrm{NC}}) = -\sqrt{\tfrac{1}{3}} \sum_{\substack{\text{all } I=\frac{1}{2} \\ \text{resonances}}} a^{\mathrm{NC}}(\mathcal{N}_1^{*+}), \quad (2.27b)$$

$$\tfrac{1}{3}(A_1^{\mathrm{NC}} + \sqrt{3}\,S_1^{\mathrm{NC}}) = +\sqrt{\tfrac{1}{3}} \sum_{\substack{\text{all } I=\frac{1}{2} \\ \text{resonances}}} a^{\mathrm{NC}}(\mathcal{N}_1^{*0}), \quad (2.27c)$$

where $\mathcal{N}_{3,1}^{*0}$, $\mathcal{N}_{3,1}^{*+}$ denote resonances (of isospin $\frac{3}{2}$ or $\frac{1}{2}$) being in zero or positively charged states, respectively.

For illustration we may form

$$A^{CC}(n\pi^+) = \sqrt{\tfrac{1}{3}} \sum a^{CC}(\mathcal{N}_3^{*+}) + \sqrt{\tfrac{2}{3}} \sum a^{CC}(\mathcal{N}_1^{*+}). \tag{2.28}$$

Now in calculating W-distributions or total cross sections where the angular dependence has already been integrated out only those resonances are allowed to interfere which have the same spin and $\mathcal{N}\pi$ orbital angular momentum. Thus, e.g., the overlapping tails of the resonances $P_{33}(1234)$ and $P_{13}(1740)$ can interfere while there is no interference between, e.g., $P_{33}(1234)$ and $P_{11}(1450)$ or $D_{33}(1730)$. More specifically, starting with Eq. (2.28) we may write

$$\begin{aligned} |A^{CC}(n\pi^+)|^2 = & \left| \sqrt{\tfrac{1}{3}} \sum a^{CC}(S_{31}^+) + \sqrt{\tfrac{2}{3}} \sum a^{CC}(S_{11}^+) \right|^2 \\ & + \sum_{j=1,3} \left| \sqrt{\tfrac{1}{3}} \sum a^{CC}(P_{3j}^+) + \sqrt{\tfrac{2}{3}} \sum a^{CC}(P_{1j}^+) \right|^2 \\ & + \sum_{j=3,5} \left| \sqrt{\tfrac{1}{3}} \sum a^{CC}(D_{3j}^+) + \sqrt{\tfrac{2}{3}} \sum a^{CC}(D_{1j}^+) \right|^2 \\ & + \sum_{j=5,7} \left| \sqrt{\tfrac{1}{3}} \sum a^{CC}(F_{3j}^+) + \sqrt{\tfrac{2}{3}} \sum a^{CC}(F_{1j}^+) \right|^2. \end{aligned} \tag{2.29}$$

Any of the charged or neutral current amplitudes $a_k(\mathcal{N}_\gamma^*)$ referring to one single resonance in a definite state of isospin, charge and helicity ($k = 2j_z$) consists of two factors describing the *production* of the resonance $\mathcal{N}_\gamma^*$ and its subsequent *decay* into the $\mathcal{N}\pi$ final state:

$$a_k^{CC,NC}(\mathcal{N}_\gamma^*) = f_k^{CC,NC}(\nu\mathcal{N} \to \mathcal{N}_\gamma^*) \cdot \eta(\mathcal{N}_\gamma^* \to \mathcal{N}\pi) \equiv f_k^{(\gamma)} \cdot \eta^{(\gamma)}. \tag{2.30}$$

The resonance production amplitudes $f_k^{(\gamma)}$ ($k = 2j_z = \pm 3, \pm 1, 0\pm$) for single resonances $\mathcal{N}_\gamma^*$ have already been introduced in Eqs. (2.17). The corresponding decay amplitudes $\eta^{(\gamma)}$ in turn can be split into three factors.

(i) First there is the Breit–Wigner factor

$$\eta_{BW}^{(\gamma)}(W) = \sqrt{\frac{\Gamma_\gamma}{2\pi}} \frac{1}{W - M_\gamma + (i/2)\,\Gamma_\gamma} \cdot \frac{1}{\sqrt{N_\gamma}}, \tag{2.31}$$

where the total resonance width Γ_γ has the usual threshold behaviour

$$\Gamma_\gamma = \Gamma_\gamma^0 \left(\frac{q_\pi(W)}{q_\pi(M_\gamma)} \right)^{2L+1} \tag{2.32}$$

with

$$q_\pi(W) = |\,\mathbf{q}_\pi\,|_{\mathcal{N}\pi\text{-}CMS} = \{(W^2 - m_{\mathcal{N}}{}^2 - m_\pi{}^2)^2 - 4m_{\mathcal{N}}{}^2 m_\pi{}^2\}^{1/2} \cdot \frac{1}{2W}$$

and a correction close to one,

$$N_\nu = \int_{W_{\min}}^{\infty} dW \frac{\Gamma_\nu}{2\pi} \frac{1}{(W - M_\nu)^2 + \Gamma_\nu^2/4}$$

has been applied for keeping the Breit–Wigner factor approximately normalized.

(ii) A second factor is the square root of the elasticity $x_E^{(\nu)}$ of the resonance taking care of the branching ratio into the $\mathcal{N}\pi$ final state.

(iii) The third factor is a pure sign. In principle, production and subsequent decay of a resonance have to be calculated in the same model in order to obtain a coherent prediction for the $\mathcal{N}\pi$ excitation amplitude. However, in replacing the latter by the *experimental* Breit–Wigner factor, the sign of the decay amplitude is lost and has to be attached as a separate factor. For single resonance production this sign would not matter. For interfering resonances, however, it is important and must be carefully included.

So we have in total for the decay amplitude of a single resonance $\mathcal{N}_\nu^*$:

$$\eta^{(\nu)} = \sqrt{x_E^{(\nu)}} \cdot \eta_{\mathrm{BW}}^{(\nu)}(W) \cdot \mathrm{sgn}(\mathcal{N}_\nu^*) \tag{2.33}$$

irrespective of its isospin, charge or helicity.

The production and decay amplitudes are now to be attached according to Eq. (2.30). Summing up all contributing resonances then gives us the full $\mathcal{N}\pi$ amplitude to be used in the cross-section formulae of Eqs. (2.14) and (2.19).

(b) *One Example in Detail*

For illustrating the procedure let us consider again the charged current reaction

$$\nu n \to \mu n \pi^+.$$

The square of a typical matrix element has been written down in Eq. (2.29). We will make the helicity information explicit:

$$A^{\mathrm{CC}}(n\pi^+) \to A_k^{n\pi^+}(q^2, W), \qquad k = \pm 3, \pm 1, 0\pm. \tag{2.34}$$

Then the helicity cross sections $\sigma_{\mathrm{L,R,}S}$ are constructed along the lines of Section 2.1 replacing everywhere the resonance mass M by the invariant energy W of the $\mathcal{N}\pi$-system.

$$\begin{aligned}
\sigma_{\substack{\mathrm{L}\\\mathrm{R}}}^{n\pi^+}(q^2, W) &= \frac{\pi W}{\kappa \cdot m_{\mathcal{N}}} \cdot \frac{1}{2}(|A_{\pm 3}^{n\pi^+}(q^2, W)|^2 + |A_{\pm 1}^{n\pi^+}(q^2, W)|^2), \\
\sigma_S^{n\pi^+}(q^2, W) &= \frac{\pi W}{\kappa \cdot m_{\mathcal{N}}} \left(\frac{Q^2}{-q^2}\right) \frac{m_{\mathcal{N}}^2}{W^2} \cdot \frac{1}{2}(|A_{0+}^{n\pi^+}(q^2, W)|^2 + |A_{0-}^{n\pi^+}(q^2, W)|^2),
\end{aligned} \tag{2.35}$$

where now Q and κ are given by

$$Q = \frac{1}{2m_{\mathcal{N}}}\{(W^2 - m_{\mathcal{N}}{}^2 - q^2)^2 - 4m_{\mathcal{N}}{}^2 q^2\}^{1/2}, \qquad \kappa = \nu + \frac{q^2}{2m_{\mathcal{N}}} = \frac{W^2 - m_{\mathcal{N}}{}^2}{2m_{\mathcal{N}}}. \tag{2.36}$$

Finally the general cross section formula reads

$$\frac{d\sigma(\nu n \to \mu n\pi^+)}{dq^2\, dW} = \frac{G^2}{4\pi^2}\left(\frac{-q^2}{Q^2}\right)\frac{W}{m_{\mathcal{N}}}\kappa\{u^2\sigma_{\mathrm{L}}^{n\pi^+}(q^2, W) + v^2\sigma_{\mathrm{R}}^{n\pi^+}(q^2, W) + 2uv\sigma_S^{n\pi^+}(q^2, W)\} \tag{2.37}$$

and a similar equation holds for the charge conjugate antineutrino reaction (2.22c') where essentially the left- and right-handed cross sections are interchanged:

$$\sigma_{\mathrm{L,R}}^{n\pi^+} \to \bar{\sigma}_{\mathrm{R,L}}^{p\pi^-} = \sigma_{\mathrm{R,L}}^{n\pi^+}. \tag{2.38}$$

(The latter equation follows from charge symmetry.) All other cross sections for single pion neutrino (antineutrino) production are obtained in exactly the same way.

2.3. *$\mathcal{N}^*$-Decay Angular Distributions in Case of Several Interfering Resonances*

Single pion neutrino production has now reached a stage where the experimental study of angular distributions of the final particles in the $\mathcal{N}^*$ rest frame becomes feasible. The theoretical analysis is relatively easy if the W-domain of a single resonance can be cut out for separate investigation. However, neighbouring resonances may well influence the result even if their cross sections are small compared with that of the leading resonance. In order to provide a kinematical framework for this possibility we thus have to generalize the usual density matrix formalism to several interfering resonances decaying simultaneously into a two particle final state.

In the preceding section we have parametrized a typical $\pi\mathcal{N}$ production amplitude as a sum of unitarized production amplitudes of single resonances

$$A_k^{\mathcal{N}\pi}(q^2, W) = \sum_{\substack{\text{all} \\ \text{resonances}}} C(I_\nu) f_k^{(\nu)}(q^2, W) \cdot \eta^{(\nu)}(W), \tag{2.39}$$

where $C(I_\nu)$ stands symbolically for the $(\mathcal{N}_\nu^* \to \mathcal{N}\pi)$-isospin Clebsch–Gordan coefficients involved.

The angular distribution should be obtained by essentially squaring Eq. (2.39). This is, however, not completely true, since every $A_k(q^2, W)$ refers to only one helicity component of the current whereas all of them are supposed to contribute. Hence we must start more generally with the transition amplitude

$$\mathfrak{M}(\nu\mathcal{N} \to \mathcal{N}\pi) = \sum_\nu \langle \mathcal{N}\pi \mid \mathcal{N}_\nu^* \rangle \langle \mathcal{N}_\nu^*, l \mid \mathscr{H}_W \mid \mathcal{N}, \nu \rangle \tag{2.40}$$

made up of resonance production amplitudes $\langle \mathcal{N}_\gamma^*, l \mid \mathcal{H}_W \mid \mathcal{N}, \nu \rangle$ and their projections $\langle \mathcal{N}\pi \mid \mathcal{N}_\gamma^* \rangle$ onto the particular $\mathcal{N}\pi$ final state. The former are taken to be unitarized, i.e., to include the resonance decay via Breit–Wigner amplitudes thus corresponding to the product $f^{(\gamma)} \cdot \eta^{(\gamma)}$ in Eq. (2.39). We will denote them by T^γ in accordance with the basic definition (2.2). The latter reduce essentially to isospin Clebsch–Gordan coefficients $C((\mathcal{N}\pi)I, I_3)$ corresponding in an obvious manner to those of Eq. (2.39) with some additional angular functions involved. If the spin states of the nucleon $\mathcal{N}$ and the resonance $\mathcal{N}_\gamma^*$ are specified by s_z and j_z, respectively, the transition matrix element T^γ is labelled accordingly: $T^\gamma_{s_z j_z}$. In squaring (2.40) we obtain various products of such transition matrix elements including those where the two factors refer to different resonances. These interference terms give rise to a generalized density matrix with elements $\rho^{j_z j_z'}_{\gamma\gamma'}$:

$$\rho^{\gamma\gamma'}_{j_z j_z'} = \tfrac{1}{2} \sum_{s_z = \pm 1/2} T^\gamma_{s_z j_z} (T^{\gamma'}_{s_z j_z'})^*. \tag{2.41}$$

They reduce to the usual form if there is only one resonance ($\gamma = \gamma'$) present. The normalization is provided by

$$\sum_{\gamma, j_z} \rho^{\gamma\gamma}_{j_z j_z} = 1. \tag{2.42}$$

With the aid of this generalized density matrix and the definition

$$Z^{jj'\lambda\pm}_{j_z j_z'}(\theta) = d^j_{j_z\lambda}(\theta)\, d^{j'}_{j_z'\lambda}(\theta) \pm d^j_{j_z-\lambda}(\theta)\, d^{j'}_{j_z'-\lambda}(\theta), \tag{2.43}$$

where the $d^j_{j_z\lambda}(\theta)$ are tabulated [14] for all interesting angular momenta j, j' and helicities λ, we may write down the desired generalized angular distribution of pions in the $\mathcal{N}\pi$ center of mass system:

$$W((\mathcal{N}\pi)\, I_3\,;\, \theta, \varphi) = \sum_{j_z, j_z'} \sum_{\substack{j, j' \\ I, I' \\ P, P'}} \sqrt{\frac{2j+1}{4\pi}} \sqrt{\frac{2j'+1}{4\pi}}\, C((\mathcal{N}\pi)\, I, I_3)\, C((\mathcal{N}\pi)\, I', I_3)$$

$$\cdot\, Z^{jj'(1/2)\sigma}_{j_z j_z'}(\theta) \cdot \mathrm{Re}\{e^{i(j_z - j_z')\varphi} \rho^{(IjP),(I'j'P')}_{j_z j_z'}\} \tag{2.44}$$

Here the set γ of quantum numbers characterizing a resonance $\mathcal{N}_\gamma^*$ has been made explicit in specifying spin, isospin and parity of $\mathcal{N}_\gamma^*$. The sign σ in $Z^{jj'(1/2)\sigma}_{j_z j_z'}(\theta)$ is positive if the interfering resonances have both equal spin and equal parities or if they have opposite parities and differ in spin by one unit. For all other configurations σ is negative.

Equation (2.44) is our general result. Its detailed derivation is deferred to the appendix. Here we will briefly discuss two cases of interest:

(i) The simplest situation occurs when only one resonance is present and the inner sum in Eq. (2.44) degenerates to a single term. Calling

$$Z^{j(1/2)+}_{j_z j'_z}(\theta) \equiv Z^{jj(1/2)+}_{j_z j'_z}(\theta) \tag{2.45a}$$

and

$$\rho_{j_z j'_z} \equiv \rho^{(Ij\,P),(Ij\,P)}_{j_z j'_z} \tag{2.45b}$$

we recover the well-known single resonance formula [15]

$$\begin{aligned} W((\mathcal{N}\pi)\, I_3\,;\,\theta,\,\varphi) &= \sum \frac{2j+1}{4\pi} \{C((\mathcal{N}\pi)\, I,\, I_3)\}^2\, Z^{j(1/2)+}_{j_z j'_z}(\theta)\, \mathrm{Re}\{e^{i(j_z - j'_z)\varphi} \rho_{j_z j'_z}\} \\ &\propto \left\{ Y_0^0 \tilde{\rho} - \frac{2}{\sqrt{5}}\, Y_2^0 \left\{ \tilde{\rho}_{33} - \frac{1}{2}\,\tilde{\rho} \right\} \right. \\ &\quad \left. + \frac{4}{\sqrt{10}}\, \mathrm{Re}\; Y_2^1 \tilde{\rho}_{31} - \frac{4}{\sqrt{10}}\, \mathrm{Re}\; Y_2^2 \tilde{\rho}_{3-1} \right\}, \end{aligned} \tag{2.46}$$

where

$$\begin{aligned} \tilde{\rho} &= \sum_{j_z} \rho_{j_z j_z}\,, \\ \tilde{\rho}_{33} &= \rho_{3/2\;3/2} + \rho_{-3/2\;-3/2}\,, \\ \tilde{\rho}_{31} &= \rho_{3/2\;1/2} - \rho_{-1/2\;-3/2}\,, \\ \tilde{\rho}_{3-1} &= \rho_{3/2\;-1/2} + \rho_{1/2\;-3/2} \end{aligned} \tag{2.47}$$

and all $\rho_{j_z j'_z}$ can be chosen real.

(ii) A less trivial example is provided by the interference of the Δ-resonance with the $P_{33}(1640)$ which is practically the only additional resonance able to contribute to the pion angular distribution in the $p\pi^+$ channel. Those two resonances have equal quantum numbers I, j, P but unequal masses and widths. Then the angular distribution has almost the same form as in (2.46) reading now:

$$\begin{aligned} W((\mathcal{N}\pi)\, I_3 = \tfrac{3}{2}\,;\,\theta,\,\varphi) \propto \left\{ Y_0^0 \tilde{\rho} - \frac{2}{\sqrt{5}} \left\{ \tilde{\rho}_{33} - \frac{1}{2}\,\tilde{\rho} \right\} + \frac{4}{\sqrt{10}}\, \mathrm{Re}\; Y_2^1\, \mathrm{Re}\; \tilde{\rho}_{31} \right. \\ \left. - \frac{4}{\sqrt{10}}\, \mathrm{Re}\; Y_2^2\, \mathrm{Re}\; \tilde{\rho}_{3-1} - \frac{4}{\sqrt{10}}\, \mathrm{Im}\; Y_2^1\, \mathrm{Im}\; \tilde{\rho}_{31} + \frac{4}{\sqrt{10}}\, \mathrm{Im}\; Y_2^2\, \mathrm{Im}\; \tilde{\rho}_{3-1} \right\} \end{aligned} \tag{2.48}$$

with the same definitions as in (2.47) apart from the more complicated structure of $\rho_{j_z j'_z}$:

$$\rho_{j_z j'_z} = \sum_{r,s=1}^{2} \rho^{rs}_{j_z j'_z}\,. \tag{2.49}$$

Since $\rho_{j_z j'_z}$ obtains contributions from two resonances differing in their production

matrix elements including the (complex) Breit–Wigner factors the nondiagonal elements with $r \neq s$ are in general also complex. This causes the angular distribution (2.48) to include some extra terms compared to (2.46) which are sometimes dubbed "illegal."

In turning to the mixed isospin channel ($\nu n \to \mu n \pi^+$) or likewise ($\bar{\nu} p \to \bar{\mu} p \pi^-$), which is easier to measure, we have to envisage the possibility of even more than two nearby resonances interfering strongly with the leading Δ-resonance. Actually we have taken into account altogether four prominent resonances. The angular distribution formula then gets rather lengthy involving also higher rank spherical harmonics. It will be given in the Appendix.

2.4. *Nonresonant Background*

The quark model approach adopted in this paper describes the final $\pi\mathcal{N}$ state entirely in terms of resonances, leaving no room for a possible nonresonant background. Some background amplitude is necessary, however, both on general grounds (for example, Born graphs [16, 17]) and on the basis of comparison with data (see Section 4). From a certain combination of charged current total cross sections, it is possible to extract the isospin $\frac{1}{2}$ to $\frac{3}{2}$ ratio $\langle A_1^{CC}/A_3^{CC} \rangle$. By comparison with the resonance model, we find that some $I = \frac{1}{2}$ nonresonant background is needed. In the spirit of the quark model, we have represented the background by a resonance amplitude of P_{11} character (like the nucleon), with the Breit–Wigner factor replaced by an adjustable constant. The corresponding cross section is added incoherently to the resonant cross section. This ansatz ensures that the background is smooth and phase-space-like and affects only the $I = \frac{1}{2}$ cross section. While subtle effects of coherence are ignored by this procedure, we are able to incorporate the background effects in a reasonable way at the expense of only one additional constant. As we shall see later, many of our results are affected only slightly by the background, which justifies the approximate treatment described above.

3. Dynamics of Single Pion Neutrino-Production

In the preceding section, we have set up a kinematical frame for calculating differential cross sections and angular distributions in terms of resonance excitation matrix elements. The dynamical task is to compute the production and decay amplitudes $f_k(q^2, W)$ and $\eta(W)$ defined in Eqs. (2.30). To this end we adopt the quark model, because of its simplicity and predictive power. The version used is that proposed by Feynman, Kislinger, and Ravndal [1] (FKR), which we outline below. Although in some respect relativistic the FKR-model depicts the basic quark–quark interaction still as an oscillator potential allowing for the definition of a three quark wave function. The transition matrix elements are then determined by the current operator and the wave function. The latter is assumed, as usual in quark models, to be largely

predicted by spin–flavor symmetry leading to a classification pattern of states in terms of SU_6 multiplets [18]. The dynamical model then gives the spatial part of the wave functions and specifies the form of the quark–current interaction.

3.1. *Brief Review of the Feynman–Kislinger–Ravndal Model*

The quark model proposed by FKR is given by the four-dimensional harmonic oscillator Hamiltonian

$$\mathscr{H} = 3(p_a^2 + p_b^2 + p_c^2) + \frac{1}{36}\Omega^2[(u_a - u_b)^2 + (u_b - u_c)^2 + (u_c - u_a)^2] + \text{const.} \tag{3.1}$$

Here p_a represents the four-momentum operator of quark a, and u_a its conjugate position, so that $p_{a\mu} = i(\partial/\partial u_a{}^\mu)$. Introducing the center-of-mass and relative coordinates

$$\begin{aligned} P &= p_a + p_b + p_c\,, & R &= \frac{1}{3}(u_a + u_b + u_c)\,, \\ \xi &= p_c + p_b - 2p_a\,, & x &= \frac{1}{6}(u_c + u_b - 2u_a), \\ \eta &= \sqrt{3}\,(p_c - p_b), & y &= \frac{1}{2\sqrt{3}}(u_c - u_b) \end{aligned} \tag{3.2}$$

one can write $\mathscr{H}$ as

$$\begin{aligned} \mathscr{H} &= P^2 - \mathfrak{N}, \\ \mathfrak{N} &= -\tfrac{1}{2}(\xi^2 + \Omega^2 x^2) - \tfrac{1}{2}(\eta^2 + \Omega^2 y^2) + \text{const.} \end{aligned} \tag{3.3}$$

showing that if $\mathscr{H}^{-1}$ is interpreted as the propagator of the three quark system, the eigenvalues of $\mathfrak{N}$ correspond to the squared masses of the baryonic states. Introducing annihilation and creation operators corresponding to the x- and y-type oscillators (with permutation symmetry α and β, respectively),

$$\begin{aligned} \xi &= \sqrt{\frac{\Omega}{2}}(a^* + a), & x &= -i\sqrt{\frac{1}{2\Omega}}(a^* - a), \\ \eta &= \sqrt{\frac{\Omega}{2}}(b^* + b), & y &= -i\sqrt{\frac{1}{2\Omega}}(b^* - b) \end{aligned} \tag{3.4}$$

satisfying the algebra

$$[a_\mu\,, a_\nu^*] = [b_\mu\,, b_\nu^*] = -g_{\mu\nu} \tag{3.5}$$

one can write $\mathfrak{N}$ as

$$\mathfrak{N} = -\Omega(a_\mu^* a^\mu + b_\mu^* b^\mu) + \text{const.}, \tag{3.6}$$

whose eigenvalues are integer multiples of Ω (up to a constant C). The baryonic spectrum in Table I is classified according to the eigenstates of this operator, and the parameter Ω is determined [1] from the Regge slope of baryon trajectories to be 1.05 GeV^2.

Electromagnetic and weak interactions are introduced into the model by the minimal coupling scheme, $\not{p}_a \to \not{p}_a - Q_a \not{A}(u_a)$, etc. (Note that $\not{p}_a \not{p}_a = p_a^2$, and the oscillator Hamiltonian in the absence of spin–orbit forces applies to each component of the quark spinor separately). Hence a vector current is given by

$$V_\mu \equiv j_\mu{}^V = 3 \sum_\alpha Q_\alpha (\not{p}_\alpha \gamma_\mu e^{iqu_\alpha} + \gamma_\mu e^{iqu_\alpha} \not{p}_\alpha), \tag{3.7}$$

where the sum is over the quarks in the nucleon, and the corresponding axial vector current operator is introduced replacing γ_μ by $Z\gamma_\mu\gamma_5$.

The unitary spin matrix Q_α specifies the SU_3 character of the current. Restriction to nonstrange baryons and baryon resonances reduces Q_α to the appropriate isospin matrix; so electromagnetic and weak neutral currents contain τ_3, whereas charged currents are characterized by $\tau_\pm$. The axial vector renormalization constant Z is introduced to compensate for the difference between the SU_6-predicted value $\frac{5}{3}$ for the nucleon's axial vector form factor at $q^2 = 0$ and its experimental value of about $\frac{5}{4}$. Consequently Z will be chosen to be $\frac{3}{4}$. Alternatively [19], abandoning SU_6 for the wave function, and coupling spin and orbital angular momentum of a quark individually, would allow us to deal with an unrenormalized axial vector current of the quark ($Z = 1$). We follow, however, the conventions in the field picking up the first alternative.

The reduction of the interaction term to a form suitable for application to resonance excitation has been carried through in Refs. [1, 3] and need not be repeated here. The result is:

$$e^u j_\mu^{V,A} = 2W(e_t F_t^{V,A} + e_z F_z^{V,A} - e_+ F_-^{V,A} - e_- F_+^{V,A}), \tag{3.8}$$

where the charged current operators read [1, 3]

$$\begin{aligned}
F_\pm{}^V &= -9\tau^+(R^V \sigma_\pm + T^V a_\mp)\, e^{-\lambda a_z}, \\
F_\pm{}^A &= \pm 9\tau^+(R^A \sigma_\pm + T^A a_\mp)\, e^{-\lambda a_z}, \\
F_0{}^V &= +9\tau^+ S e^{-\lambda a_z}, \\
F_0{}^A &= -9\tau^+[C\sigma_z + B(\boldsymbol{\sigma}\mathbf{a})]\, e^{-\lambda a_z}.
\end{aligned} \tag{3.9}$$

Application to transitions from the ground-state baryons (the nucleons) makes the $\mathbf{a}^*$ operators inoperative, so that they can be dropped. The neutral current operators, according to the Salam–Weinberg theory [20], are obtained replacing τ^+ by $\frac{1}{2}\tau^3 - 2\sin^2\theta_w \cdot \tau^{\mathrm{em}}$ for the vector current, and by $\frac{1}{2}\tau_3$ for the axial vector current, respectively. Charged and neutral currents contain unitary spin operators (τ^+, τ^3, $\tau^{\mathrm{em}} =$

$(\tau^3 + 1)/2)$ and spin operators $(1, \sigma)$ acting on the SU_6 part of the resonance wave functions. The oscillator operators

$$a_z\,, a_\pm = \mp \frac{1}{\sqrt{2}}(a_x \mp i a_y), \tag{3.10}$$

act on the spatial part. The coefficients in Eq. (3.8) are the same as in Ravndal's paper (Ref. [3]) with the resonance mass M replaced by the $\pi\mathcal{N}$ invariant energy W. We will quote them for the reader's convenience:

$$\begin{aligned}
\lambda &= \sqrt{\frac{2}{\Omega}}\,\frac{m_{\mathcal{N}}}{W}\,Q,\\
T^V &= \frac{1}{3W}\sqrt{\frac{\Omega}{2}}\,G^V(q^2) = T,\\
R^V &= \sqrt{2}\,\frac{m_{\mathcal{N}}}{W}\,\frac{(W + m_{\mathcal{N}})\,Q}{(W + m_{\mathcal{N}})^2 - q^2}\,G^V(q^2) = R,\\
S &= \left(\frac{-q^2}{Q^2}\right)\frac{3Wm_{\mathcal{N}} + q^2 - m_{\mathcal{N}}^2}{6m_{\mathcal{N}}^2}\,G^V(q^2),\\
T^A &= \frac{2}{3}Z\sqrt{\frac{\Omega}{2}}\,\frac{m_{\mathcal{N}}}{W}\,\frac{Q}{(W + m_{\mathcal{N}})^2 - q^2}\,G^A(q^2),\\
R^A &= \frac{Z\sqrt{2}}{6W}\left(W + m_{\mathcal{N}} + \frac{2n\Omega W}{(W + m_{\mathcal{N}})^2 - q^2}\right)G^A(q^2),\\
B &= \frac{Z}{3W}\sqrt{\frac{\Omega}{2}}\left(1 + \frac{W^2 - m_{\mathcal{N}}^2 + q^2}{(W + m_{\mathcal{N}})^2 - q^2}\right)G^A(q^2),\\
C &= \frac{Z}{6m_{\mathcal{N}}Q}\left(W^2 - m_{\mathcal{N}}^2 + n\Omega\,\frac{W^2 - m_{\mathcal{N}}^2 + q^2}{(W + m_{\mathcal{N}})^2 - q^2}\right)G^A(q^2).
\end{aligned} \tag{3.11}$$

The final comment concerns the transition form factors $G^{V,A}(q^2)$ included in the quantities of Eq. (3.11). These are assumed to have the form

$$G^{V,A}(q^2) = \left(1 - \frac{q^2}{4m_{\mathcal{N}}^2}\right)^{1/2-n}\left(\frac{1}{1 - q^2/m_{V,A}^2}\right)^2. \tag{3.12}$$

The dipole factor represents the experimentally measured elastic form factors, the parameters m_V and m_A taking the values [21]

$$\begin{aligned}
m_V &= 0.84\ \text{GeV/c},\\
m_A &= 0.95\ \text{GeV/c}.
\end{aligned} \tag{3.13}$$

The additional factor $(1 - q^2/4m_{\mathcal{N}}^2)^{1/2-n}$ depends on the number n of oscillator

quanta present in the final resonance. It is an ad hoc factor introduced in order to remedy certain unphysical aspects of the model associated with the existence of time-like excitations [1].

3.2. *Transition Amplitudes for Neutrino Reactions*

From the vector and axialvector currents (3.9) we form the relevant $(V-A)$-combinations needed for evaluating the transition matrix elements between a nucleon and a nucleon resonance. For the charged current operators we then find:

$$F_{\pm}^{CC} = F_{\pm}^{V} - F_{\pm}^{A} = 9\tau^{+} \cdot \{T^{\pm} a_{\mp} + R^{\pm}\sigma_{\pm}\}\, e^{-\lambda a_z}, \tag{3.14a}$$

$$F_{0}^{CC} = F_{0}^{V} - F_{0}^{A} = 9\tau^{+} \cdot \{S + C\sigma_z + B\boldsymbol{\sigma}\mathbf{a}\}\, e^{-\lambda a_z}, \tag{3.14b}$$

where

$$T^{\pm} = -(T^{V} \pm T^{A}), \qquad R^{\pm} = -(R^{V} \pm R^{A}). \tag{3.15}$$

The neutral current operators are composed of isovector parts $F_{\pm}^{I_3}$, $F_{0}^{I_3}$ which are the same as $F_{\pm,0}^{CC}$ apart from the replacement of τ^{+} by $\tau_3/2$ in Eqs. (3.14), and of electromagnetic pieces

$$F_{\pm}^{em} = 9\,\frac{\tau_3 + 1}{2}\,(T^{V} a_{\mp} + R^{V}\sigma_{\pm})\, e^{-\lambda a_z}, \tag{3.16a}$$

$$F_{0}^{em} = 9\,\frac{\tau_3 + 1}{2}\, S e^{-\lambda a_z}. \tag{3.16b}$$

We therefore obtain

$$F_{\pm}^{NC} = F_{\pm}^{I_3} - 2\sin^2\theta_w \cdot F_{\pm}^{em}, \tag{3.17a}$$

$$F_{0}^{NC} = F_{0}^{I_3} - 2\sin^2\theta_w \cdot F_{0}^{em}. \tag{3.17b}$$

The exponential function may be expanded to second order in a_z (we are not interested in resonances corresponding to more than two units of radial excitation). This gives, e.g.,

$$F_{\pm}^{I_3} = 9\,\frac{\tau_3}{2}\Big\{R^{\pm}\sigma_{\pm} + [T^{\pm}a_{\mp} - \lambda R^{\pm}\sigma_{\pm}a_z] + \Big[-\lambda T^{\pm}a_{\mp}a_z + \frac{\lambda^2}{2}\,R^{\pm}\sigma_{\pm}a_z^{2}\Big] + \cdots\Big\} \tag{3.18a}$$

and similarly

$$F_0^{I_3} = 9\frac{\tau_3}{2}\Big\{S + C\sigma_z + [(B - \lambda C)\,\sigma_z a_z - \lambda S a_z - B\sqrt{2}\,\sigma_+ a_+ + B\sqrt{2}\,\sigma_- a_-] + \Big[-\Big(B\lambda - \frac{\lambda^2}{2}C\Big)\,\sigma_z a_z^2 + \frac{\lambda^2}{2}S a_z^2 + B\sqrt{2}\,(\sigma_+ a_+ a_z - \sigma_- a_- a_z)\,\lambda\Big] + \cdots\Big\} \tag{3.18b}$$

with corresponding expansions for $F_\pm^{\mathrm{em}}$ and F_0^{em}.

The first line applies to resonances with $n = 0$, the second to singly excited $[70, 1^-]_1$ resonances and the third to twice excited resonances belonging to $[56, 0^+]_2$ or $[56, 2^+]_2$, $[70, 0^+]_2$ and $[70, 2^+]_2$.

The application of these operators to the resonance states now proceeds along the lines indicated in the Appendix of the FKR paper [1]. For proper construction of the baryonic wave functions one may also consult Ref. [17]. The procedure thus need not be repeated here, in fact some of the tables given there can immediately be used for our purposes. Hence we will display in Table II only the final results on

$$\begin{aligned} f_{-3} &= \langle \mathcal{N}, \tfrac{1}{2} \mid F_- \mid \mathcal{N}^*, \tfrac{3}{2}\rangle, \\ f_{-1} &= \langle \mathcal{N}, -\tfrac{1}{2} \mid F_- \mid \mathcal{N}^*, \tfrac{1}{2}\rangle, \\ f_{+1} &= \langle \mathcal{N}, \tfrac{1}{2} \mid F_+ \mid \mathcal{N}^*, -\tfrac{1}{2}\rangle, \\ f_{+3} &= \langle \mathcal{N}, -\tfrac{1}{2} \mid F_+ \mid \mathcal{N}^*, -\tfrac{3}{2}\rangle, \\ f_{0\pm} &= \langle \mathcal{N}, \pm\tfrac{1}{2} \mid F_0 \mid \mathcal{N}^*, \pm\tfrac{1}{2}\rangle, \end{aligned} \tag{3.19}$$

where for charged currents $F_{\pm,0}^{CC}$ the incoming nucleon $\mathcal{N}$ is taken to be a neutron whereas for neutral (and electromagnetic) currents $F_{\pm,0}^{NC}$ both positively charged and neutral states have to be considered.

Decay Signs

As indicated before, however, the production amplitudes f_j ($j = \pm 3, \pm 1, 0\pm$) are not directly measured in single pion neutrino production. The decay amplitudes of the resonances into a particular $\mathcal{N}\pi$-state are equally necessary before comparing the calculation with data. The same problem has also been met in single pion photo- and electroproduction [22, 23]. Now the respective decay amplitudes are calculable in the framework of the FKR model if the usual PCAC assumptions are incorporated. It is the divergence of the axial current operator which causes the decay of a resonance into a nucleon and a pseudoscalar meson and this divergence is given in the model. It will be sufficient to consider only π^0 emission described by the transition operator

$$\mathfrak{N}^P = 6G^A(q^2)\,\tau_3\{\gamma\sigma_z - [\lambda\gamma(1 + \delta) - \beta]\,\sigma_z a_z - \sqrt{2}\,\beta[\sigma_+ a_+ - \sigma_- a_-] + \tfrac{1}{2}\lambda[\lambda\gamma(1 + 2\delta) - 2\beta]\,\sigma_z a_z^2 + \lambda\sqrt{2}\,\beta[\sigma_+ a_+ a_z - \sigma_- a_- a_z] + \cdots\}, \tag{3.20}$$

TABLE

Production Amplitudes for Positively Charged (P) or Neutral (N) Resonances Produce

Resonance (Multiplet)	Helicity ampl.	Electromagnetic P	Electromagnetic N	Weak CC N
$P_{33}(1234)$	f_{-3}	$-\sqrt{6}\,R$		$+\sqrt{6}\,R^-$
$^4(10)_{3/2}[56, 0^+]_0$	f_{-1}	$-\sqrt{2}\,R$		$+\sqrt{2}\,R^-$
	f_{+1}	$+\sqrt{2}\,R$	$N = P$	$-\sqrt{2}\,R^+$
	f_{+3}	$+\sqrt{6}\,R$		$-\sqrt{6}\,R^+$
	f_{0+}	0		$-2\sqrt{2}\,C$
	f_{0-}	0		$-2\sqrt{2}\,C$
$S_{11}(1540)$	f_{-1}	$+\sqrt{3}\,T + \sqrt{\frac{3}{2}}\,\lambda R$	$-\sqrt{3}\,T - \frac{1}{\sqrt{6}}\,\lambda R$	$+2\sqrt{3}\,T^- + \frac{4}{\sqrt{6}}\,\lambda R^-$
$^2(8)_{1/2}[70, 1^-]_1$	f_{+1}	$-\sqrt{3}\,T - \sqrt{\frac{3}{2}}\,\lambda R$	$+\sqrt{3}\,T + \frac{1}{\sqrt{6}}\,\lambda R$	$-2\sqrt{3}\,T^+ - \frac{4}{\sqrt{6}}\,\lambda R^+$
	f_{0+}	$+\sqrt{\frac{3}{2}}\,\lambda S$	$-\sqrt{\frac{3}{2}}\,\lambda S$	$+\sqrt{6}\,\lambda S + 2\sqrt{\frac{2}{3}}\,(\lambda C - 3B)$
	f_{0-}	$-\sqrt{\frac{3}{2}}\,\lambda S$	$+\sqrt{\frac{3}{2}}\,\lambda S$	$-\sqrt{6}\,\lambda S + 2\sqrt{\frac{2}{3}}\,(\lambda C - 3B)$
$D_{13}(1525)$	f_{-3}	$+\sqrt{\frac{9}{2}}\,T$	$-\sqrt{\frac{9}{2}}\,T$	$+2\sqrt{\frac{9}{2}}\,T^-$
$^2(8)_{3/2}[70, 1^-]_1$	f_{-1}	$+\sqrt{\frac{3}{2}}\,T - \sqrt{3}\,\lambda R$	$-\sqrt{\frac{3}{2}}\,T + \sqrt{\frac{1}{3}}\,\lambda R$	$+\sqrt{6}\,T^- - \frac{4}{\sqrt{3}}\,\lambda R^-$
	f_{+1}	$+\sqrt{\frac{3}{2}}\,T - \sqrt{3}\,\lambda R$	$-\sqrt{\frac{3}{2}}\,T + \sqrt{\frac{1}{3}}\,\lambda R$	$+\sqrt{6}\,T^+ - \frac{4}{\sqrt{3}}\,\lambda R^+$
	f_{+3}	$+\sqrt{\frac{9}{2}}\,T$	$-\sqrt{\frac{9}{2}}\,T$	$+2\sqrt{\frac{9}{2}}\,T^+$
	f_{0+}	$-\sqrt{3}\,\lambda S$	$+\sqrt{3}\,\lambda S$	$-2\sqrt{3}\,\lambda S - \frac{4}{\sqrt{3}}\,\lambda C$
	f_{0-}	$-\sqrt{3}\,\lambda S$	$+\sqrt{3}\,\lambda S$	$-2\sqrt{3}\,\lambda S + \frac{4}{\sqrt{3}}\,\lambda C$

y Electromagnetic, Weak Charged and Neutral Currents in the FKR-Model

Weak NC (Salam–Weinberg, $x = \sin^2 \theta_w$)	
P	N
$-\sqrt{6}\,(R^- + 2xR)$	
$\sqrt{2}\,(R^- + 2xR)$	
$-\sqrt{2}\,(R^+ + 2xR)$	
$\sqrt{6}\,(R^+ + 2xR)$	$N = P$
$2\sqrt{2}\,C$	
$-2\sqrt{2}\,C$	
$-\sqrt{3}\,(T^- + 2xT) + \sqrt{\frac{2}{3}}\lambda\left(R^- + 2x\cdot\frac{3}{2}R\right)$	$-\sqrt{3}\,(T^- + 2xT) - \sqrt{\frac{2}{3}}\lambda\left(R^- + 2x\cdot\frac{1}{2}R\right)$
$\sqrt{3}\,(T^+ + 2xT) - \sqrt{\frac{2}{3}}\lambda\left(R^+ + 2x\cdot\frac{3}{2}R\right)$	$+\sqrt{3}\,(T^+ + 2xT) + \sqrt{\frac{2}{3}}\lambda\left(R^+ + 2x\cdot\frac{1}{2}R\right)$
$-\sqrt{\frac{3}{2}}\lambda S(1-2x) + \sqrt{\frac{2}{3}}(\lambda C - 3B)$	$-\sqrt{\frac{3}{2}}\lambda S(1-2x) - \sqrt{\frac{2}{3}}(\lambda C - 3B)$
$-\sqrt{\frac{3}{2}}\lambda S(1-2x) + \sqrt{\frac{2}{3}}(\lambda C - 3B)$	$+\sqrt{\frac{3}{2}}\lambda S(1-2x) - \sqrt{\frac{2}{3}}(\lambda C - 3B)$
$-\sqrt{\frac{9}{2}}(T^- + 2xT)$	$-\sqrt{\frac{9}{2}}(T^- + 2xT)$
$-\sqrt{\frac{3}{2}}(T^- + 2xT) - \sqrt{\frac{4}{3}}\lambda\left(R^- + 2x\cdot\frac{3}{2}R\right)$	$-\sqrt{\frac{3}{2}}(T^- + 2xT) + \sqrt{\frac{4}{3}}\lambda\left(R^- + 2x\cdot\frac{1}{2}R\right)$
$\sqrt{\frac{3}{2}}(T^+ + 2xT) - \sqrt{\frac{4}{3}}\lambda\left(R^+ + 2x\cdot\frac{3}{2}R\right)$	$-\sqrt{\frac{3}{2}}(T^+ + 2xT) + \sqrt{\frac{4}{3}}\lambda\left(R^+ + 2x\cdot\frac{1}{2}R\right)$
$\sqrt{\frac{9}{2}}(T^+ + 2xT)$	$-\sqrt{\frac{9}{2}}(T^+ + 2xT)$
$\sqrt{3}\,\lambda S(1-2x) - \frac{2}{\sqrt{3}}\lambda C$	$+\sqrt{3}\,\lambda S(1-2x) + \frac{2}{\sqrt{3}}\lambda C$
$\sqrt{3}\,\lambda S(1-2x) + \frac{2}{\sqrt{3}}\lambda C$	$+\sqrt{3}\,\lambda S(1-2x) - \frac{2}{\sqrt{3}}\lambda C$

Table continued

TABLE

Resonance (Multiplet)	Helicity ampl.	Electromagnetic P	Electromagnetic N	Weak CC N
$S_{11}(1640)$	f_{-1}	0	$-\sqrt{\frac{1}{6}}\lambda R$	$+\sqrt{\frac{1}{6}}\lambda R^-$
$^4(8)_{1/2}[70, 1^-]_1$	f_{+1}	0	$+\sqrt{\frac{1}{6}}\lambda R$	$-\sqrt{\frac{1}{6}}\lambda R^+$
	f_{0+}	0	0	$-\sqrt{\frac{2}{3}}(\lambda C - 3B)$
	f_{0-}	0	0	$-\sqrt{\frac{2}{3}}(\lambda C - 3B)$
$D_{13}(1670)$	f_{-3}	0	$-\sqrt{\frac{9}{10}}\lambda R$	$+\sqrt{\frac{9}{10}}\lambda R^-$
$^4(8)_{3/2}[70, 1^-]_1$	f_{-1}	0	$-\sqrt{\frac{1}{30}}\lambda R$	$+\sqrt{\frac{1}{30}}\lambda R^-$
	f_{+1}	0	$-\sqrt{\frac{1}{30}}\lambda R$	$+\sqrt{\frac{1}{30}}\lambda R^+$
	f_{+3}	0	$-\sqrt{\frac{9}{10}}\lambda R$	$+\sqrt{\frac{9}{10}}\lambda R^+$
	f_{0+}	0	0	$-\sqrt{\frac{2}{15}}\lambda C$
	f_{0-}	0	0	$+\sqrt{\frac{2}{15}}\lambda C$
$D_{15}(1680)$	f_{-3}	0	$+\sqrt{\frac{3}{5}}\lambda R$	$-\sqrt{\frac{3}{5}}\lambda R^-$
$^4(8)_{5/2}[70, 1^-]_1$	f_{-1}	0	$+\sqrt{\frac{3}{10}}\lambda R$	$-\sqrt{\frac{3}{10}}\lambda R^-$
	f_{+1}	0	$-\sqrt{\frac{3}{10}}\lambda R$	$+\sqrt{\frac{3}{10}}\lambda R^+$
	f_{+3}	0	$-\sqrt{\frac{3}{5}}\lambda R$	$+\sqrt{\frac{3}{5}}\lambda R^+$

-Continued

Weak NC (Salam–Weinberg, $x = \sin^2\theta_w$)	
P	N
$+\frac{1}{2}\sqrt{\frac{1}{6}}\lambda R^-$	$-\frac{1}{2}\sqrt{\frac{1}{6}}\lambda(R^- + 4xR)$
$-\frac{1}{2}\sqrt{\frac{1}{6}}\lambda R^+$	$+\frac{1}{2}\sqrt{\frac{1}{6}}\lambda(R^+ + 4xR)$
$-\sqrt{\frac{1}{5}}(\lambda C - 3B)$	$+\sqrt{\frac{1}{6}}(\lambda C - 3B)$
$-\sqrt{\frac{1}{6}}(\lambda C - 3B)$	$+\sqrt{\frac{1}{6}}(\lambda C - 3B)$
$+\frac{1}{2}\sqrt{\frac{9}{10}}\lambda R^-$	$-\frac{1}{2}\sqrt{\frac{9}{10}}\lambda(R^- + 4xR)$
$+\frac{1}{2}\sqrt{\frac{1}{30}}\lambda R^-$	$-\frac{1}{2}\sqrt{\frac{1}{30}}\lambda(R^- + 4xR)$
$+\frac{1}{2}\sqrt{\frac{1}{30}}\lambda R^+$	$-\frac{1}{2}\sqrt{\frac{1}{30}}\lambda(R^+ + 4xR)$
$+\frac{1}{2}\sqrt{\frac{9}{10}}\lambda R^+$	$-\frac{1}{2}\sqrt{\frac{9}{10}}\lambda(R^+ + 4xR)$
$-\frac{1}{2}\sqrt{\frac{2}{15}}\lambda C$	$+\frac{1}{2}\sqrt{\frac{2}{15}}\lambda C$
$+\frac{1}{2}\sqrt{\frac{2}{15}}\lambda C$	$-\frac{1}{2}\sqrt{\frac{2}{15}}\lambda C$
$\frac{1}{2}\sqrt{\frac{3}{5}}\lambda R^-$	$+\frac{1}{2}\sqrt{\frac{3}{5}}\lambda(R^- + 4xR)$
$-\frac{1}{2}\sqrt{\frac{3}{10}}\lambda R^-$	$+\frac{1}{2}\sqrt{\frac{3}{10}}\lambda(R^- + 4xR)$
$+\frac{1}{2}\sqrt{\frac{3}{10}}\lambda R^+$	$-\frac{1}{2}\sqrt{\frac{3}{10}}\lambda(R^+ + 4xR)$
$+\frac{1}{2}\sqrt{\frac{3}{5}}\lambda R^+$	$-\frac{1}{2}\sqrt{\frac{3}{5}}\lambda(R^+ + 4xR)$

Table continued

TABLE

Resonance (Multiplet)	Helicity ampl.	Electromagnetic P	Electromagnetic N	Weak CC N
	f_{0+}	0	0	$+\sqrt{\frac{6}{5}}\lambda C$
	f_{0-}	0	0	$+\sqrt{\frac{6}{5}}\lambda C$
$S_{31}(1620)$	f_{-1}	$+\sqrt{3}\,T-\sqrt{\frac{1}{6}}\lambda R$		$-\sqrt{3}\,T^{-}+\sqrt{\frac{1}{6}}\lambda R^{-}$
$^2(10)_{1/2}[70,1^-]_1$	f_{+1}	$-\sqrt{3}\,T+\sqrt{\frac{1}{6}}\lambda R$	$N=P$	$+\sqrt{3}\,T^{+}-\sqrt{\frac{1}{6}}\lambda R^{+}$
	f_{0+}	$+\sqrt{\frac{3}{2}}\lambda S$		$-\sqrt{\frac{3}{2}}\lambda S+\sqrt{\frac{1}{6}}(\lambda C-3\beta)$
	f_{0-}	$-\sqrt{\frac{3}{2}}\lambda S$		$+\sqrt{\frac{3}{2}}\lambda S+\sqrt{\frac{1}{6}}(\lambda C-3\beta)$
$D_{33}(1730)$	f_{-3}	$+\sqrt{\frac{9}{2}}\,T$		$-\sqrt{\frac{9}{2}}\,T^{-}$
$^2(10)_{3/2}[70,1^-]_1$	f_{-1}	$+\sqrt{\frac{3}{2}}\,T+\sqrt{\frac{1}{3}}\lambda R$		$-\sqrt{\frac{3}{2}}\,T^{-}-\sqrt{\frac{1}{3}}\lambda R^{-}$
	f_{+1}	$+\sqrt{\frac{3}{2}}\,T+\sqrt{\frac{1}{3}}\lambda R$	$N=P$	$-\sqrt{\frac{3}{2}}\,T^{+}-\sqrt{\frac{1}{3}}\lambda R^{+}$
	f_{+3}	$+\sqrt{\frac{9}{2}}\,T$		$-\sqrt{\frac{9}{2}}\,T^{+}$
	f_{0+}	$-\sqrt{3}\,\lambda S$		$+\sqrt{3}\,\lambda S-\sqrt{\frac{1}{3}}\lambda C$
	f_{0-}	$-\sqrt{3}\,\lambda S$		$+\sqrt{3}\,\lambda S+\sqrt{\frac{1}{3}}\lambda C$
$P_{11}(1450)$	f_{-1}	$-\sqrt{\frac{3}{4}}\lambda^2 R$	$+\sqrt{\frac{1}{3}}\lambda^2 R$	$-\frac{5}{6}\sqrt{3}\,\lambda^2 R^{-}$
$^2(8)_{1/2}[56,0^+]_2$	f_{+1}	$-\sqrt{\frac{3}{4}}\lambda^2 R$	$+\sqrt{\frac{1}{3}}\lambda^2 R$	$-\frac{5}{6}\sqrt{3}\,\lambda^2 R^{+}$

Continued

Weak NC (Salam–Weinberg, $x = \sin^2 \theta_w$)	
P	N
$\sqrt{\frac{3}{10}}\lambda C$	$-\sqrt{\frac{3}{10}}\lambda C$
$\sqrt{\frac{3}{10}}\lambda C$	$-\sqrt{\frac{3}{10}}\lambda C$
$\sqrt{3}\,(T^- + 2xT) - \sqrt{\frac{1}{6}}\lambda(R^- + 2xR)$	
$\sqrt{3}\,(T^+ + 2xT) + \sqrt{\frac{1}{6}}\lambda(R^+ + 2xR)$	$N = P$
$\sqrt{\frac{3}{2}}\lambda S(1 - 2x) - \sqrt{\frac{1}{6}}(\lambda C - 3B)$	
$\sqrt{\frac{3}{2}}\lambda S(1 - 2x) - \sqrt{\frac{1}{6}}(\lambda C - 3B)$	
$\sqrt{\frac{9}{2}}\,(T^- + 2xT)$	
$\sqrt{\frac{3}{2}}\,(T^- + 2xT) + \sqrt{\frac{1}{3}}\lambda(R^- + 2xR)$	
$\sqrt{\frac{3}{2}}\,(T^+ + 2xT) + \sqrt{\frac{1}{3}}\lambda(R^+ + 2xR)$	$N = P$
$\sqrt{\frac{9}{2}}\,(T^+ + 2xT)$	
$\sqrt{3}\,\lambda S(1 - 2x) + \sqrt{\frac{1}{3}}\lambda C$	
$\sqrt{3}\,\lambda S(1 - 2x) - \sqrt{\frac{1}{3}}\lambda C$	
$\frac{5}{12}\sqrt{3}\,\lambda^2\left(R^- + 2x \cdot \frac{6}{5}R\right)$	$+\frac{5}{12}\sqrt{3}\,\lambda^2\left(R^- + 2x \cdot \frac{4}{5}R\right)$
$\frac{5}{12}\sqrt{3}\,\lambda^2\left(R^+ + 2x \cdot \frac{6}{5}R\right)$	$+\frac{5}{12}\sqrt{3}\,\lambda^2\left(R^+ + 2x \cdot \frac{4}{5}R\right)$

Table continued

TABLE

Resonance (Multiplet)	Helicity ampl.	Electromagnetic P	Electromagnetic N	Weak CC N
	f_{0+}	$-\sqrt{\frac{3}{4}}\lambda^2 S$	0	$-\sqrt{\frac{3}{4}}\lambda^2 S - \frac{5}{6}\sqrt{3}\lambda(\lambda C - 2$
	f_{0-}	$-\sqrt{\frac{3}{4}}\lambda^2 S$	0	$-\sqrt{\frac{3}{4}}\lambda^2 S + \frac{5}{6}\sqrt{3}\lambda(\lambda C - 2$
$P_{33}(1640)$	f_{-3}	$+\frac{1}{\sqrt{2}}\lambda^2 R$		$-\frac{1}{\sqrt{2}}\lambda^2 R^-$
$^4(10)_{3/2}[56, 0^+]_2$	f_{-1}	$+\frac{1}{\sqrt{6}}\lambda^2 R$		$-\frac{1}{\sqrt{6}}\lambda^2 R^-$
	f_{+1}	$-\frac{1}{\sqrt{6}}\lambda^2 R$	$N = P$	$+\frac{1}{\sqrt{6}}\lambda^2 R^+$
	f_{+3}	$-\frac{1}{\sqrt{2}}\lambda^2 R$		$+\frac{1}{\sqrt{2}}\lambda^2 R^+$
	f_{0+}	0		$+\sqrt{\frac{2}{3}}\lambda(\lambda C - 2B)$
	f_{0-}	0		$+\sqrt{\frac{2}{3}}\lambda(\lambda C - 2B)$
$P_{13}(1740)$	f_{-3}	$+\sqrt{\frac{9}{10}}\lambda T$	0	$+\sqrt{\frac{9}{10}}\lambda T^-$
$^2(8)_{3/2}[56, 2^+]_2$	f_{-1}	$-\sqrt{\frac{27}{10}}\lambda T - \sqrt{\frac{3}{5}}\lambda^2 R$	$+\sqrt{\frac{4}{15}}\lambda^2 R$	$-\sqrt{\frac{27}{10}}\lambda T^- - \sqrt{\frac{5}{3}}\lambda^2 R^-$
	f_{+1}	$+\sqrt{\frac{27}{10}}\lambda T + \sqrt{\frac{3}{5}}\lambda^2 R$	$-\sqrt{\frac{4}{15}}\lambda^2 R$	$+\sqrt{\frac{27}{10}}\lambda T^+ + \sqrt{\frac{5}{3}}\lambda^2 R^+$
	f_{+3}	$-\sqrt{\frac{9}{10}}\lambda T$	0	$-\sqrt{\frac{9}{10}}\lambda T^+$

Continued

Weak NC (Salam–Weinberg, $x = \sin^2\theta_w$)	
P	N
$\frac{1}{2}\sqrt{\frac{3}{4}}\lambda^2 S(1-4x) - \frac{5}{12}\sqrt{3}\,\lambda(\lambda C - 2B)$	$+\frac{1}{2}\sqrt{\frac{3}{4}}\lambda^2 S + \frac{5}{12}\sqrt{3}\,\lambda(\lambda C - 2B)$
$\frac{1}{2}\sqrt{\frac{3}{4}}\lambda^2 S(1-4x) + \frac{5}{12}\sqrt{3}\,\lambda(\lambda C - 2B)$	$+\frac{1}{2}\sqrt{\frac{3}{4}}\lambda^2 S - \frac{5}{12}\sqrt{3}\,\lambda(\lambda C - 2B)$
$\frac{1}{\sqrt{2}}\lambda^2(R^- + 2xR)$	
$\frac{1}{\sqrt{6}}\lambda^2(R^- + 2xR)$	
$\frac{1}{\sqrt{6}}\lambda^2(R^+ + 2xR)$	
$\frac{1}{\sqrt{2}}\lambda^2(R^+ + 2xR)$	$N = P$
$\sqrt{\frac{2}{3}}\lambda(\lambda C - 2B)$	
$\sqrt{\frac{2}{3}}\lambda(\lambda C - 2B)$	
$\frac{1}{2}\sqrt{\frac{9}{10}}\lambda(T^- + 4xT)$	$-\frac{1}{2}\sqrt{\frac{9}{10}}\lambda T^-$
$\frac{1}{2}\sqrt{\frac{27}{10}}\lambda(T^- + 4xT)$	$+\frac{1}{2}\sqrt{\frac{27}{10}}\lambda T^-$
$-\frac{1}{2}\sqrt{\frac{5}{3}}\lambda^2\left(R^- + 2x\cdot\frac{6}{5}R\right)$	$+\frac{1}{2}\sqrt{\frac{5}{3}}\lambda^2\left(R^- + 2x\cdot\frac{4}{5}R\right)$
$\frac{1}{2}\sqrt{\frac{27}{10}}\lambda(T^+ + 4xT)$	$-\frac{1}{2}\sqrt{\frac{27}{10}}\lambda T^+$
$+\frac{1}{2}\sqrt{\frac{5}{3}}\lambda^2\left(R^+ + 2x\cdot\frac{6}{5}R\right)$	$-\frac{1}{2}\sqrt{\frac{5}{3}}\lambda^2\left(R^+ + 2x\cdot\frac{4}{5}R\right)$
$\frac{1}{2}\sqrt{\frac{9}{10}}\lambda(T^+ + 4xT)$	$+\frac{1}{2}\sqrt{\frac{9}{10}}\lambda T^+$

Table continued

TABLE

Resonance (Multiplet)	Helicity ampl.	Electromagnetic P	Electromagnetic N	Weak CC N
	f_{0+}	$-\sqrt{\frac{3}{5}}\lambda^2 S$	0	$-\sqrt{\frac{3}{5}}\lambda^2 S - \sqrt{\frac{5}{3}}\lambda(\lambda C + 5B$
	f_{0-}	$+\sqrt{\frac{3}{5}}\lambda^2 S$	0	$+\sqrt{\frac{3}{5}}\lambda^2 S - \sqrt{\frac{5}{3}}\lambda(\lambda C - 5B$
$F_{15}(1680)$	f_{-3}	$-\sqrt{\frac{18}{5}}\lambda T$	0	$-\sqrt{\frac{18}{5}}\lambda T^-$
$^2(8)_{5/2}[56, 2^+]_2$	f_{-1}	$-\sqrt{\frac{9}{5}}\lambda T + \sqrt{\frac{9}{10}}\lambda^2 R$	$-\sqrt{\frac{2}{5}}\lambda^2 R$	$-\sqrt{\frac{9}{5}}\lambda T^- + \sqrt{\frac{5}{2}}\lambda^2 R^-$
	f_{+1}	$-\sqrt{\frac{9}{5}}\lambda T + \sqrt{\frac{9}{10}}\lambda^2 R$	$-\sqrt{\frac{2}{5}}\lambda^2 R$	$-\sqrt{\frac{9}{5}}\lambda T^+ + \sqrt{\frac{5}{2}}\lambda^2 R^+$
	f_{+3}	$-\sqrt{\frac{18}{5}}\lambda T$	0	$-\sqrt{\frac{18}{5}}\lambda T^+$
	f_{0+}	$+\sqrt{\frac{9}{10}}\lambda^2 S$	0	$+\sqrt{\frac{9}{10}}\lambda^2 S + \sqrt{\frac{5}{2}}\lambda^2 C$
	f_{0-}	$+\sqrt{\frac{9}{10}}\lambda^2 S$	0	$+\sqrt{\frac{9}{10}}\lambda^2 S - \sqrt{\frac{5}{2}}\lambda^2 C$
$P_{31}(1920)$	f_{-1}	$-\sqrt{\frac{1}{15}}\lambda^2 R$		$+\sqrt{\frac{1}{15}}\lambda^2 R^-$

Continued

Weak NC (Salam–Weinberg, $x = \sin^2\theta_w$)	
P	N
$\frac{1}{2}\sqrt{\frac{3}{5}}\lambda^2 S(1-4x) - \frac{1}{2}\sqrt{\frac{5}{3}}\lambda(\lambda C - 5B)$	$+\frac{1}{2}\sqrt{\frac{3}{5}}\lambda^2 S + \frac{1}{2}\sqrt{\frac{5}{3}}\lambda(\lambda C - 5B)$
$\frac{1}{2}\sqrt{\frac{3}{5}}\lambda^2 S(1-4x) - \frac{1}{2}\sqrt{\frac{5}{3}}\lambda(\lambda C - 5B)$	$-\frac{1}{2}\sqrt{\frac{3}{5}}\lambda^2 S + \frac{1}{2}\sqrt{\frac{5}{3}}\lambda(\lambda C - 5B)$
$\frac{1}{2}\sqrt{\frac{18}{5}}\lambda(T^- + 4xT)$	$+\frac{1}{2}\sqrt{\frac{18}{5}}\lambda T^-$
$\frac{1}{2}\sqrt{\frac{9}{5}}\lambda(T^- + 4xT)$	$+\frac{1}{2}\sqrt{\frac{9}{5}}\lambda T^- - \frac{1}{2}\sqrt{\frac{5}{2}}\lambda^2\left(R^- + 2x\cdot\frac{4}{5}R\right)$
$+\frac{1}{2}\sqrt{\frac{5}{2}}\lambda^2\left(R^- + 2x\cdot\frac{6}{5}R\right)$	
$\frac{1}{2}\sqrt{\frac{9}{5}}\lambda(T^+ + 4xT)$	$+\frac{1}{2}\sqrt{\frac{9}{5}}\lambda T^+ - \frac{1}{2}\sqrt{\frac{5}{2}}\lambda^2\left(R^+ + 2x\cdot\frac{4}{5}R\right)$
$+\frac{1}{2}\sqrt{\frac{5}{2}}\lambda^2\left(R^+ + 2x\cdot\frac{6}{5}R\right)$	
$\frac{1}{2}\sqrt{\frac{18}{5}}\lambda(T^+ + 4xT)$	$+\frac{1}{2}\sqrt{\frac{18}{5}}\lambda T^+$
$\frac{1}{2}\sqrt{\frac{9}{10}}\lambda^2 S(1-4x) + \frac{1}{2}\sqrt{\frac{5}{2}}\lambda^2 C$	$-\frac{1}{2}\sqrt{\frac{9}{10}}\lambda^2 S - \frac{1}{2}\sqrt{\frac{5}{2}}\lambda^2 C$
$\frac{1}{2}\sqrt{\frac{9}{10}}\lambda^2 S(1-4x) - \frac{1}{2}\sqrt{\frac{5}{2}}\lambda^2 C$	$-\frac{1}{2}\sqrt{\frac{9}{10}}\lambda^2 S + \frac{1}{2}\sqrt{\frac{5}{2}}\lambda^2 C$
$\sqrt{\frac{1}{15}}\lambda^2(R^- + 2xR)$	

Table continued

TABLE

Resonance (Multiple)	Helicity ampl.	Electromagnetic P	Electromagnetic N	Weak CC N
$^4(10)_{1/2}[56, 2^+]_2$	f_{+1}	$-\sqrt{\frac{1}{15}}\lambda^2 R$	$N = P$	$+\sqrt{\frac{1}{15}}\lambda^2 R^+$
	f_{0+}	0		$-\sqrt{\frac{4}{15}}\lambda(\lambda C - 5B)$
	f_{0-}	0		$+\sqrt{\frac{4}{15}}\lambda(\lambda C - 5B)$
$P_{33}(1960)$	f_{-3}	$-\sqrt{\frac{1}{5}}\lambda^2 R$	$N = P$	$+\sqrt{\frac{1}{5}}\lambda^2 R^-$
$^4(10)_{3/2}[56, 2^+]_2$	f_{-1}	$+\sqrt{\frac{1}{15}}\lambda^2 R$		$-\sqrt{\frac{1}{15}}\lambda^2 R^-$
	f_{+1}	$-\sqrt{\frac{1}{15}}\lambda^2 R$		$+\sqrt{\frac{1}{15}}\lambda^2 R^+$
	f_{+3}	$+\sqrt{\frac{1}{5}}\lambda^2 R$		$-\sqrt{\frac{1}{5}}\lambda^2 R^+$
	f_{0+}	0		$+\sqrt{\frac{4}{15}}\lambda(\lambda C - 5B)$
	f_{0-}	0		$+\sqrt{\frac{4}{15}}\lambda(\lambda C - 5B)$
$F_{35}(1920)$	f_{-3}	$+\sqrt{\frac{18}{35}}\lambda^2 R$	$N = P$	$-\sqrt{\frac{18}{35}}\lambda^2 R^-$
$^4(10)_{5/2}[56, 2^+]_2$	f_{-1}	$+\sqrt{\frac{1}{35}}\lambda^2 R$		$-\sqrt{\frac{1}{35}}\lambda^2 R^-$
	f_{+1}	$+\sqrt{\frac{1}{35}}\lambda^2 R$		$-\sqrt{\frac{1}{35}}\lambda^2 R^+$
	f_{+3}	$+\sqrt{\frac{18}{35}}\lambda^2 R$		$-\sqrt{\frac{18}{35}}\lambda^2 R^+$
	f_{0+}	0		$+\sqrt{\frac{4}{35}}\lambda^2 C$

Continued

Weak NC (Salam–Weinberg, $x = \sin^2 \theta_w$)

P	N
$\sqrt{\frac{1}{15}}\,\lambda^2(R^+ + 2xR)$	$N = P$
$\sqrt{\frac{4}{15}}\,\lambda(\lambda C - 5B)$	
$\sqrt{\frac{4}{15}}\,\lambda(\lambda C - 5B)$	
$\sqrt{\frac{1}{5}}\,\lambda^2(R^- + 2xR)$	$N = P$
$\sqrt{\frac{1}{15}}\,\lambda^2(R^- + 2xR)$	
$\sqrt{\frac{1}{15}}\,\lambda^2(R^+ + 2xR)$	
$\sqrt{\frac{1}{5}}\,\lambda^2(R^+ + 2xR)$	
$\sqrt{\frac{4}{15}}\,\lambda(\lambda C - 5B)$	
$\sqrt{\frac{4}{15}}\,\lambda(\lambda C - 5B)$	
$\sqrt{\frac{18}{35}}\,\lambda^2(R^- + 2xR)$	$N = P$
$\sqrt{\frac{1}{35}}\,\lambda^2(R^- + 2xR)$	
$\sqrt{\frac{1}{35}}\,\lambda^2(R^+ + 2xR)$	
$\sqrt{\frac{18}{35}}\,\lambda^2(R^+ + 2xR)$	
$\sqrt{\frac{4}{35}}\,\lambda^2 C$	

Table continued

TABLE

Resonance (Multiple)	Helicity ampl.	Electromagnetic P	Electromagnetic N	Weak CC N
	f_{0-}	0		$-\sqrt{\frac{4}{35}}\lambda^2 C$
$F_{37}(1950)$	f_{-3}	$-\sqrt{\frac{2}{7}}\lambda^2 R$		$+\sqrt{\frac{2}{7}}\lambda^2 R^-$
$^4(10)_{3/2}[56, 2^+]_2$	f_{-1}	$-\sqrt{\frac{6}{35}}\lambda^2 R$		$+\sqrt{\frac{6}{35}}\lambda^2 R^-$
	f_{+1}	$+\sqrt{\frac{6}{35}}\lambda^2 R$	$N = P$	$-\sqrt{\frac{6}{35}}\lambda^2 R^+$
	f_{+3}	$+\sqrt{\frac{2}{7}}\lambda^2 R$		$-\sqrt{\frac{2}{7}}\lambda^2 R^+$
	f_{0+}	0		$-2\sqrt{\frac{6}{35}}\lambda^2 C$
	f_{0-}	0		$-2\sqrt{\frac{6}{35}}\lambda^2 C$
$P_{11}(1710)$	f_{-1}	$+\sqrt{\frac{3}{8}}\lambda^2 R$	$-\sqrt{\frac{1}{24}}\lambda^2 R$	$+\sqrt{\frac{2}{3}}\lambda^2 R^-$
$^2(8)_{1/2}[70, 0^+]_2$	f_{+1}	$+\sqrt{\frac{3}{8}}\lambda^2 R$	$-\sqrt{\frac{1}{24}}\lambda^2 R$	$+\sqrt{\frac{2}{3}}\lambda^2 R^+$
	f_{0+}	$+\sqrt{\frac{3}{8}}\lambda^2 S$	$-\sqrt{\frac{3}{8}}\lambda^2 S$	$+\sqrt{\frac{3}{2}}\lambda^2 S + \sqrt{\frac{2}{3}}\lambda(\lambda C$
	f_{0-}	$+\sqrt{\frac{3}{8}}\lambda^2 S$	$-\sqrt{\frac{3}{8}}\lambda^2 S$	$+\sqrt{\frac{3}{2}}\lambda^2 S - \sqrt{\frac{2}{3}}\lambda(\lambda C -$
$F_{17}(1970)$	f_{-3}	0	$+\sqrt{\frac{1}{7}}\lambda^2 R$	$-\sqrt{\frac{1}{7}}\lambda^2 R^-$
$^4(8)_{7/2}[70, 2^+]_2$	f_{-1}	0	$+\sqrt{\frac{3}{35}}\lambda^2 R$	$-\sqrt{\frac{3}{35}}\lambda^2 R^-$
	f_{+1}	0	$-\sqrt{\frac{3}{35}}\lambda^2 R$	$+\sqrt{\frac{3}{35}}\lambda^2 R^+$

Continued

Weak NC (Salam–Weinberg, $x = \sin^2 \theta_w$)	
P	N
$-\sqrt{\frac{4}{35}}\lambda^2 C$	
$-\sqrt{\frac{2}{7}}\lambda^2(R^- + 2xR)$	
$\sqrt{\frac{6}{35}}\lambda^2(R^- + 2xR)$	
$-\sqrt{\frac{6}{35}}\lambda^2(R^+ + 2xR)$	$N = P$
$\sqrt{\frac{2}{7}}\lambda^2(R^+ + 2xR)$	
$2\sqrt{\frac{6}{35}}\lambda^2 C$	
$2\sqrt{\frac{6}{35}}\lambda^2 C$	
$\sqrt{\frac{1}{6}}\lambda^2\left(R^- + 2x \cdot \frac{3}{2}R\right)$	$-\sqrt{\frac{1}{6}}\lambda^2\left(R^- + 2x \cdot \frac{1}{2}R\right)$
$\sqrt{\frac{1}{6}}\lambda^2\left(R^+ + 2x \cdot \frac{3}{2}R\right)$	$-\sqrt{\frac{1}{6}}\lambda^2\left(R^+ + 2x \cdot \frac{1}{2}R\right)$
$\sqrt{\frac{3}{8}}\lambda^2 S(1-2x) + \sqrt{\frac{1}{6}}\lambda(\lambda C - 2B)$	$-\sqrt{\frac{3}{8}}\lambda^2 S(1-2x) - \sqrt{\frac{1}{6}}\lambda(\lambda C - 2B)$
$\sqrt{\frac{3}{8}}\lambda^2 S(1-2x) - \sqrt{\frac{1}{6}}\lambda(\lambda C - 2B)$	$-\sqrt{\frac{3}{8}}\lambda^2 S(1-2x) + \sqrt{\frac{1}{6}}\lambda(\lambda C - 2B)$
$\frac{1}{2}\sqrt{\frac{1}{7}}\lambda^2 R^-$	$+\frac{1}{2}\sqrt{\frac{1}{7}}\lambda^2(R^- + 4xR)$
$\frac{1}{2}\sqrt{\frac{3}{35}}\lambda^2 R^-$	$+\frac{1}{2}\sqrt{\frac{3}{35}}\lambda^2(R^- + 4xR)$
$\frac{1}{2}\sqrt{\frac{3}{35}}\lambda^2 R^+$	$-\frac{1}{2}\sqrt{\frac{3}{35}}\lambda^2(R^+ + 4xR)$

table continued

TABLE I

Resonane (Multiple)	Helicity ampl.	Electromagnetic		Weak CC
		P	N	N
	f_{+3}	0	$-\sqrt{\frac{1}{7}}\lambda^2 R$	$+\sqrt{\frac{1}{7}}\lambda^2 R^+$
	f_{0+}	0	0	$+\sqrt{\frac{6}{35}}\lambda^2 C$
	f_{0-}	0	0	$+\sqrt{\frac{6}{35}}\lambda^2 C$

where λ and $G^A(q^2)$ have the same meaning as in Eqs. (3.11), (3.12) but

$$Q = \frac{1}{2M}\{(M^2 - m_{\mathcal{N}}{}^2 - m_\pi{}^2)^2 - 4m_{\mathcal{N}}{}^2 m_\pi{}^2\}^{1/2}$$

and

$$\gamma = MQ\left(1 + \frac{3m_\pi{}^2}{(M + m_{\mathcal{N}})^2 - m_\pi{}^2}\right) > 0,$$

$$\beta = \sqrt{\frac{\Omega}{2}}(M - m_{\mathcal{N}}) > 0, \tag{3.21}$$

$$\gamma\delta = MQ\frac{\Omega}{(M + m_{\mathcal{N}})^2 - m_\pi{}^2} > 0.$$

Sandwiching $\mathfrak{N}^P/G^A(q^2)$ between resonance state and nucleon state results in Table III.

We have included this table since we differ in sign in some entries with the corresponding Table II of FKR (Ref. [1]). Likewise we should mention that our table of production matrix elements (Table II) does not coincide in sign with Table I of FKR at every point of overlap. The photoproduction amplitudes $A_{3/2}^{p,n}$, $A_{1/2}^{p,n}$, however, as given by FKR and extended to higher resonances by Moorhouse *et al.* (Ref. [2]) were reproduced by us without exceptions. This gives us confidence that our production matrix elements (Table II) and decay signs (Table III) are indeed correct. As an independent check we compared our production amplitudes with those calculated by Ravndal for electroproduction [24] and charged current neutrino production [3] of resonances up to $M = 1.7$ GeV/c^2 finding complete agreement in the electroproduction case and almost complete agreement (except for a sign difference at $S_{11}(1640)$ and $D_{15}(1680)$) in the neutrino production case.

Ultimately, for the decay part of the single pion production process it is just the sign of the resonance decay amplitude which must be calculated in the quark model since the size of the decay matrix element is more accurately accounted for by the

Continued

Weak (NC (Salam–Weinberg, $x = \sin^2\theta_w$)	
P	N
$+\frac{1}{2}\sqrt{\frac{1}{7}}\lambda^2 R^+$	$-\frac{1}{2}\sqrt{\frac{1}{7}}\lambda^2(R^+ + 4xR)$
$+\frac{1}{2}\sqrt{\frac{6}{35}}\lambda^2 C$	$-\frac{1}{2}\sqrt{\frac{6}{35}}\lambda^2 C$
$+\frac{1}{2}\sqrt{\frac{6}{35}}\lambda^2 C$	$-\frac{1}{2}\sqrt{\frac{6}{35}}\lambda^2 C$

usual complex Breit–Wigner factor $\eta^{(\nu)}(W)$ (see Eq. (2.33)) containing the experimental mass, width and elasticity x_E of the resonance. An overall sign is fixed requiring the $P_{33}(1236)$ to have a positive isospin Clebsch–Gordan coefficient for its decay into $p\pi^0$ channels. So we may directly use the last column of Table III to obtain sgn (A^*) entering the single pion production amplitudes $a_k^{\mathrm{CC,NC}}$ of Eq. (2.30).

4. Results

4.1. *Excitation of Single Resonances*

(a) *General Features*

Having now all production matrix elements at hand (Table II) the computation of cross sections for the excitation of single isolated resonances proceeds along the lines of Section 2.1. First we may obtain the helicity cross sections $\sigma_{\mathrm{L,R}}(q^2)$ and $\sigma_S(q^2)$ for every resonance separately by integrating out the W-dependence mainly located in the Breit–Wigner factor $\eta(W)$. These helicity cross sections $\sigma_{\mathrm{L,R,}S}(q^2)$ do not depend on the incident neutrino energy. Once they are known the ordinary differential cross sections for resonance production are available at any neutrino (antineutrino) energy by essentially attaching the appropriate energy dependent kinematical factors. It appears as a general feature of neutrino production of resonances that σ_{L} is substantially larger than σ_{R} and σ_S. This was known [3] for charged current reactions and resonances below 1.7 GeV/c^2. Now it turns out to be true also for higher resonances up to 2 GeV/c^2 and for neutral current reactions. This means that quite generally neutrino cross sections for resonance excitation lie above the corresponding antineutrino cross sections. There is, however, one exception [3]: the $S_{31}(1620)$ is predicted to have $\sigma_{\mathrm{L}} < \sigma_{\mathrm{R}}$, σ_S leading to almost equal production cross sections for neutrinos and antineutrinos. The q^2-dependence of individual resonances is hardly measurable,

TABLE III

Resonance Decay Amplitudes for $\mathcal{N}^{*+} \to p\pi^0$ in the FKR-Model

Resonance	$\langle P, \frac{1}{2} \mid \mathfrak{N}^P \mid N^{*+}, \frac{1}{2}\rangle / G^A(q^2)$	Numerical value of $\langle \mid \mid \rangle / G^A$	Decay sign
$P_{33}(1236)$	$+\frac{8}{3}\sqrt{2}\,\gamma$	+0.28	+
$D_{13}(1525)$	$-\frac{8}{9}\sqrt{3}\,[\gamma\lambda(1+\delta)]$	−0.82	−
$S_{11}(1540)$	$+\frac{4}{9}\sqrt{6}\,[\gamma\lambda(1+\delta)-3\beta]$	−0.83	−
$D_{15}(1680)$	$+\frac{2}{15}\sqrt{30}\,[\gamma\lambda(1+\delta)]$	+0.61	+
$S_{31}(1620)$	$-\frac{2}{9}\sqrt{6}\,[\gamma\lambda(1+\delta)-3\beta]$	+0.41	+
$D_{33}(1730)$	$+\frac{4}{9}\sqrt{3}\,\gamma\lambda(1+\delta)$	+0.64	+
$S_{11}(1640)$	$-\frac{2}{9}\sqrt{6}\,[\gamma\lambda(1+\delta)-3\beta]$	+0.41	+
$D_{13}(1670)$	$-\frac{2}{45}\sqrt{30}\,\gamma\lambda(1+\delta)$	−0.20	−
$P_{11}(1450)$	$-\frac{5}{9}\sqrt{3}\,\lambda[\gamma\lambda(1+2\delta)-2\beta]$	+0.16	+
$P_{33}(1640)$	$-\frac{4}{9}\sqrt{6}\lambda[\gamma\lambda(1+2\delta)-2\beta]$	+0.12	+
$F_{15}(1680)$	$+\frac{1}{3}\sqrt{10}\lambda[\gamma\lambda(1+2\delta)]$	+0.82	+
$P_{13}(1740)$	$-\frac{2}{9}\sqrt{15}\lambda[\gamma\lambda(1+2\delta)-5\beta]$	+1.28	+
$P_{31}(1920)$	$+\frac{8}{45}\sqrt{15}\lambda[\gamma\lambda(1+2\delta)-5\beta]$	−1.27	−
$P_{33}(1960)$	$-\frac{8}{45}\sqrt{15}\lambda[\gamma\lambda(1+2\delta)-5\beta]$	+1.29	+
$F_{35}(1920)$	$-\frac{8}{105}\sqrt{35}\lambda[\gamma\lambda(1+2\delta)]$	−0.78	−
$F_{37}(1950)$	$+\frac{8}{105}\sqrt{210}\lambda[\gamma\lambda(1+2\delta)]$	+2.10	+
$P_{11}(1710)$	$+\frac{2}{9}\sqrt{6}\lambda[\gamma\lambda(1+2\delta)-2\beta]$	+0.02	+
$F_{17}(1970)$	$+\frac{2}{105}\sqrt{210}\lambda[\gamma\lambda(1+2\delta)]$	+0.56	+

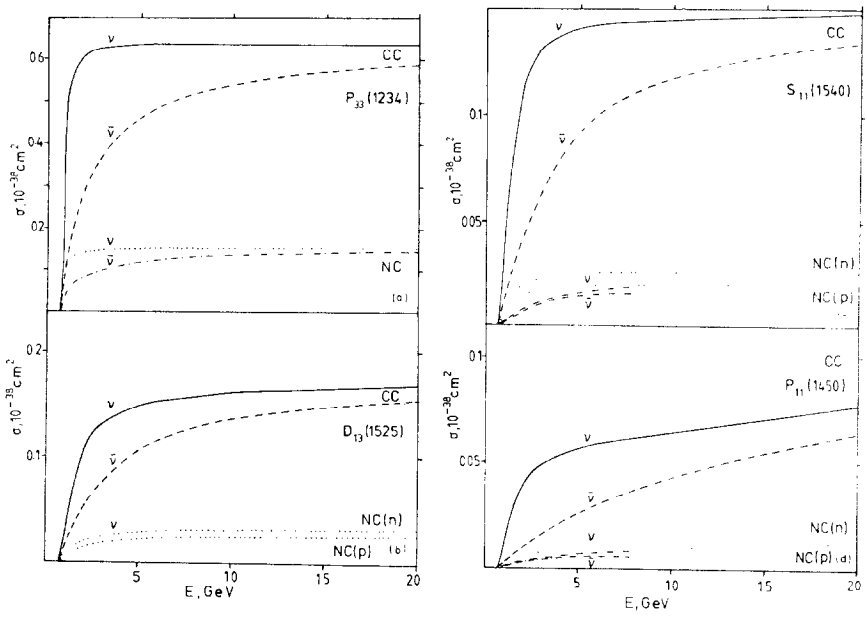

FIG. 1. Single resonance cross sections of (a) $P_{33}(1234)$, (b) $D_{13}(1525)$, (c) $S_{11}(1540)$, (d) $P_{11}(1450)$; for charged and neutral current reactions induced by neutrinos or antineutrinos.

except in the case of the $\Delta(1234)$ which will be discussed subsequently in some detail. Here we focus on the integrated cross sections as a function of the incident neutrino/antineutrino energy.

We have calculated $\sigma(E)$ for charged and neutral current resonance excitation at various energies using a realistic form of the Breit–Wigner decay probability with L-dependent decay width Γ. These cross sections are plotted in Figs. 1a–d for the lowest lying resonances $\Delta(1234)$, $P_{11}(1450)$, $D_{13}(1525)$ and $S_{11}(1540)$ which are also most prominently excited in neutrino reactions (at least at low and moderate energies). For all higher resonances we will give $\sigma(E)$ only at two typical values, 2 and 20 GeV, which are approximately the peak energies of the neutrino beams at CERN/Brookhaven and CERN–SPS/Fermilab, respectively. These values are listed in Table IV. Quite generally the resonance cross sections rise steeply with energy as can be read off Fig. 1, and subsequently saturate at higher energies. Both neutrino and antineutrino cross sections approach each other with increasing energy levelling off asymptotically at a common value. This is the same as in elastic neutrino nucleon scattering processes and can be interpreted as the consequence of the fast decrease of the resonance form factors. There are, however, differences in the energies where the cross sections start to flatten out. While the lower lying resonances belonging to the oscillator states with $n = 0$ and 1 level off between 10 and 20 GeV the resonances with $n = 2$ still have rising cross sections, thus becoming relatively more important at higher energies (Fig. 1). This is clearly a dynamical consequence of the model and could in principle first be tested in the region of the Roper resonance $P_{11}(1450)$.

For neutrino energies $E_\nu \lesssim 2$ GeV, the invariant mass region $W < 2$ GeV is the only one accessible. It is thus of interest to see if the inclusive ν and $\bar{\nu}$ cross sections at such energies can be reproduced by the above model. The total resonant cross section on an "average" nucleon at an energy 2 GeV is found to be

$$\sigma_{\text{res}} = 0.71 \cdot 10^{-38}\ \text{cm}^2, \qquad \bar{\sigma}_{\text{res}} = 0.30 \cdot 10^{-38}\ \text{cm}^2$$

for ν and $\bar{\nu}$, respectively. At the same energy the elastic channel contributes [25, 26]

$$\sigma_{\text{elast}} = 0.40 \cdot 10^{-38}\ \text{cm}^2, \qquad \bar{\sigma}_{\text{elast}} = 0.23 \cdot 10^{-38}\ \text{cm}^2.$$

As will be seen later, the nonresonant background which we introduce into the model in a phenomenological way, gives a contribution of the same order as the $I = \frac{1}{2}$ resonance part

$$\sigma_{\text{nonres}} \approx 0.20 \cdot 10^{-38}\ \text{cm}^2, \qquad \bar{\sigma}_{\text{nonres}} \approx 0.08 \cdot 10^{-38}\ \text{cm}^2.$$

Taken together these cross sections amount to

$$\sigma = 1.31 \cdot 10^{-38}\ \text{cm}^2, \qquad \bar{\sigma} = 0.61 \cdot 10^{-38}\ \text{cm}^2 \tag{4.1}$$

at $E = 2$ GeV and thus yield "slope" parameters

$$\langle \sigma/E \rangle = 0.66 \cdot 10^{-38}\ \text{cm}^2, \qquad \langle \bar{\sigma}/E \rangle = 0.31 \cdot 10^{-38}\ \text{cm}^2. \tag{4.2}$$

These numbers are in reasonable agreement with the corresponding parameters measured in the Gargamelle experiment [27]:

$$\langle \sigma/E \rangle_{\text{exp}} = 0.74 \cdot 10^{-38}\ \text{cm}^2, \qquad \langle \bar{\sigma}/E \rangle_{\text{exp}} = 0.28 \cdot 10^{-38}\ \text{cm}^2.$$

Turning now to neutral current resonance cross sections inspection of Fig. 1 and Table IV shows a general suppression of neutral current cross sections compared with the corresponding charged current cross sections. The suppression factor depends on the isospin of the resonance ranging from 1–2 for $I = \frac{3}{2}$ resonances to 4–6 for $I = \frac{1}{2}$ resonances. This confirms earlier considerations of almost model independent nature [28] concluding that the ratio

$$R(\mathcal{N}^*) = \frac{\sigma(\nu p \to \nu \mathcal{N}^{*+}) + \sigma(\nu n \to \nu \mathcal{N}^{*0})}{2\sigma(\nu n \to \mu \mathcal{N}^{*+})} \tag{4.3}$$

should not exceed $\frac{1}{4}$ if $\mathcal{N}^*$ carries isospin $\frac{1}{2}$, whereas for the Δ-resonance with isospin $\frac{3}{2}$ this same ratio should be close to 1 (in fact we find $\sim$0.7). In all other respects the neutral current cross sections follow their charged current counterparts. For isospin $\frac{3}{2}$ resonances the NC cross sections off protons and neutrons are equal, since there only

TABLE IV

Resonance Production Cross Sections in Units of 10^{-40} cm^2 at Incident Energies of 2 and 20 GeV ($m_A = 0.95$ GeV/c^2, $\sin^2\theta_w = 0.22$)

	Charged current				Neutral current					
	$\sigma_{CC}(\nu n \to \mu R^+)$		$\sigma_{CC}(\bar{\nu} p \to \bar{\mu} R^0)$		$\sigma_{NC}(\nu p \to \nu R^+)$		$\sigma_{NC}(\nu n \to \nu R^0)$		$\sigma_{NC}(\bar{\nu} p \to \bar{\nu} R^+)$	
Resonance	$E=2$	$E=20$	$E=2$	$E=20$	$E=2$	$E=20$	$E=2$	$E=20$	$E=2$	$E=20$
$P_{33}(1234)$	20.0	22.58	8.7	20.65	13.6	16.22	13.6	16.22	7.27	15.15
$P_{11}(1450)$	3.90	10.93	0.66	8.92	0.56	1.89	0.69	2.15	0.18	1.66
$D_{13}(1525)$	9.57	18.12	4.46	16.57	1.32	2.91	1.86	3.51	0.95	2.79
$S_{11}(1540)$	9.88	14.28	3.50	12.54	1.28	1.95	1.71	2.50	0.60	1.78
$S_{31}(1620)$	0.20	0.57	0.23	0.56	0.12	0.31	0.12	0.31	0.14	0.30
$S_{11}(1640)$	0.48	0.89	0.27	0.83	0.12	0.22	0.08	0.18	0.07	0.21
$P_{33}(1640)$	0.88	4.54	0.08	3.66	0.55	3.49	0.55	3.49	0.10	3.00
$D_{13}(1670)$	1.15	2.04	0.14	1.65	0.29	0.51	0.10	0.23	0.03	0.41
$D_{11}(1680)$	1.52	3.73	0.52	3.36	0.38	0.93	0.19	0.66	0.13	0.84
$F_{11}(1680)$	4.16	10.96	1.34	9.68	0.74	2.12	0.78	2.28	0.35	1.96
$P_{11}(1710)$	0.86	5.65	0.10	4.55	0.10	0.99	0.16	1.21	0.03	0.89
$D_{33}(1730)$	1.24	2.57	0.41	2.32	0.68	1.48	0.68	1.48	0.21	1.34
$P_{13}(1740)$	3.89	15.06	1.29	11.82	0.58	2.56	0.82	3.75	0.33	2.20
$P_{31}(1920)$	0.13	1.28	0.08	1.15	0.11	1.14	0.11	1.14	0.09	1.07
$F_{33}(1920)$	0.64	2.20	0.05	1.75	0.40	1.49	0.40	1.49	0.08	1.24
$F_{33}(1950)$	0.67	4.33	0.22	3.94	0.49	3.72	0.49	3.72	0.24	3.50
$P_{33}(1960)$	0.24	2.22	0.07	1.68	0.17	1.66	0.17	1.66	0.08	1.36
$F_{11}(1970)$	0.26	1.55	0.05	1.34	0.07	0.39	0.03	0.27	0.01	0.34

the isovector part of the neutral current can be operative, and the relevant isospin Clebsch–Gordan-coefficients are the same. Also for $I = \frac{1}{2}$ resonances there is approximate equality for most of the NC cross sections off protons and neutrons as can be read off Table IV. In contrast to charged current reactions the neutrino and antineutrino cross sections do not differ appreciably from each other. This is because the Salam–Weinberg theory predicts the axial vector cross section to be quite dominant, the corresponding vector cross section being reduced by the interference with the electromagnetic part of the current. This will be obvious from Figs. 10d–g where the vector and axial vector cross sections are shown together with the total cross sections.

(b) *Detailed Discussion of* Δ^{++}

The Δ-resonance $P_{33}(1234)$ is excited by neutrinos as prominently as by photons or electrons. A special advantage available to neutrinos is the possibility to excite the Δ^{++}, a charge mode not accessible to photoproduction or electroproduction. Since the Δ^{++}

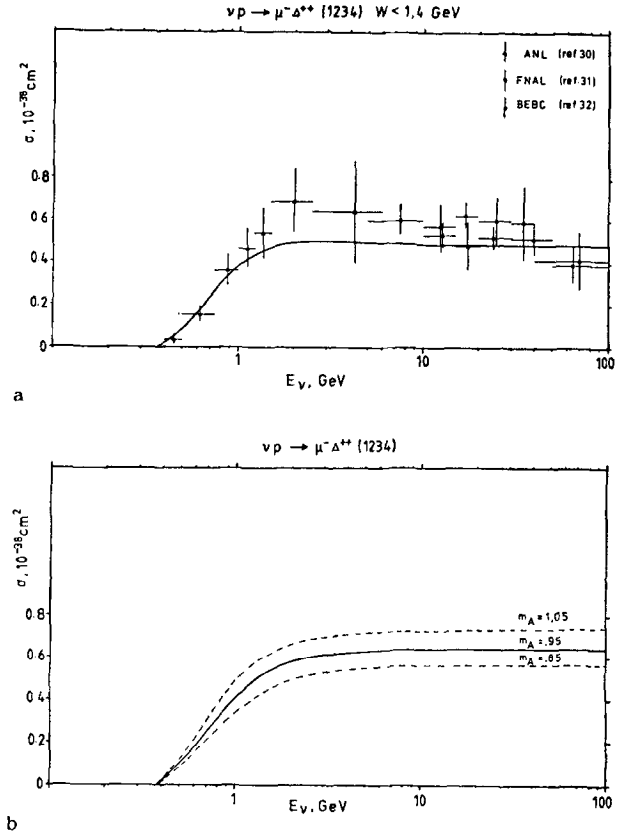

FIG. 2. Δ^{++} cross section, as a function of neutrino energy; (a) comparison with data (Refs. [30–32]) for $W < 1{,}4$ GeV, (b) full excitation curve (without W-cut) for $m_A = 0.85, 0.95, 1.05$ GeV/c².

is produced with a large cross section, and is well separated from higher $I = \frac{3}{2}$ resonances in the $p\pi^+$ channel, it offers a clean testing ground for models of resonance production.

On the basis of the FKR model, we have calculated the Δ^{++} cross section as a function of neutrino energy. The mass parameter in the axial vector form factor was chosen as $m_A = 0.95$ GeV/c^2 which is the average result of recent quasi-elastic neutrino nucleon scattering experiments [25, 26, 29]. The shape of the resonance was assumed to be of a normalized P-wave Breit–Wigner form. For reasons of comparison with experiments [30–32] our result, as shown in Fig. 2a, refers to the Δ^{++} with the tail of its Breit–Wigner factor cut off at $W = 1.4$ GeV. Also indicated in Fig. 2b is our prediction for the full excitation curve of the Δ^{++} resonance without any restriction in W. We found, for a value $m_A = 0.95$ GeV/c²:

$$\sigma(\Delta^{++};\, E_\nu \gg 1 \text{ GeV}) = 0.65 \cdot 10^{-38} \text{ cm}^2. \tag{4.4}$$

This compares well with the experimental values:

$$\sigma_{\text{exp}}(\Delta^{++};\, E_\nu > 15\ \text{GeV}) = \begin{cases} 0.63 \pm 0.09 \\ 0.59 \pm 0.06 \end{cases} \cdot 10^{-38}\ \text{cm}^2 \quad \begin{matrix} \text{(Ref. [31])} \\ \text{(Ref. [32])} \end{matrix} \tag{4.5}$$

Note that the calculation is sensitive to the choice of the axial mass parameter: a 10% variation of the value of m_A changes the cross section by about 12% in the same direction. On the other hand the cross section depends very little on the assumed shape of the resonance. (The data, in fact, fit better to an S-wave type of Breit–Wigner formula, or to a P-wave form modified by a threshold factor [32]).

The q^2-distribution of the Δ^{++} channel at $E_\nu = 20$ GeV (again cut at $W = 1.4$ GeV) is compared in Fig. 3 with data from two sources [31, 32]. There is good agreement in the whole q^2-region. One might, however, question the value of $d\sigma/dq^2$ at $q^2 = 0$. This is determined entirely by the divergence of the axial vector current, and so can be estimated by PCAC without recourse to a dynamical model. The FKR model, in fact, predicts for the Δ^{++} a value

$$\left.\frac{d\sigma}{dq^2}\right|_{q^2=0} = 1.18 \left\{1 - \frac{\nu}{E}\right\} \cdot 10^{-38}\ \text{cm}^2\ \text{GeV}^{-2}. \tag{4.6}$$

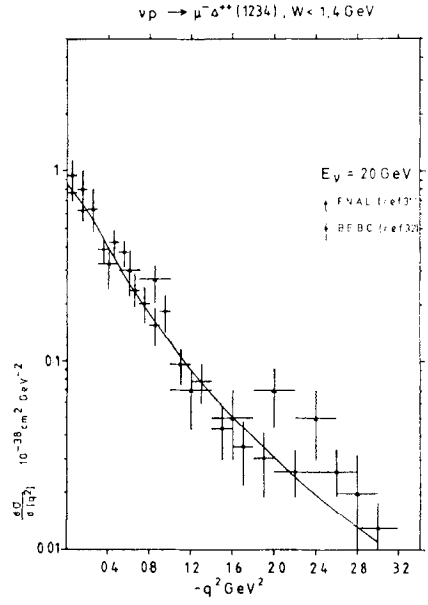

FIG. 3. $d\sigma(\Delta^{++})/dq^2$ for $E_\nu = 20$ GeV and $W < 1.4$ GeV compared with data ($m_A = 0.95$ GeV/c²).

As shown by Ravndal [3] this is numerically very close to what one obtains from Adler's PCAC formula

$$\left.\frac{d\sigma}{d\nu\, dq^2}\right|_{q^2=0} = \frac{G^2}{\pi^2}\frac{E'}{E}\frac{F_\pi^2}{Q}\,\sigma_{\pi N\to\Delta^{++}}(W), \tag{4.7}$$

after integrating over W. Thus the FKR model satisfies PCAC rather closely. The value of $d\sigma/dq^2\,|_{q^2=0}$ indicated in Fig. 3 is somewhat lower than the value in Eq. (4.6), owing to the cut $W < 1.4$ GeV, which removes the high-mass tail of the Δ^{++}. The data fit nicely to the theoretical expectation, which may be considered a success of the PCAC idea.

A separate determination of the vector, axial vector and interference terms in the cross section $\sigma(\Delta^{++})$ is useful as a basis for distinguishing competing models of resonance production. Our results are shown in Fig. 4. For comparison with other calculations we quote the values at $E_\nu = 1$ GeV:

$$\{\sigma_V\,,\ \sigma_A\,,\ \sigma_I\}_{E_\nu=1} = \{0.095,\ 0.155,\ 0.154\}\cdot 10^{-38}\ \text{cm}^2$$

giving a total $\sigma(E_\nu = 1) = 0.404\cdot 10^{-38}$ cm^2. The fact that $\sigma_A > \sigma_V$ reflects the dominance of the axial contribution in the low q^2-region. This is evident in Fig. 5, where we have separated the V, A and I contributions to $d\sigma/dq^2$ for $E_\nu = 2$ GeV. At $E_\nu = 1$ GeV the curves appear to be the same except for being scaled down by the ratio of the total cross sections at 1 and 2 GeV. Our numerical values are close to those extracted from the Adler model [6, 33]:

$$\{\sigma_V\,,\ \sigma_A\,,\ \sigma_I\}_{\text{Adler},\ E_\nu=1} = \{0.104,\ 0.151,\ 0.157\}\cdot 10^{-38}\ \text{cm}^2.$$

They are, however, at variance with the static model calculation of Lee [34], which gave a ratio $\sigma_V : \sigma_A : \sigma_I = 0.263{:}0.202{:}0.235$, implying in particular that $\sigma_V > \sigma_A$, in contrast to our findings. We have also compared our results with those obtained in

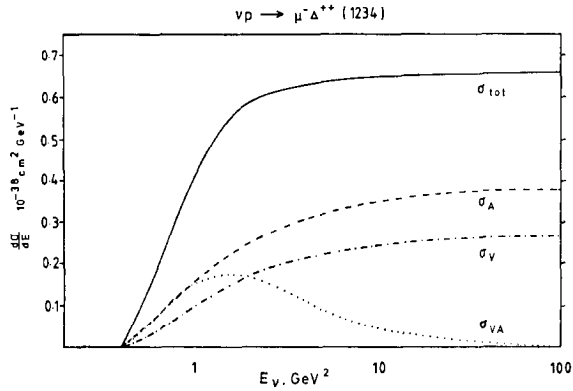

FIG. 4. Vector, axialvector, and VA-interference parts of the Δ^{++} cross section as functions of E_ν ($m_A = 0.95$ GeV/c^2).

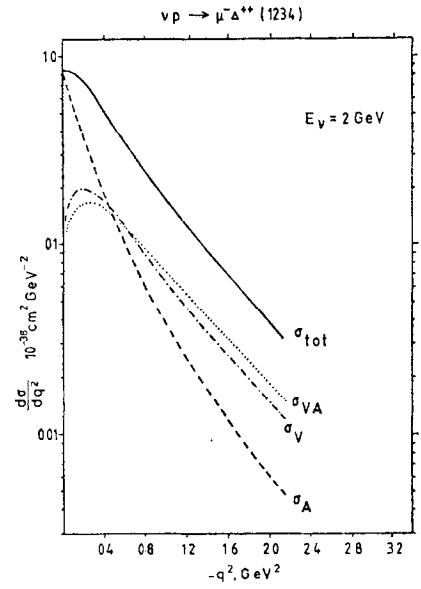

FIG. 5. Vector, axialvector, and VA-interference parts of $d\sigma/dq^2$ at $E_\nu = 2$ GeV ($m_A = 0.95$ GeV/c^2).

the model of Fogli and Nardulli [11]. From the paper of Fogli (Ref. [35]) one can extract the values of σ_V, σ_A and σ_I appropriate to Δ^{++} production in the Gargamelle neutrino spectrum, and one finds:

$$\{\sigma_V, \sigma_A, \sigma_I\}_{\text{GGM,Fogli}} = \{0.23, 0.17, 0.10\} \cdot 10^{-38} \text{ cm}^2.$$

The corresponding result obtained by us is

$$\{\sigma_V, \sigma_A, \sigma_I\}_{\text{GGM,FKR}} = \{0.14, 0.20, 0.14\} \cdot 10^{-38} \text{ cm}^2.$$

Once again we note a significant difference in the relative size of σ_V to σ_A. This illustrates the general fact, summarized in Table V, that different models can differ quite strongly in their detailed predictions even though they give almost identical results for the total Δ^{++} cross section.

To conclude this subsection, we give below our results for density matrix elements in the Δ^{++} region. At low energies ($E_\nu \cong 1$ GeV) these are essentially the same as those obtained by Ravndal [3], and are almost identical with the predictions of the Adler model as well as the model of Andreadis *et al.* [9] and fairly compatible with the data [37]. We note that their dependence on the neutrino energy is very weak, at least on top of the Δ^{++}-resonance peak where we have investigated them (see Fig. 6). For comparison with the BEBC and Fermilab data we have computed q^2-averaged density

TABLE V

Comparison of Various Models for Δ^{++} Production

E_ν	Model	$\sigma_V : \sigma_A : \sigma_I$	$\sigma(\Delta^{++})$ $(10^{-38}\ \text{cm}^2)$	Reference
1 GeV	Ours (FKR)	1: 1.63: 1.62	0.41	
	Adler	1: 1.45: 1.51	0.41	[6, 13, 33]
	B. W. Lee	1: 0.79: 0.89	—	[34]
	Le Yaouanc *et al.*	1: 1.98: 1.89	0.43	[9]
Gargamelle spectrum	Ours (FKR)	1: 1.43: 1.0	0.48	
	Adler	1: 1.23: 0.73	0.51	[6, 33]
	Le Yaouanc *et al.*	1: 2.13: 1.10	0.49	[9]
	Fogli	1: 0.74: 0.43	0.50	[11, 35]

matrix elements for the Δ^{++} folding in the appropriate neutrino spectrum. The results and the corresponding measurements are as follows:

$$\langle\tilde{\rho}_{33}\rangle = 0.582 \qquad \left(\text{Expt:} \begin{array}{r} 0.90 \pm 0.09 \text{ Ref. [31]} \\ 0.60 \pm 0.08 \text{ Ref. [36]} \end{array}\right),$$

$$\langle\tilde{\rho}_{31}\rangle = -0.184 \qquad \left(\text{Expt:} \begin{array}{r} 0.01 \pm 0.05 \text{ Ref. [31]} \\ -0.03 \pm 0.04 \text{ Ref. [36]} \end{array}\right),$$

$$\langle\tilde{\rho}_{3-1}\rangle = 0.035 \qquad \left(\text{Expt:} \begin{array}{r} -0.07 \pm 0.06 \text{ Ref. [31]} \\ -0.03 \pm 0.04 \text{ Ref. [36]} \end{array}\right).$$

It should be remarked that there is a weak indication in the BEBC and Fermilab data for the occurrence of nonzero "illegal" density matrix elements, reflected in an asymmetry of the angular distribution around $\cos\Theta = 0$ and around $\phi = \pi$. These asymmetries require an interference between the dominant $I = \frac{3}{2}$ Δ^{++}-amplitude and a background of the same isospin. Within a resonance model, the only possibility is to invoke an interference with the tail of a higher lying $I = \frac{3}{2}$ resonance, but this turns out to be negligibly small. The observed asymmetries thus suggest the existence of a small nonresonant $I = \frac{3}{2}$ background amplitude interfering with the Δ-resonance. Models that contain background contributions of this kind can, in principle, explain such effects. It appears that the Adler model does not reproduce the sign or magnitude of the observed asymmetries whereas the model of Fogli *et al.* (Ref. [35]) seems to be more successful in this respect.

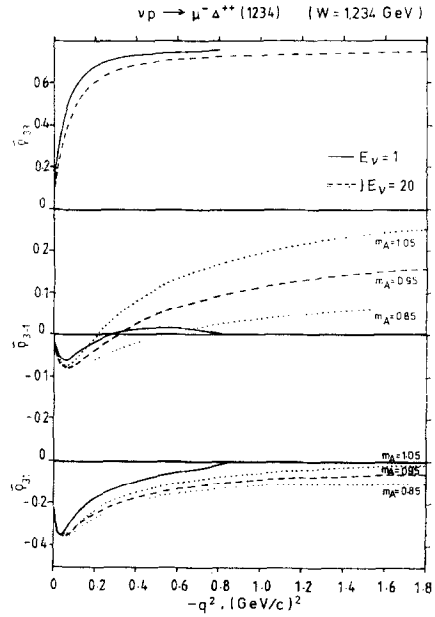

FIG. 6. Density matrix elements of the $\Delta^{++}(1234)$ as functions of $-q^2$ for two values of neutrino energy: $E_\nu = 1$ GeV (full line), $E_\nu = 20$ GeV (dashed), (a) $\tilde{\rho}_{33}(q^2)$, (b) $\tilde{\rho}_{3-1}(q^2)$, (c) $\tilde{\rho}_{31}(q^2)$, ($m_A = 0.95$ GeV/c^2; variation with m_A is indicated by dotted lines).

4.2. *Cross Sections*

(a) $\sigma(E)$ *for Mixed Isospin Channels*

Of the 14 single pion channels that can be excited by charged or neutral weak currents, only two ($\mu^- p\pi^+$ and $\mu^+ n\pi^-$) are pure in isospin. In these two cases the $\pi\mathcal{N}$ system has $I = \frac{3}{2}$, and the cross section is dominated by the $\Delta(1234)$ resonance, which has been discussed in the preceding section. We wish now to focus on the remaining channels, which necessarily involve both $I = \frac{1}{2}$ and $I = \frac{3}{2}$ amplitudes. The discussion of these channels is complicated by two factors. (a) In any given mass range, there is a large number of resonances (of either isospin) which generally overlap and have to be added coherently. (b) There exists the possibility of a nonresonant background that is not included in a pure resonance description.

The first problem can be solved within the framework of the FKR resonance model, since both the absolute magnitudes and relative phases of the single resonance terms are specified. We are thus able to take account of all interference effects between resonances and derive a resonant cross section for every $\mathcal{N}\pi$ channel that includes in a realistic way the elasticity of each resonance, its shape, and the effects of its overlap with neighbouring resonances. It may be recalled that as long as one is interested in angle-integrated cross sections, interferences can occur only between resonances that have identical (L, j) quantum numbers. Since such resonances are

often well separated, the interference effects can, in practice, turn out to be small.

As to the question of a nonresonant background, we have represented it by an incoherent $I = \frac{1}{2}$ cross section generated so as to resemble a phase space distribution in the $\pi\mathcal{N}$ invariant mass. This was done by means of a simple and economic ansatz (described in Section 2.4) leaving only a scale factor free for adjustment. To determine this factor, we have appealed to low energy data [29, 37] on the charged current channels $\mu^- p\pi^+$, $\mu^- n\pi^+$ and $\mu^- p\pi^0$, which allows one to extract the ratio of the average $I = \frac{1}{2}$ and $I = \frac{3}{2}$ amplitudes:

$$\frac{\langle A_1^{CC}\rangle}{\langle A_3^{CC}\rangle} = \left\{\frac{3\cdot[\sigma(\nu n \to \mu^- p\pi^0) + \sigma(\nu n \to \mu^- n\pi^+)] - \sigma(\nu p \to \mu^- p\pi^+)}{2\sigma(\nu p \to \mu^- p\pi^+)}\right\}^{1/2}. \quad (4.8)$$

The scale factor needed to reproduce the above ratio turned out to be approximately one, in the sense that our background amplitude corresponded to a nucleon-like excitation with the usual Breit–Wigner factor replaced by unity. In Table VI, we list the cross sections predicted by the model at various energies, both with and without the background contribution. As evident from the comparison with GGM and ANL data (also listed in the table) the inclusion of background improves agreement. It may be noted that the incoherent nature of our background implies that the average

TABLE VI

Total Charged Current Cross Sections for Single Pion Neutrino Production[a]

	ANL-Spectrum			GGM-Spectrum		
	Res.	Res. + BG	Data (Ref. [29])	Res.	Res. + BG	Data (Ref. [37])
$\sigma(\mu^- p\pi^+)$	0.214	0.214		0.483	0.483	0.52 ± 0.09
$\sigma(\mu^- p\pi^0)$	0.055	0.067		0.151	0.192	0.18 ± 0.06
$\sigma(\mu^- n\pi^+)$	0.039	0.063		0.134	0.216	0.37 ± 0.08
$R^+ = \frac{(n\pi^+)}{(p\pi^0)}$	0.71	0.94	0.89 ± 0.17	0.89	1.13	2.2 ± 0.76
$R^{++} = \frac{(n\pi^+) + (p\pi^0)}{(p\pi^+)}$	0.44	0.61	0.55 ± 0.07	0.59	0.84	1.03 ± 0.17
$\frac{\langle A_1^{CC}\rangle}{\langle A_3^{CC}\rangle}$	0.40	0.64	0.66 ± 0.06	0.62	0.88	1.03 ± 0.15
$\langle\phi\rangle$		90.3^0	$(90 \pm 9)^0$		90.4^0	$(73^{+12}_{-10})^0$

[a] Values given for (a) the FKR resonance model, (b) the same model including $I = \frac{1}{2}$ nonresonant background, compared with low energy data (in units of 10^{-38} cm^2).

phase between the A_1^{CC} and A_3^{CC} amplitudes is unchanged from the pure resonance value. As seen from the table, this phase defined by

$$\cos\phi = \mathrm{Re}\left\{\frac{\langle A_3^{CC} A_1^{CC*}\rangle}{\langle A_3^{CC}\rangle\langle A_1^{CC}\rangle}\right\}$$

$$= \frac{\sigma(\nu n \to \mu^- n\pi^+) - 2\sigma(\nu n \to \mu^- p\pi^0) + \frac{1}{3}\sigma(\nu p \to \mu^- p\pi^+)}{\{\frac{8}{3}\sigma(\nu p \to \mu^- p\pi^+)[\sigma(\nu n \to \mu^- n\pi^+) + \sigma(\nu n \to \mu^- p\pi^0) - \frac{1}{3}\sigma(\nu p \to \mu^- p\pi^+)]\}^{1/2}} \tag{4.9}$$

is in quite adequate agreement with the data.

Having calibrated the background contribution, we proceed to detailed predictions for all charged and neutral current channels. As before, we have chosen the mass parameter m_A to be 0.95 GeV. Changes in this parameter produce changes in the overall scale of the cross sections, but with little effect on relative ratios as those of Eqs. (4.8) and (4.9). For neutral current channels we use the Salam–Weinberg model with $\sin^2\theta_w = 0.22$, investigating also the dependence on this parameter in some cases.

The results for $\sigma(E)$ are plotted in Figs. 7 and 8 for neutrino and antineutrino reactions, respectively. These refer to $W < 2$ GeV, which is essentially the whole mass region excited in the $\mathcal{N}\pi$ channels even at high energies. Data have been inserted where available [30, 36–40]. We have also calculated flux-averaged cross sections for all $\mathcal{N}\pi$ channels for direct comparison with various experiments. These are displayed in Table VII. The variation of the neutral current cross sections with $x_w = \sin^2\theta_w$ has been studied separately for the Gargamelle spectrum and presented

TABLE VII

Flux Averaged Total Cross Section Predictions for Various Experiments (Nonresonant Background Included), in Units of 10^{-38} cm^2

Channel	ANL	GGM	BEBC	FNAL
$(\mu^- p\pi^+)$	0.214	0.483	0.643	
$(\mu^- p\pi^0)$	0.067	0.192	0.309	
$(\mu^- n\pi^+)$	0.063	0.216	0.379	
$(\nu p\pi^0)$	0.035	0.083	0.124	
$(\nu n\pi^+)$	0.022	0.062	0.108	
$(\nu n\pi^0)$	0.036	0.086	0.128	
$(\nu p\pi^-)$	0.023	0.068	0.118	
$(\mu^+ n\pi^-)$		0.251		0.597
$(\mu^+ n\pi^0)$		0.095		0.292
$(\mu^+ p\pi^-)$		0.101		0.356
$(\bar{\nu} p\pi^0)$		0.053		0.117
$(\bar{\nu} n\pi^+)$		0.040		0.103
$(\bar{\nu} n\pi^0)$		0.053		0.121
$(\bar{\nu} p\pi^-)$		0.041		0.112

same as BEBC

same as FNAL

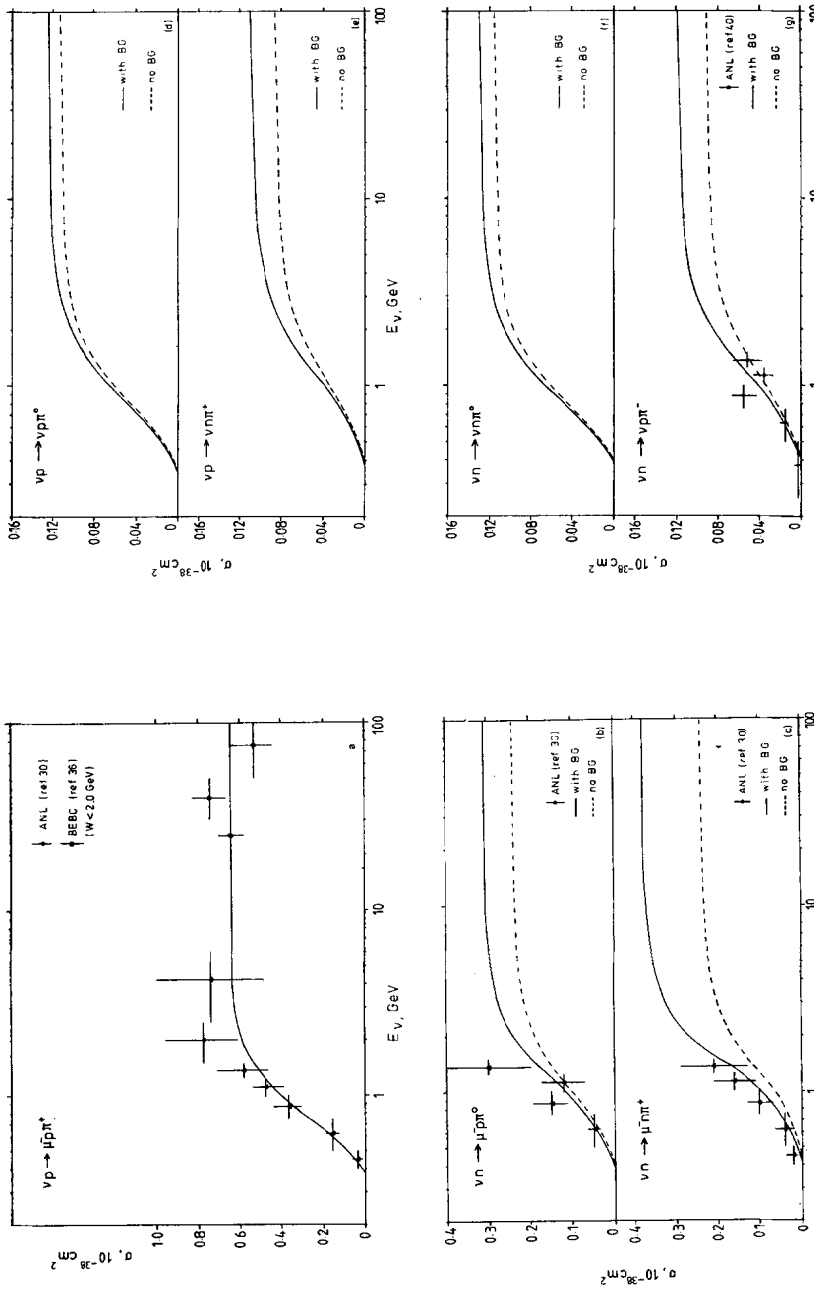

FIG. 7. Total neutrino cross sections for charged current $\mathcal{N}\pi$ production (a–c), and neutral current $\mathcal{N}\pi$ production (d–g); predictions are made for the pure resonance model (dashed line) and for resonances plus incoherent nonresonant background (full line); data from ANL (Ref. [30]) and BEBC (Ref. [36]). ($m_A = 0.95$ GeV/c^2, $\sin^2\theta_w = 0.22$).

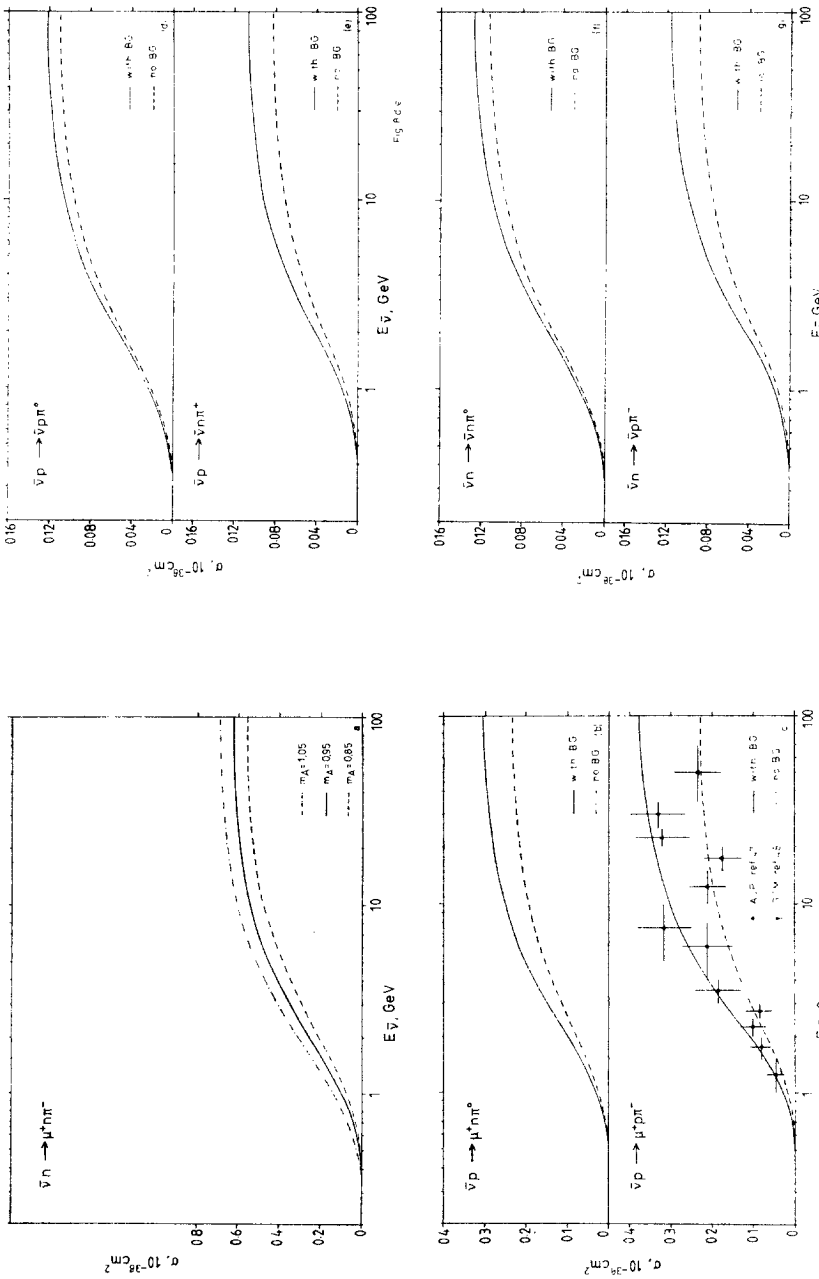

FIG. 8. The same as Fig. 7 but for antineutrinos. In addition variation with m_A indicated on Fig. 8a.

TABLE VIII

Variation of Neutral Current Cross Sections with $x_w = \sin^2\theta_w$ for the GGM Neutrino Experiment (and Other Experiments with the Same Neutrino Flux)

	$x_w = 0.20$	$x_w = 0.25$	$x_w = 0.30$	$x_w = 0.35$	$x_w = 0.22$
$\sigma(\nu p\pi^0)$	0.0867	0.0788	0.0717	0.0655	0.0834
$\sigma(\nu n\pi^+)$	0.0646	0.0587	0.0535	0.0500	0.0622
$\sigma(\nu n\pi^0)$	0.0894	0.0817	0.0748	0.0687	0.0862
$\sigma(\nu p\pi^-)$	0.0704	0.0652	0.0604	0.0561	0.0682
$R_0 = \dfrac{(\nu p\pi^0) + (\nu n\pi^0)}{2(\mu p\pi^0)}$	0.46	0.42	0.38	0.35	0.45

Note. Cross sections in units of 10^{-38} cm^2.

in Table VIII. These results apply equally to other experiments using a similar flux, e.g., the Aachen–Padova and CIR experiments. It should be noted that because of the saturation of cross sections, the precise shape of the $\nu/\bar{\nu}$ flux for the higher energy experiments is rather unimportant. We have chosen therefore to give results for one neutrino experiment (BEBC ν) and one antineutrino experiment (FNAL $\bar{\nu}$) of that class.

Data on absolute cross sections are not always given explicitly but often cross section ratios are available, especially for neutral current channels. The following ratios will be considered:

(i) charged current case

$$R_1 = \frac{\sigma(\nu n \to \mu^- p\pi^0)}{\sigma(\nu p \to \mu^- p\pi^+)} \qquad \bar{R}_1 = \frac{\sigma(\bar{\nu}p \to \mu^+ n\pi^0)}{\sigma(\bar{\nu}n \to \mu^+ n\pi^-)},$$
$$R_2 = \frac{\sigma(\nu n \to \mu^- n\pi^+)}{\sigma(\nu p \to \mu^- p\pi^+)} \qquad \bar{R}_2 = \frac{\sigma(\bar{\nu}p \to \mu^+ p\pi^-)}{\sigma(\bar{\nu}n \to \mu^+ n\pi^-)}. \tag{4.10}$$

Note that sometimes instead of R_1, R_2 the combinations $R^+ = R_2/R_1$ or $R^{++} = R_1 + R_2$ are given experimentally. These were included in Table VI.

(ii) neutral current case

$$R_0 = \frac{\sigma(\nu p \to \nu p\pi^0) + \sigma(\nu n \to \nu n\pi^0)}{2\sigma(\nu n \to \mu^- p\pi^0)}, \qquad \bar{R}_0 = \frac{\sigma(\bar{\nu}p \to \bar{\nu}p\pi^0) + \sigma(\bar{\nu}n \to \bar{\nu}n\pi^0)}{2\sigma(\bar{\nu}p \to \mu^+ n\pi^0)},$$
$$r_1 = \frac{\sigma(\nu p \to \nu p\pi^0) + \sigma(\nu n \to \nu n\pi^0)}{\sigma(\nu p \to \nu n\pi^+)}, \qquad \bar{r}_1 = \frac{\sigma(\bar{\nu}p \to \bar{\nu}p\pi^0) + \sigma(\bar{\nu}n \to \bar{\nu}n\pi^0)}{\sigma(\bar{\nu}n \to \bar{\nu}p\pi^-)},$$
$$r_{\mathrm{NC}} = \frac{\sigma(\bar{\nu}p \to \bar{\nu}p\pi^0) + \sigma(\bar{\nu}n \to \bar{\nu}n\pi^0)}{\sigma(\nu p \to \nu p\pi^0) + \sigma(\nu n \to \nu n\pi^0)}, \tag{4.11}$$

TABLE IX

Total Cross-Section Ratios for Typical Experimental Neutrino/Antineutrino Spectra[a]

	ANL ν		ν GGM/AC–PD		$\bar{\nu}$		ν BEBC/FNAL	$\bar{\nu}$
	Model	Data	Model	Data	Model	Data	Model	Model
R_1, $\bar{R}_1$	0.32		0.40	0.32 ± 0.09 GGM [41]	0.38		0.48	0.49
R_2, $\bar{R}_2$	0.29		0.45	0.71 ± 0.14 GGM [41]	0.40		0.59	0.60
				0.45 ± 0.08 GGM [41][b]		$0.57\ ^{+0.11}_{-0.10}$ GGM [44]		
R_0, $\bar{R}_0$	0.52		0.45	0.47 ± 0.06 AC–PD [42][b] 0.17 ± 0.04 CIR [43]	0.56	0.62 ± 0.08 AC–PD [42][b] 0.39 ± 0.18 CIR [43]	0.41	0.41
r_1, $\bar{r}_1$	3.20		2.73	—	2.67	$2.4\ ^{+0.8}_{-0.6}$ GGM [44]	2.33	2.33
$r_{NC} = \frac{\sigma_{NC}(\bar{\nu})}{\sigma_{NC}(\nu)}$					Model: 0.63 Data: 0.50 ± 0.09 AC–PD [42]		0.96 —	
$\frac{\sigma(\nu p\pi^0)}{\sigma(\nu n\pi^+)}$	1.59	3.1 ± 2.2 ANL [39]	1.34	1.65 ± 0.36 GGM [41]			1.14	
$\frac{\sigma(\nu p\pi^0)}{\sigma(\mu p\pi^+)}$	0.16	0.09 ± 0.05 ANL [39]	0.17	0.23 ± 0.03 "			0.19	
$\frac{\sigma(\nu n\pi^+)}{\sigma(\mu p\pi^+)}$	0.10	0.13 ± 0.04 ANL [39]	0.13	0.15 ± 0.04 "			0.17	
$\frac{\sigma(\nu p\pi^-)}{\sigma(\mu n\pi^+)}$	0.37	0.38 ± 0.11 ANL [39]	0.32	0.32 ± 0.11 "			0.31	
$\frac{\sigma(\nu p\pi^-)}{\sigma(\mu p\pi^+)}$	0.11	0.11 ± 0.022 ACP [40]	0.14	—			0.18	

[a] (a) The low energy Argonne spectrum (ANL), (b) the spectrum of Gargamelle, Aachen–Padova and Brookhaven experiments (GGM/AC–PD), (c) the high energy wideband beam of CERN–SPS and Fermilab (BEBC/FNAL); predictions for $m_A = 0.95$ (including nonres. BG) and $\sin^2\theta_w = 0.22$.

[b] Corrected for nuclear effects.

Comparison of all these cross-section ratios (including some additional combinations useful for framing experimental results) with experiment [39–44] is made in Table IX.

Table X shows how the FKR model compares with other theoretical models. While essentially all models agree about the cross section of the $p\pi^+$-channel, i.e., the Δ^{++}-excitation, there is somewhat more spread in the theoretical prediction of the mixed isospin channels; however, experimental data are not yet advanced enough to distinguish between these models.

Inspection of Table X reveals the very near equality of neutral current π^0 production off protons and neutrons in all three models; essentially the same is true for neutral current π^+ and π^- production. This shows that despite the presence in the Weinberg–Salam model of a neutral current with both isovector and isoscalar components, the interference of these components produces very little asymmetry between the $\nu p\pi^0$ and $\nu n\pi^0$ channels (or between $\nu p\pi^-$ and $\nu n\pi^+$). In this connection, it is worth mentioning that NC single π^0 production near threshold can be related to elastic scattering $\nu\mathcal{N} \to \nu\mathcal{N}$ by a theorem of Adler [45]. Using this theorem we find $\sigma(\nu n\pi^0) > \sigma(\nu p\pi^0)$ near threshold. If we calculate the difference $\sigma(\nu n\pi^0) - \sigma(\nu p\pi^0)$, assuming the theorem to hold over the whole W-interval covered by the Gargamelle spectrum, we find a result of only 0.01×10^{-38} cm^2, consistent with the very small difference produced by our model [46]. Thus the findings of the Gargamelle experiment, indicating a two standard deviation difference ($\approx -0.06 \cdot 10^{-38}$ cm^2) between $\sigma(\nu p\pi^0)$ and $\sigma(\nu n\pi^0)$, remain unexplained.

(b) *Invariant Mass Distributions*

More detailed information than contained in total cross sections is exhibited by the W-distributions in every $\mathcal{N}\pi$-channel. These we have calculated for a W-interval between $\mathcal{N}\pi$-threshold (1.08 GeV) and $W = 2$ GeV. In order to facilitate direct comparison with measured W-distributions we have again folded in neutrino/antineutrino spectra typical for experiments at Argonne, CERN/BNL and CERN/Fermilab. Our results are displayed in Figs. 9–13 and compared with the corresponding experimental histograms where they exist.

The agreement between theoretical and experimental W-distributions is in general quite satisfactory throughout the whole energy range covered by experiments. In particular the measurement of the FNAL antineutrino collaboration [47] of the $\mu^+p\pi^-$ channel are remarkably well reproduced by the model. This channel is of course highly nontrivial and interesting since just here the $I = \frac{1}{2}$ part of the $\mathcal{N}\pi$-production amplitude is strongly favored against the $I = \frac{3}{2}$ part by isospin combination rules. This can be verified looking at Eqs. (2.24) and (2.25). Consequently this antineutrino channel $\mu^+p\pi^-$, and its charge conjugate counterpart $\mu^-n\pi^+$ in neutrino reactions, are most sensitive to resonance excitation beyond the $\Delta(1234)$ where the $I = \frac{1}{2}$ resonances play a prominent role. The $I = \frac{1}{2}$ enhancement is more pronounced at higher energies where all resonances are fully excited but could also be studied at Gargamelle energies if there is sufficient statistics. At FNAL and CERN–SPS energies, however, the resonance region around 1.5 GeV for the first time shows up more

TABLE X

Comparison of Our Flux Averaged Cross-Section Predictions (FKR) for Neutrinos with Those of the Models of Adler [6] and of Fogli and Nardulli [11] (In Units of 10^{-38} cm^2)

	ANL Spectrum					GGM Spectrum				
	FKR		Adler	FN		FKR		Adler	FN	
	$W < 1.4$	$W < 2$	$W < 1.4$	$W < 1.4$	$W < 1.6$	$W < 1.4$	$W < 2$	$W < 1.4$	$W < 1.4$	$W < 1.6$
$\sigma(\mu p\pi^+)$	0.200	0.214	0.219	0.231	0.243	0.416	0.483	0.427	0.502	0.585
$\sigma(\mu p\pi^0)$	0.056	0.067	0.073	0.079	0.085	0.118	0.192	0.147	0.187	0.263
$\sigma(\mu n\pi^+)$	0.044	0.063	0.057	0.052	0.065	0.097	0.216	0.129	0.147	0.281
$\sigma(\nu p\pi^0)^a$	0.032	0.035	0.028		0.036	0.066	0.083	0.053	0.068	0.090
$\sigma(\nu n\pi^+)$	0.018	0.022	0.020		0.031	0.039	0.062	0.038	0.064	0.097
$\sigma(\nu n\pi^0)$	0.033	0.036	0.029		0.038	0.067	0.086	0.054	0.075	0.105
$\sigma(\nu p\pi^-)$	0.019	0.023	0.019		0.028	0.041	0.068	0.037	0.061	0.100

[a] Neutral current cross sections evaluated for $\sin^2\theta_w = 0.22$ (FKR and FN) or $\sin^2\theta_w = 0.35$ (Adler).

prominently in a particular $\mathcal{N}\pi$-channel than the lowest lying $\Delta(1234)$-resonance —and this is predicted by the FKR-quark model of resonance excitation!

In the case $\nu p \to \mu^- p\pi^+$ where no $I = \frac{1}{2}$ resonances can contribute the BEBC experiment [32] with its high statistics allowed also for a closer inspection of the line shape of the Δ^{++}. There it was found that instead of a P-wave Breit–Wigner-factor —which would be a natural choice (and was used by us)—an S-wave form or alternatively a modified P-wave essentially equivalent to an S-wave gave the best fit. This seems to be a general feature of all neutrino/antineutrino experiments as indicated by the plots of Figs. 9–13. While such a modification was also found necessary in photoproduction analyses of resonances [16] the unprecedented small width of the Δ^{++} also found at BEBC [32] has no immediate interpretation: although the production

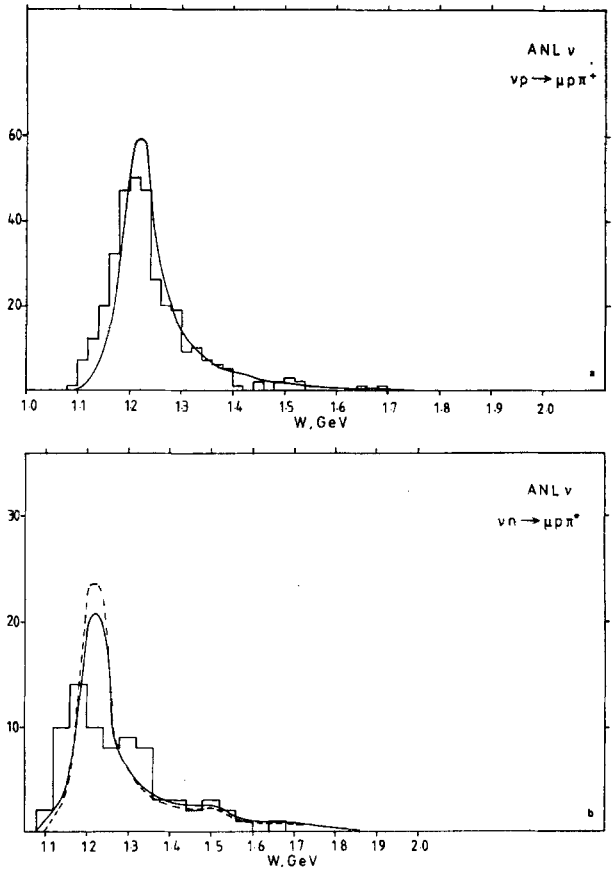

FIG. 9. W-distributions of charged current (a–c) and neutral current (d–g) $\mathcal{N}\pi$ events, flux averaged for ANL ν spectrum; area normalized to total event number of histogram, where data available (Ref. [30]), ($m_A = 0.95$ GeV/c², $\sin^2\theta_w = 0.22$), dotted lines for pure resonance model without nonresonant background.

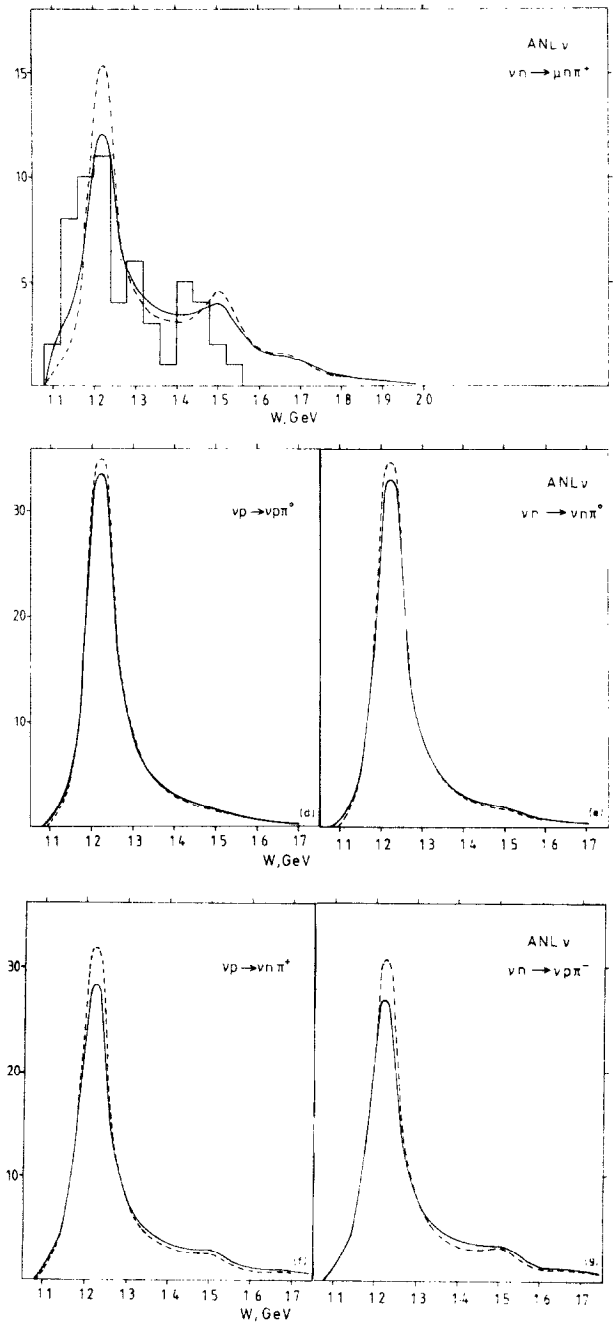

FIG. 9.—*Continued*

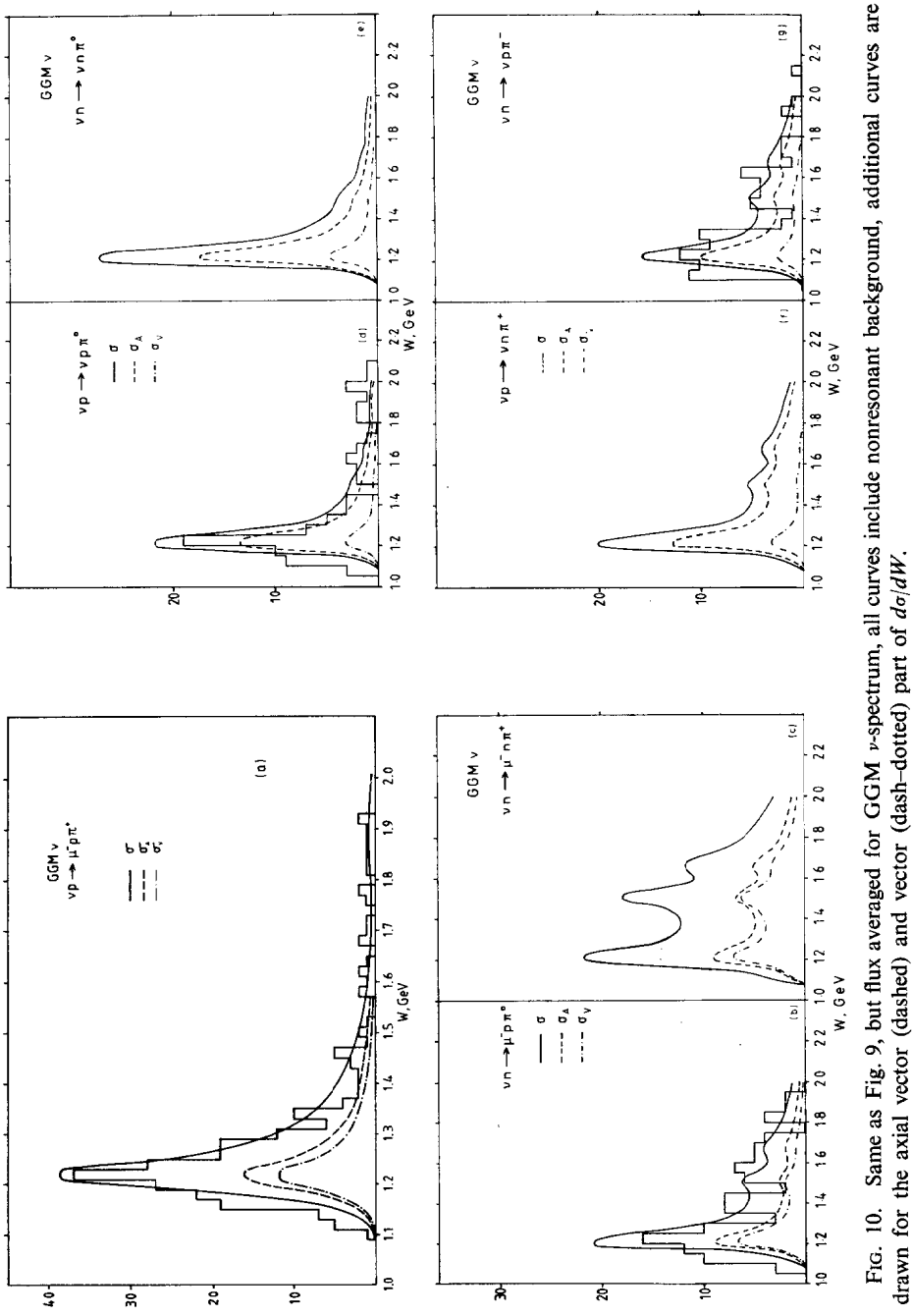

FIG. 10. Same as Fig. 9, but flux averaged for GGM ν-spectrum, all curves include nonresonant background, additional curves are drawn for the axial vector (dashed) and vector (dash–dotted) part of $d\sigma/dW$.

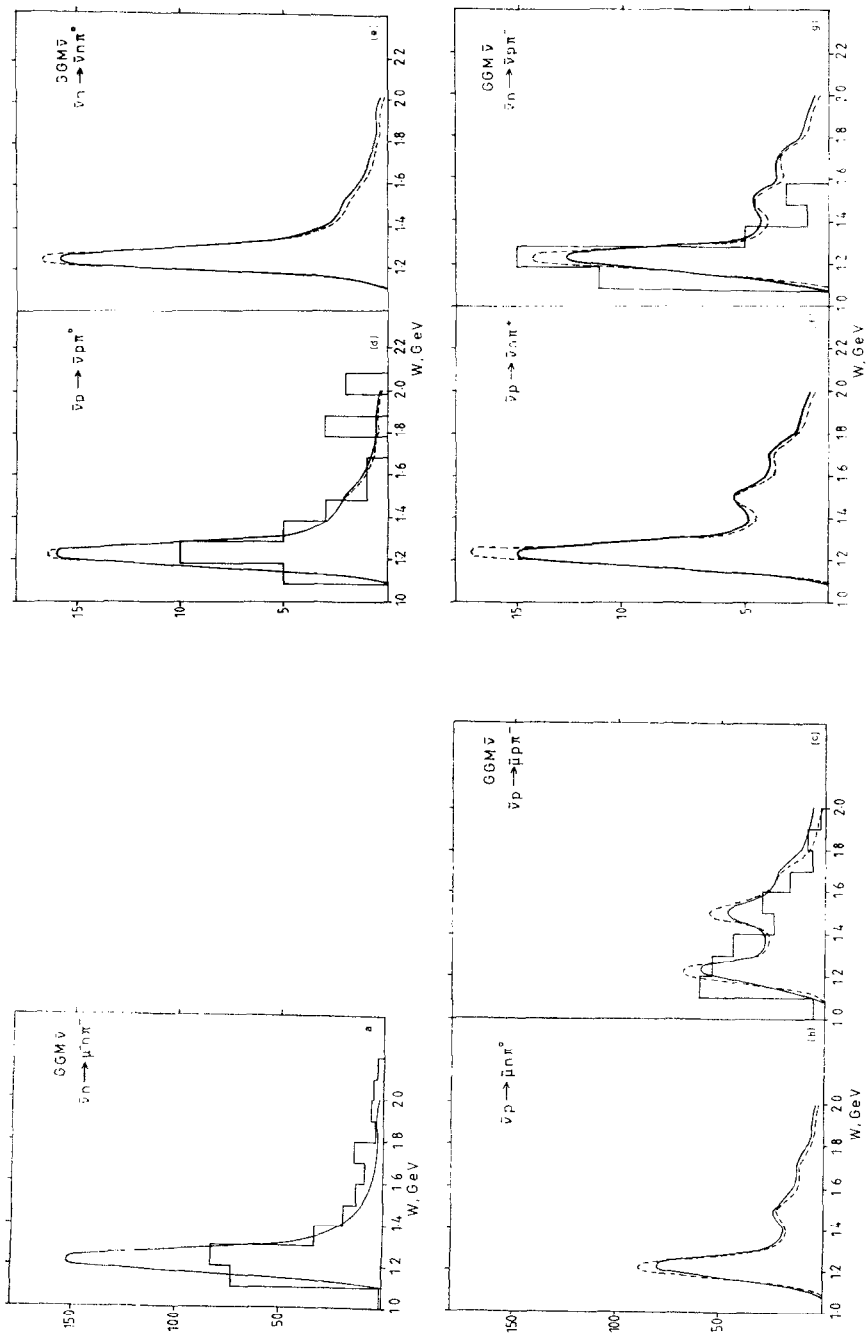

FIG. 11. Same as Fig. 9, but flux averaged for GGM ν̄-spectrum, data from Ref. [48].

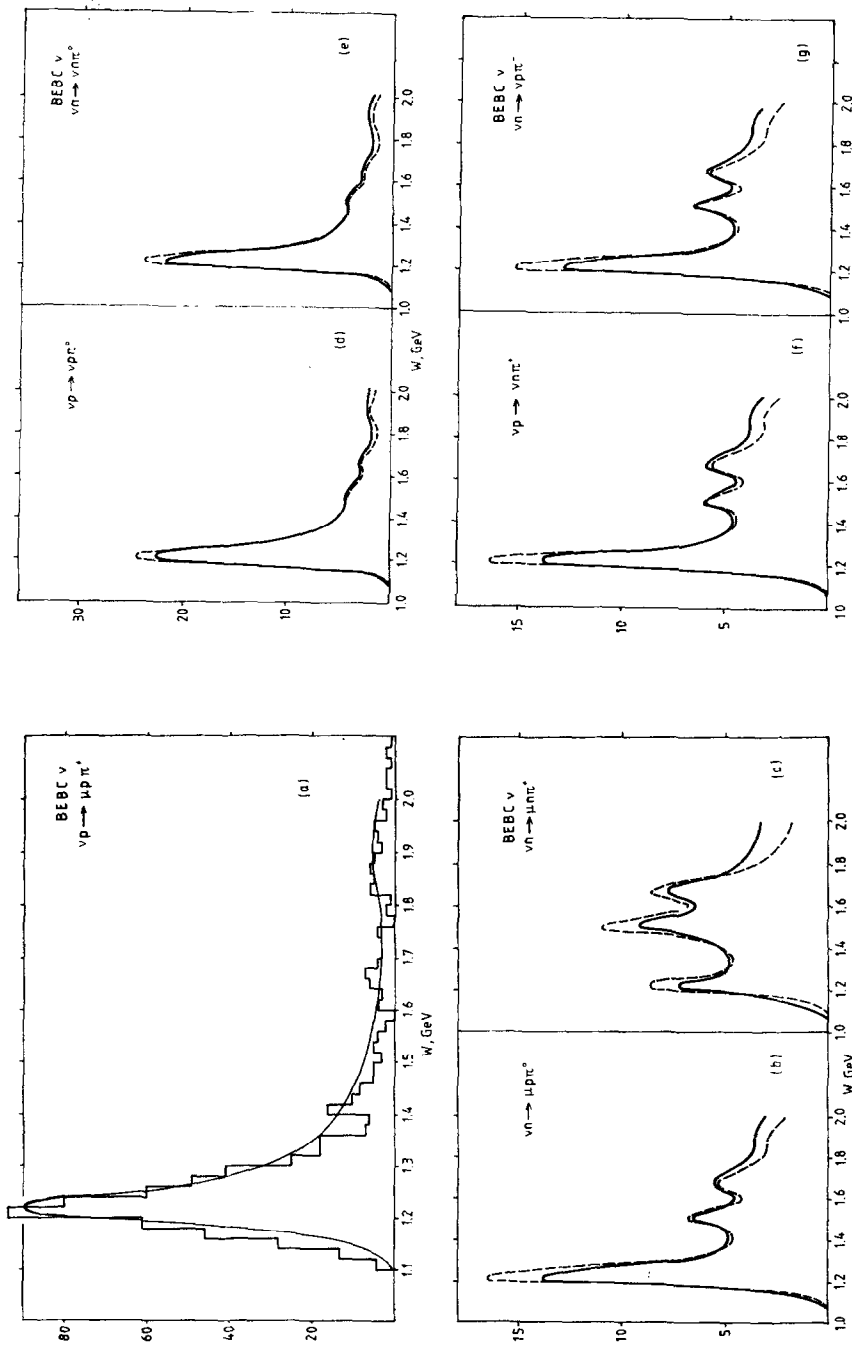

FIG. 12. Same as Fig. 9, but flux averaged for BEBC ν-spectrum, data from Ref. [32].

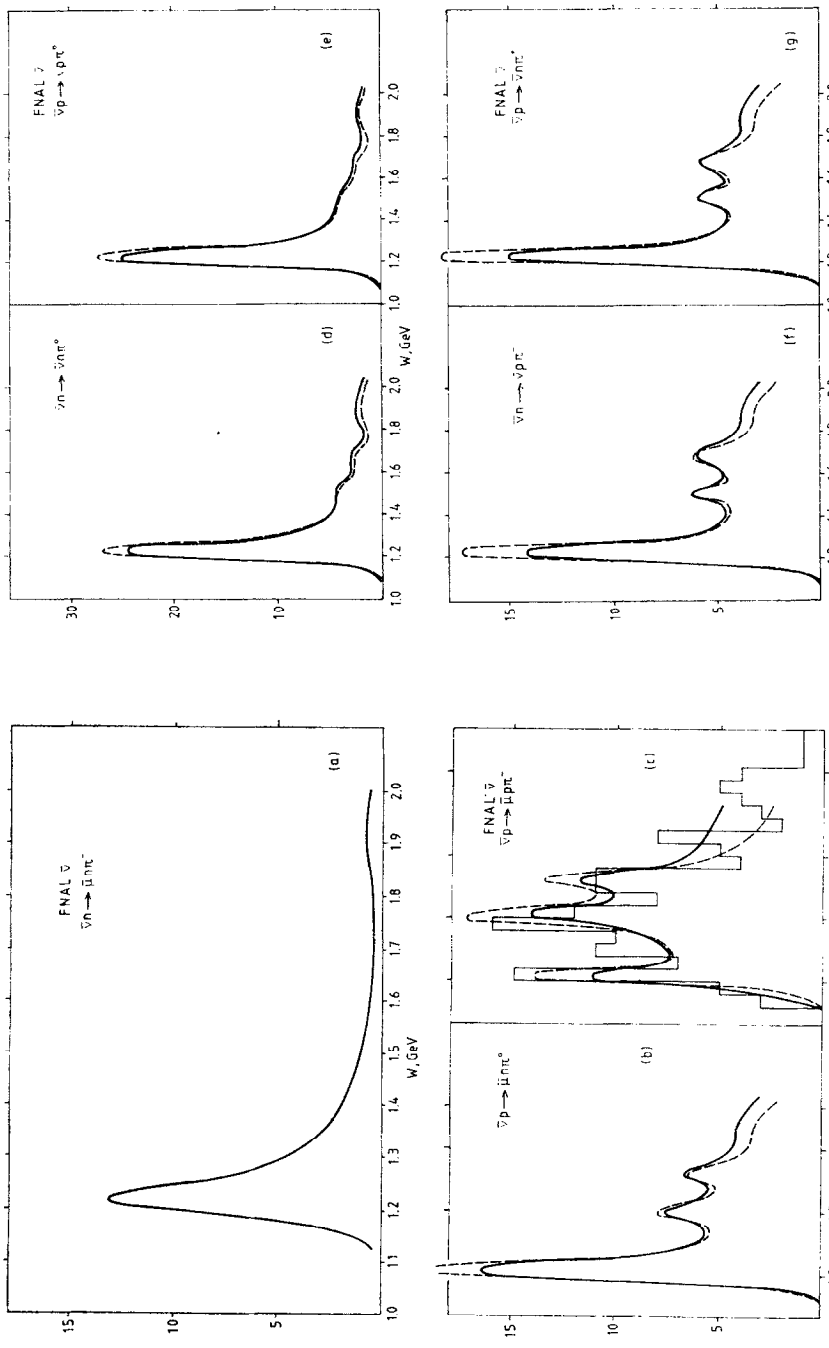

FIG. 13. Same as Fig. 9, but flux averaged for FNAL $\bar{\nu}$-spectrum, data from Ref. [47].

amplitudes have some W-dependence this does not lead to a large distortion of the resonance shape in $\mathcal{N}\pi$-production. So we must leave this as an open question for future theoretical and experimental investigation.

4.3. *Angular Distributions in Case of Several Interfering Resonances*

(a) *Two Interfering P_{33} Resonances in the $p\pi^+$ Channel*

Although the $\mu^- p\pi^+$ channel, as we have seen, is largely dominated by one single resonance $\Delta^{++} = P_{33}^{++}(1234)$ alone there are definitely higher $I = \frac{3}{2}$ resonances present, and even if they contribute only little to the cross section of that channel their interference with the leading $\Delta(1234)$ might not be so negligible. The $\mathcal{N}\pi$ angular distribution originating from the Δ^{++} decay alone was described in terms of density matrix elements $\tilde{\rho}_{33}$, $\tilde{\rho}_{31}$ and $\tilde{\rho}_{3-1}$, defined in Section 2.3. They are functions of q^2 and we have studied them in some detail in Section 4.1b. Now we consider the interference of the $\Delta(1234)$ with its nearest $I = \frac{3}{2}$ neighbour $P_{33}(1640)$ carrying the same quantum numbers I, j, P as the Δ itself. The next higher $I = \frac{3}{2}$ resonances are still further away from the $\Delta(1234)$ and therefore are assumed to give less contributions. The interference of the two P_{33} resonances causes the $\tilde{\rho}_{ik}$ to obtain also imaginary parts measuring essentially the overlap between the interfering states.

If two (or more) separate resonances do interfere we found it more natural to study the density matrix elements—or more generally, the coefficients of the spherical harmonics in the $\mathcal{N}\pi$ angular distribution—as a function of W rather than of q^2. This has the advantage of revealing quite clearly the changes which these quantities undergo when approaching the location of the perturbing resonance. We thus have plotted in Fig. 14, as one representative of the ρ_{ik}, the normalized quantity

$$\tilde{\rho}_{33,\mathrm{norm}}(W) = \{\rho_{3/2\,3/2}(W) + \rho_{-3/2\,-3/2}(W)\}/\tilde{\rho}(W) \equiv \hat{\rho}_{33}(W), \tag{4.12}$$

where

$$\tilde{\rho}(W) = \rho_{3/2\,3/2}(W) + \rho_{-3/2\,-3/2}(W) + \rho_{1/2\,1/2}(W) + \rho_{-1/2\,-1/2}(W).$$

For obtaining averaged numbers to be compared with experimental averages we integrated both the numerator and the denominator in Eq. (4.12) over an appropriate W-interval which was chosen here to range from threshold to $W = 2$ GeV. If there were no higher Δ's—as also indicated in Fig. 14—$\tilde{\rho}_{33,\mathrm{norm}}(W)$ would be a structureless, monotonically decreasing function of W. Because of the $P_{33}(1640)$, however, its slope changes when W approaches the higher resonance thus exhibiting nicely the effect of the interference. Although this effect is quite pronounced it would nevertheless be hard to measure it, since there are only a few events in this W-region and the statistical error is necessarily large.

(b) *Several Interfering Resonances in the Mixed Isospin Channel ($\mu^+ p\pi^-$)*

A more promising channel for investigating the effect of interfering resonances in the $\mathcal{N}\pi$ angular distribution is provided by the reaction $\bar{\nu}n \to \mu^+ p\pi^-$ at high energies

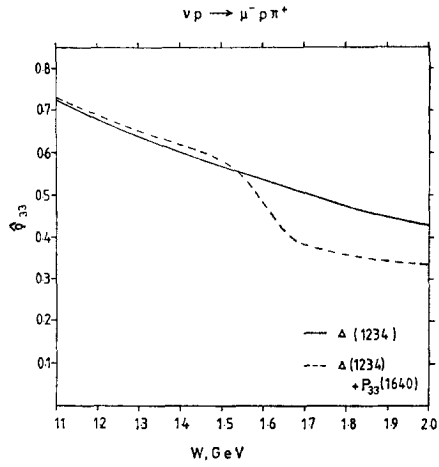

FIG. 14. $\hat{\rho}_{33}$ as function of W in the channel $\mu^- p\pi^+$ at BEBC assuming Δ^{++} to be the only resonance (full line), or assuming $\Delta^{++} - P_{33}(1640)$ interference (dashed).

which has been explored recently by the Carnegie–Mellon–Argonne–Purdue collaboration at Fermilab [47]. As evident from Fig. 13c the measured cross section does not lack in events in the resonance region around 1.5 GeV although the overall statistics is still small. The relatively high cross section in this W-domain, however, suggests the possibility of a substantial interference between the lowest lying $\Delta(1234)$ and the next higher $I = \frac{1}{2}$ resonances. So we may expect quite drastic distortions of the angular distribution as compared to the pure Δ case. In the following we thus pursue the interference of the four most important resonances below 1.7 GeV which are also most adjacent to each other. These are the $P_{33}(1234)$ or Δ-resonance and three $I = \frac{1}{2}$ resonances: $D_{13}(1525)$, $S_{11}(1540)$ and the Roper resonance $P_{11}(1450)$. Among those the Roper resonance, although least pronounced, is the most interesting object since it is the only resonance where the FKR model seemed to fail in predicting the sign of the photoproduction amplitude. It would be quite important to see whether this failure can be confirmed or disproved in neutrino reactions.

To this end we focussed our attention on the changes of the angular distribution terms which arise from reversing the sign of the production amplitudes of the Roper resonance. In order to keep disturbing interplay from higher resonances small we limited ourselves to the W region between threshold and $\sim$1.5 GeV. At $W = 1.5$ GeV essentially all higher resonances are off by more than half a width and hence should safely be negligible. The angular distribution of the pion in the $\mathcal{N}\pi$ center of mass system can be written in the form (see Appendix for more details):

$$\begin{aligned} W((p\pi^-);\theta,\phi) \propto \{&a_{00}Y_0^0 + a_{10}Y_1^0 + a_{20}Y_2^0 + a_{30}Y_3^0 \\ &+ a_{11}\mathrm{Re}\ Y_1^1 + a_{21}\mathrm{Re}\ Y_2^1 + a_{22}\mathrm{Re}\ Y_2^2 \\ &+ a_{31}\mathrm{Re}\ Y_3^1 + a_{32}\mathrm{Re}\ Y_3^2 \\ &+ b_{11}\mathrm{Im}\ Y_1^1 + b_{21}\mathrm{Im}\ Y_2^1 + b_{22}\mathrm{Im}\ Y_2^2 \\ &+ b_{31}\mathrm{Im}\ Y_3^1 + b_{32}\mathrm{Im}\ Y_3^2\}. \end{aligned} \tag{4.13}$$

The coefficients a_{ik}, b_{ik} are measurable relatively to each other at every value of W or in every W-interval. So it is convenient to normalize them with respect to a_{00} calling

$$\hat{a}_{ik}(W) = \frac{a_{ik}(W)}{a_{00}(W)}, \qquad \hat{b}_{ik}(W) = \frac{b_{ik}(W)}{a_{00}(W)}. \tag{4.14}$$

Then all $\hat{a}_{ik}$, $\hat{b}_{ik}$ attain values between -1 and $+1$. They are expressible in terms of generalized density matrix elements as given in the Appendix.

The angular distribution (4.13) originating from four interfering resonances with rather different quantum numbers I, J, P is much more involved than the corresponding formula (4.12) where only two resonances of equal quantum numbers were allowed to interfere. This complexity limits the number of resonances that can be included in considerations of this kind—not in principle, but in practice. In the present case, there exists a fairly extended W-domain where not more than four interfering resonances need to be considered. Even so the representations of the a_{ik} and b_{ik} in terms of generalized density matrix elements ρ_{ik}^{rs}, which in turn are products of single resonance production amplitudes, appeared to be so complicated that they had to be banished to the Appendix. Nevertheless everything is fixed by the model and all coefficients a_{ik} and b_{ik} are calculable as functions of the $\mathcal{N}\pi$ invariant energy W.

The coefficient a_{00} which serves as a normalization factor was evaluated to see whether it agrees grossly with the W-distribution—a_{00} would coincide in shape with the W-distribution if no interference term entered $d\sigma/dW$. This coming out correctly we selected those coefficients $\hat{a}_{ik}$, $\hat{b}_{ik}$ for display which showed appreciable size and variation in W. These have been plotted in Fig. 15a–f for three options:

(i) the signs of the Roper resonance matrix elements are chosen according to the prescriptions of the FKR model,

(ii) the Roper resonance is completely neglected,

(iii) the signs of the Roper resonance matrix elements are chosen opposite to those given by the FKR model.

All other coefficients are predicted to be in general nonzero but small.

Two features of the results are worth noting: First we observe that among the various coefficients the $\hat{b}_{11}$ and $\hat{b}_{21}$—corresponding to the imaginary parts of generalized density matrix elements—are quite large and comparable to the coefficients $\hat{a}_{10}$, $\hat{a}_{20}$, $\hat{a}_{11}$, $\hat{a}_{21}$ which contain only real parts of the ρ_{ik}^{rs}. This means that it would be misleading to term the $\hat{b}_{ik}$ or some of the $\hat{a}_{ik}$ "illegal" since all of them are really expected to exist in case of several interfering resonances and some of them are quite respectable.

A second equally important point concerns the behaviour of these coefficients under a change of sign of the Roper resonance. Inspection of Fig. 15 shows rather pronounced differences, concentrated between 1.3 and 1.5 GeV. This should be recognizable experimentally even if the data are not too abundant.

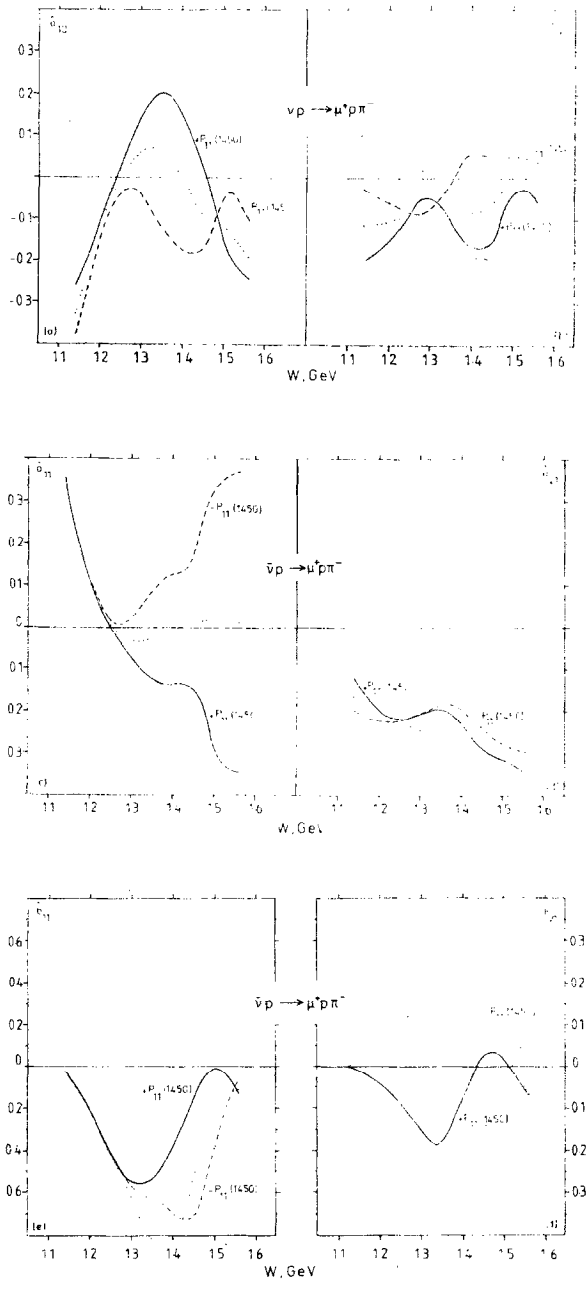

FIG. 15. Some coefficients $\hat{a}_{ik}$ and $\hat{b}_{ik}$ of the angular distribution in the $\mu^+p\pi^-$ channel at FNAL for interfering resonances $\Delta 1234$), $D_{13}(1525)$, $S_{11}(1540)$, $P_{11}(1450)$. Our prediction (full line) is compared with the cases $P_{11}(1450) \to -P_{11}(1450)$ (dashed) and $P_{11}(1450) \to 0$ (dotted).

TABLE XI

Selected Angular Coefficients in the $\mu^+ p\pi^-$ Channel at Fermilab/BEBC Energies (Flux Averaged), Normalized to $\int a_{00}(W)dW$ in the Interval: $1.08 < W < 1.4\ (1.55)$ GeV

	$\langle \hat{a}_{10} \rangle$		$\langle \hat{a}_{11} \rangle$		$\langle \hat{b}_{11} \rangle$		$\langle \hat{b}_{21} \rangle$	
	$W < 1.4$	$W < 1.55$	$W < 1.4$	$W < 1.55$	$W < 1.4$	$W < 1.55$	$W < 1.4$	$W < 1.55$
$\Delta(1234) + D_{13}(1525) + S_{11}(1540) + P_{11}(1450)$	+0.02	−0.04	+0.01	−0.10	−0.35	−0.25	−0.09	−0.06
$\Delta(1234) + D_{13}(1525) + S_{11}(1540)$	−0.05	−0.08	+0.05	+0.04	−0.42	−0.36	+0.01	+0.01
$\Delta(1234) + D_{13}(1525) + S_{11}(1540) - P_{11}(1450)$	−0.11	−0.11	+0.08	+0.17	−0.39	−0.39	+0.10	+0.08

Some average coefficients

$$\langle \hat{a}_{ik} \rangle = \int_{W_{\min}}^{W_1} dW\, a_{ik}(W) \Big/ \int_{W_{\min}}^{W_1} dW\, a_{00}(W) \tag{4.15}$$

($W_1 = 1.4$ or 1.55 GeV undergoing significant changes under sign reversal of the Roper matrix elements are collected in Table XI.

We should, however, keep in mind that all interference between resonances and nonresonant background has been left out so far although this might not be completely true. Thus our conclusions on angular distributions could change if such resonance–background interference turned out to be appreciable.

5. Conclusion

In this paper we made an attempt to explain all single pion production data up to an invariant $\mathcal{N}\pi$ energy of $W = 2$ GeV in a simple and coherent way using a suitable and well-tested quark model, the relativistic harmonic oscillator quark model of Feynman, Kislinger, and Ravndal. Extending the application of the model to the whole W domain between the $\mathcal{N}\pi$-threshold and 2 GeV and including essentially all resonances of that mass region, allowing them to interfere where they overlap we have gone beyond previous approaches in this field. Now at the end it is worthwhile to recall the assumptions on which calculations were based, and the conclusions which are to be drawn from successes and failures of resulting predictions.

The basic idea was to describe the amplitude for every final $\mathcal{N}\pi$ state (14 in all for CC and NC neutrino and antineutrino reactions) as a coherent superposition of all nucleon resonances between 1 and 2 GeV contributing to the particular $\mathcal{N}\pi$ channel under consideration. The charged and neutral current induced transition matrix elements from a ground state nucleon to a resonance are calculable in the oscillator quark model once the resonance state is specified by its SU_6 classification and its radial excitation mode. The only parameter of the model to be newly adjusted is the axial form factor mass m_A which was fixed to be $m_A = 0.95$ GeV. For neutral current interactions we employed the Salam–Weinberg theory with $\sin^2\theta_w$ put at 0.22. (The variation of some of the results with $\sin^2\theta_w$ was studied but no better agreement with data emerged from a different choice.) The resonance decay part, aside from a relative sign provided by the model, has been taken as an experimental input. In fact we assumed the resonance decay amplitude to be a Breit–Wigner form properly shaped and normalized, and including the measured elasticity factor which represents the probability amplitude for singling out the $\pi\mathcal{N}$ state among the decay products. In addition to resonances a small amount of a simple incoherent nonresonant background was included improving the agreement with experiment on cross sections and various cross section ratios at the expense of one additional constant.

As a result of calculations based on the FKR model, complemented by these addi-

tional assumptions, we found cross sections, W-distributions and angular distributions nicely in agreement with experimental measurements wherever data exist at lower or at higher energies. The most prominent Δ^{++} resonance as studied in the $\mu^- p\pi^+$ channel is well described by the FKR model. This is not surprising since its excitation in neutrino reactions is mostly determined by CVC and PCAC, and all models fulfilling these requirements agree among themselves on the Δ-cross section. A more striking result appears in the $(\bar{\nu}p \to \mu^+ p\pi^-)$ channel. This is the first place where higher resonances of isospin $\frac{1}{2}$ outshine the lowest lying Δ resonance which was by far the brightest one in other channels. There our calculations have almost quantitatively reproduced the measured excitation pattern up to 2 GeV. Our consideration of decay angular distributions led us to a generalization of the existing density matrix formalism adapted to the case of several interfering resonances. In the $\mu^- p\pi^+$ channel dominated by the Δ^{++} resonance we found small distortions of the angular distribution caused by a higher P_{33} resonance at $W = 1.64$ GeV/c^2 interfering with the tail of the $\Delta(1234)$. Quite substantial changes, however, are predicted to occur in the $I = \frac{1}{2}$ enhanced channels $\mu^- n\pi^+$ and $\mu^+ p\pi^-$, respectively. Here the four lowest lying resonances are found to interfere quite strongly leading to an angular distribution sensitive to any changes of relative signs. We show how various coefficients in the multipole expansion of this angular distribution change under reversal of the sign of the Roper resonance. This would constitute an independent determination of the signs of production amplitudes of this resonance which, unambiguously predicted by the FKR model, are the only ones at variance with experiments in photoproduction. It would be interesting to see whether the same discrepancy arises in neutrino-production experiments.

Comparison with other models reveals no dramatic differences in the low W-domain, which is the only domain in which predictions have previously been made. However, the models do differ in detail, and particularly in the vector/axial vector decomposition of cross sections, as exemplified by Table V. We have also tried to check the sensitivity of our results to specific ingredients of the FKR model, for example the damping factor $(1 - q^2/4m_{\mathcal{N}}^2)^{1/2-n}$ in the resonance transition form factor which depends on the number n of oscillator excitations. We found that dropping this factor led to a significant enhancement of the higher resonance region in compelling disagreement with data.

In comparing the model with experiment, we encountered only two possible signs of disagreement. The model—in common with other competing models—does not produce any sizeable asymmetry between neutral current π^0 production off protons and neutrons. The experimentally observed asymmetry [41] (which is, however, only a two standard deviation effect) ought to be checked by other measurements. Also, with our assumption of an incoherent $I = \frac{1}{2}$ background, we are unable to generate any angular asymmetries (around $\theta = \pi/2$ and $\phi = \pi$) in the $\mu^- p\pi^+$ channel, for which some hint exists in the data. This deficiency, however, is directly linked to our approximate treatment of the background amplitude, and does not detract from the success of the model in describing resonance production. We must conclude that the FKR model, embellished with a small amount of nonresonant background, can

provide a comprehensive understanding of a large amount of data on neutrino-production of single pions, giving added support to the basic picture of this process as a transition between different states of a 3-quark system, induced by external currents acting on quark constituents.

APPENDIX: ($N\pi$)-DENSITY MATRIX FORMALISM IN CASE OF SEVERAL INTERFERING RESONANCES

Our starting point is the general transition amplitude

$$\mathfrak{M}(\nu\mathcal{N} \to l\mathcal{N}\pi) = \sum_{\gamma} \langle \mathcal{N}\pi \mid \mathcal{N}_{\gamma}^{*} \rangle \langle \mathcal{N}_{\gamma}^{*}, l \mid \mathscr{H}_{W} \mid \mathcal{N}, \nu \rangle, \tag{A.1}$$

where the contributing resonances $\mathcal{N}_{\gamma}^{*}$ are labelled by a set of quantum numbers γ including isospin, spin and parity. The unitarized production amplitude $\langle \mathcal{N}_{\gamma}^{*}, l \mid \mathscr{H}_{W} \mid \mathcal{N}, \nu \rangle$ is denoted by T^{γ} and we call the projection amplitude on the final $\mathcal{N}\pi$ state

$$B^{\gamma} = \langle \mathcal{N}\pi \mid \mathcal{N}_{\gamma}^{*} \rangle. \tag{A.2}$$

For evaluating the angular distribution of the emitted particle π (or $\mathcal{N}$) in the rest frame of the resonance $\mathcal{N}_{\gamma}^{*}$ (identical to the CMS of particles π and $\mathcal{N}$) we have to specify their angles relative to a fixed direction. According to Gottfried and Jackson [15] this is best done in terms of helicity amplitudes and we shall follow their guidelines. Let $|(N\pi)\theta, \phi; \lambda_{\mathcal{N}}, \lambda_{\pi} = 0\rangle$ denote the two particle plane wave state containing helicity and angular information of the final state configuration. It can be expanded into angular momentum eigenstates according to

$$|(\mathcal{N}\pi), \theta, \varphi; \lambda_{\mathcal{N}}, \lambda_{\pi}\rangle = \sum_{j, j_z} |j, j_z, \lambda_{\mathcal{N}}, \lambda_{\pi}\rangle \sqrt{\frac{2j+1}{4\pi}}\, D^{j}_{j_z\lambda}(\varphi, \theta, 0) \tag{A.3}$$

with the usual definitions

$$\lambda = \lambda_{\mathcal{N}} - \lambda_{\pi} = \lambda_{\mathcal{N}},$$

$$D^{j}_{j_z\lambda}(\varphi, \theta, 0) = e^{-ij_z\varphi}\, d^{j}_{j_z\lambda}(\theta). \tag{A.4}$$

Separating the angular momentum quantum numbers from the rest of γ we may write more explicitly instead of (A.2)

$$B^{\gamma}_{j_z}(\theta, \varphi; \lambda_{\mathcal{N}}, \lambda_{\pi}) = \langle (\mathcal{N}\pi), \theta, \varphi; \lambda_{\mathcal{N}}, \lambda_{\pi} \mid \gamma; j, j_z \rangle$$

$$= \sqrt{\frac{2j+1}{4\pi}} \langle j, j_z; \lambda_{\mathcal{N}}, \lambda_{\pi} \mid \gamma; j, j_z \rangle\, D^{j*}_{j_z\lambda}(\varphi, \theta, 0). \tag{A.5}$$

Obviously the matrix element in the angular momentum basis is rotationally invariant

and does not depend on the magnetic quantum number j_z. It contains, however, the parity and isospin assignments of the states involved.

We may therefore abbreviate $\langle j, j_z ; \lambda_N, \lambda_\pi \mid \gamma ; j, j_z \rangle$ by $K^\nu(\lambda_N, \lambda_\pi) = K^\nu(\lambda)$ showing the reflection symmetry property

$$K^\nu(-\lambda_\mathcal{N}, -\lambda_\pi) = \zeta_\mathcal{N}\zeta_\pi\zeta_\nu(-1)^{j-s_\mathcal{N}-s_\pi} \cdot K^\nu(\lambda\ldots, \lambda_\pi) \tag{A.6}$$

with ζ_N, ζ_π, ζ_ν denoting the intrinsic paritties of the corresponding particles. Since $s_\pi = \lambda_\pi = 0$ and $s_\mathcal{N} = \frac{1}{2}$ there is only one $K^\nu(\lambda)$ for each resonance $\mathcal{N}^*_\nu$ with definite I, j, P, and this reduces to an isospin Clebsch–Gordan coefficient

$$C[(N\pi)\, I, I_3] = \begin{pmatrix} I^N & I^\pi \\ I_3{}^N & I_3{}^\pi \end{pmatrix} \Bigg| \begin{matrix} I \\ I_3 \end{matrix}\Bigg).$$

In the following we may drop λ_π without losing transparency.

The whole transition matrix element (A.1) then takes the form

$$\mathfrak{M}\left[\nu + \mathcal{N}(s_z) \to l + \sum_\nu \mathcal{N}^*_\nu \to l + \{(\mathcal{N}(\lambda_\mathcal{N}), \pi(\lambda_\pi)), \theta, \varphi\}\right]$$

$$= \sum_{\nu, j_z} T^\nu_{s_z j_z} \cdot B^\nu_{j_z}(\theta, \varphi; \lambda_\mathcal{N}) \tag{A.7}$$

and the (normalized) decay angular distribution is given by

$$W(\theta, \varphi) = \frac{\sum \mathfrak{M}\mathfrak{M}^*}{\int d\Omega \sum \mathfrak{M}\mathfrak{M}^*} \propto \sum T^\nu_{s_z j_z}(T^{\nu'}_{s_z j'_z})^*\, B^\nu_{j_z}(\theta, \varphi; \lambda_\mathcal{N})[B^{\nu'}_{j'_z}(\theta, \varphi; \lambda_\mathcal{N})]^*, \tag{A.8}$$

where we have to sum over the intermediate quantum numbers j_z, j'_z and $\gamma\gamma'$ and on final and initial helicities if no nucleon polarization is measured. Hence

$$W((\mathcal{N}\pi)\, I_3 ; \theta, \varphi)$$

$$= \frac{1}{2s_N + 1} \sum_{s_z = \pm 1/2} \sum_{\lambda = \pm 1/2} \sum_{j_z, j'_z} \sum_{\nu, \nu'} \sqrt{\frac{2j+1}{4\pi}} \sqrt{\frac{2j'+1}{4\pi}}$$

$$\times D^{j*}_{j_z \lambda}(\varphi, \theta, 0)\, D^{j'}_{j'_z \lambda}(\varphi, \theta, 0)\, K^\nu(\lambda)(K^{\nu'}(\lambda))^*\, T^\nu_{s_z j_z}(T^{\nu'}_{s_z j'_z})^*$$

$$= \sum_{j_z, j'_z} \sum_{\nu, \nu'} \sqrt{\frac{2j+1}{4\pi}} \sqrt{\frac{2j'+1}{4\pi}} \sum_{\lambda = \pm 1/2} e^{i(j_z - j'_z)\varphi}\, d^j_{j_z \lambda}(\theta)\, d^{j'}_{j'_z \lambda}(\theta)\, K^\nu(\lambda)\, K^{\nu'*}(\lambda)\, \rho^{\nu\nu'}_{j_z j'_z}, \tag{A.9}$$

where γ stands for the triple of quantum numbers (I, j, P) of the resouance $\mathcal{N}^*$. We have defined a *generalized* density matrix by

$$\rho^{\nu\nu'}_{j_z j'_z} = \tfrac{1}{2} \sum_{s_z = \pm 1/2} T^\nu_{s_z j_z}(T^{\nu'}_{s_z j'_z})^* \tag{A.10}$$

which may be normalized according to

$$\sum_{\nu, j_z} \rho^{\nu\nu}_{j_z j_z} = 1. \tag{A.11}$$

Expression (A.9) can be simplified by use of Eq. (A.6)

$$K^{\nu}(-\lambda) = (-1)^{j+1/2}\zeta_{\nu} C[(\mathcal{N}\pi)I, I_3]. \tag{A.12}$$

Defining

$$Z^{jj'\lambda\pm}_{j_z j'_z}(\theta) = d^{j}_{j_z\lambda}(\theta)\, d^{j'}_{j'_z\lambda}(\theta) \pm d^{j}_{j_z-\lambda}(\theta)\, d^{j'}_{j'_z-\lambda}(\theta) \tag{A.13}$$

with the obvious symmetry property

$$Z^{jj'\lambda\pm}_{j_z j_z}(\theta) = Z^{j'j\lambda\pm}_{j'_z j_z}(\theta) \tag{A.14}$$

we then obtain the desired generalized angular distribution of pions in the $\mathcal{N}\pi$-center of mass frame:

$$W((\mathcal{N}\pi)\, I_3\, ;\, \theta, \varphi) = \sum_{j_z j'_z} \sum_{\substack{j, j', I, I' \\ P, P'}} \sqrt{\frac{2j+1}{4\pi}} \sqrt{\frac{2j'+1}{4\pi}}\, C[(\mathcal{N}\pi)\, I, I_3]\, C[(\mathcal{N}\pi)\, I', I_3]$$

$$\times\, Z^{jj'\mathbf{1}/2\sigma}_{j_z j'_z}(\theta)\, \mathrm{Re}\{e^{i(j_z - j'_z)\varphi} \rho^{(IjP),(I'j'P')}_{j_z j'_z}\}, \tag{A.15}$$

where the sign σ, obtained by means of Eq. (A.12), is positive if the interfering resonances have both equal spins (note that $2j$ is always odd) and equal parities, or if they have unequal parities and spins differing by one unit. For all other configurations σ is negative.

Equation (A.15) is our general result used in Section 2.3, and will be subsequently discussed in some detail.

(i) A first remark applies to interfering resonances of equal parity. Since the decay process conserves parity the decay angular distribution can include only spherical harmonics of even rank. Consider for example two resonances with $j^P = \frac{3}{2}^+$. Then all angular momenta between 0 and $2J = 3$ could occur but parity selects only two of them, namely $l = 0, 2$. On the other hand resonances with equal j but different parities—which may well be produced simultaneously through the parity violating weak interaction—will generate all spherical harmonics up to $l_{\max} = 2j$.

(ii) In the $(p\pi^+)$ channel probably the dominant interference takes place between two resonances of the same (I, j, P), namely, $P_{33}(1236)$ and $P_{33}(1640)$. In this case the angular distribution is only slightly different from the corresponding distribution of a pure P_{33} resonance:

$$W(\theta, \varphi) = \sqrt{\frac{1}{\pi}}\frac{1}{\rho}\left\{Y_0^0\rho - \frac{2}{\sqrt{5}}Y_2^0\left(\tilde{\rho}_{33} - \frac{1}{2}\rho\right) + \frac{4}{\sqrt{10}}\,\mathrm{Re}\,Y_2^1\,\mathrm{Re}\,\tilde{\rho}_{31}\right.$$
$$\left. - \frac{4}{\sqrt{10}}\,\mathrm{Re}\,Y_2^2\,\mathrm{Re}\,\tilde{\rho}_{3-1} - \frac{4}{\sqrt{10}}\,\mathrm{Im}\,Y_2^1\,\mathrm{Im}\,\tilde{\rho}_{31} + \frac{4}{\sqrt{10}}\,\mathrm{Im}\,Y_2^2\,\mathrm{Im}\,\tilde{\rho}_{3-1}\right\}. \tag{A.16}$$

We only have to note the more complicated structure of $\rho_{mm'}$:

$$\rho_{mm'} = \sum_{r,s=1}^{2} \rho_{mm'}^{rs}, \qquad \rho = \sum_m \rho_{mm}\,. \tag{A.17}$$

Since $\rho_{mm'}$ now gets contributions from two resonances differing in their production matrix elements including the Breit–Wigner phases the nondiagonal elements with $r \neq s$ are in general complex. This was also noted in the text.

(iii) In the mixed isospin channel ($\nu n \to \mu n\pi^+$) or likewise ($\bar{\nu}p \to \mu^+ p\pi^-$), which is easier to measure things get more complicated since at least three prominent $I = \frac{1}{2}$ resonances are close to the leading $P_{33}(1236)$. Those are the even parity $P_{11}(1450)$ and the odd parity resonances $D_{13}(1525)$ and $S_{11}(1540)$. We have developed our basic formula (A.15) to cover this situation and found the following result containing contributions from all $\pi\mathcal{N}$ orbital angular momenta up to $l = 3$.

$$W(\theta, \varphi) = \frac{1}{3}\sqrt{\frac{1}{\pi}}\{a_{00}Y_0^0 + a_{10}Y_1^0 + a_{20}Y_2^0 + a_{30}Y_3^0$$
$$+ a_{11}\,\mathrm{Re}\,Y_1^1 + a_{21}\,\mathrm{Re}\,Y_2^1 + a_{22}\,\mathrm{Re}\,Y_2^2$$
$$+ a_{31}\,\mathrm{Re}\,Y_3^1 + a_3^2\,\mathrm{Re}\,Y_3^2 + b_{11}\,\mathrm{Im}\,Y_1^1 + b_{21}\,\mathrm{Im}\,Y_2^1$$
$$+ b_{22}\,\mathrm{Im}\,Y_2^2 + b_{31}\,\mathrm{Im}\,Y_3^1 + b_{32}\,\mathrm{Im}\,Y_3^2 + a_{33}\,\mathrm{Re}\,Y_3^3 + b_{33}\,\mathrm{Im}\,Y_3^3\}. \tag{A.18}$$

The coefficients a_{ik} , b_{ik} are rather complicated combinations of generalized density matrix elements given by the following set of equations where:

$$a_{00} = \{\rho^{\Delta\Delta} + 2(\rho^{DD} + \rho^{PP} + \rho^{SS})\}, \tag{A.19a}$$

$$a_{10} = \mathrm{Re}\left\{\frac{2}{5}\sqrt{6}\,(\rho^{\Delta D}_{3/2\,3/2} - \rho^{\Delta D}_{-3/2\,-3/2}) + \frac{2}{15}\sqrt{6}\,(\rho^{\Delta D}_{1/2\,1/2} - \rho^{\Delta D}_{-1/2\,-1/2})\right.$$
$$+ \frac{4}{3}\sqrt{3}\,(\rho^{PS}_{1/2\,1/2} - \rho^{PS}_{-1/2\,-1/2})$$
$$\left. + \frac{4}{3}\sqrt{3}\,(\rho^{\Delta S}_{1/2\,1/2} + \rho^{\Delta S}_{-1/2\,-1/2}) + \frac{4}{3}\sqrt{6}\,(\rho^{DP}_{1/2\,1/2} + \rho^{DP}_{-1/2\,-1/2})\right\}, \tag{A.19b}$$

$$a_{20} = -\frac{2}{5}\sqrt{5}\left(\rho^{\Delta\Delta}_{3/2\,3/2}+\rho^{\Delta\Delta}_{-3/2\,-3/2}-\frac{1}{2}\rho^{\Delta\Delta}\right)$$
$$-\frac{4}{5}\sqrt{5}\left(\rho^{DD}_{3/2\,3/2}+\rho^{DD}_{-3/2\,-3/2}-\frac{1}{2}\rho^{DD}\right)$$
$$-\mathrm{Re}\left\{\frac{4}{5}\sqrt{5}\,(\rho^{\Delta P}_{1/2\,1/2}-\rho^{\Delta P}_{-1/2\,-1/2})+\frac{4}{5}\sqrt{10}\,(\rho^{DS}_{1/2\,1/2}-\rho^{DS}_{-1/2\,-1/2})\right\}, \tag{A.19c}$$

$$a_{30} = \mathrm{Re}\left\{-\frac{6}{35}\sqrt{14}\,(\rho^{\Delta D}_{3/2\,3/2}-\rho^{\Delta D}_{-3/2\,-3/2})-\frac{18}{35}\sqrt{14}\,(\rho^{\Delta D}_{1/2\,1/2}-\rho^{\Delta D}_{-1/2\,-1/2})\right\}, \tag{A.19d}$$

$$a_{11} = \mathrm{Re}\left\{-\frac{4}{5}\,(\rho^{\Delta D}_{3/2\,1/2}+\rho^{\Delta D}_{-1/2\,-3/2}+\rho^{\Delta D}_{1/2\,3/2}+\rho^{\Delta D}_{-3/2\,-1/2})\right.$$
$$-\frac{4}{3}\sqrt{6}\,(\rho^{PS}_{1/2\,-1/2}+\rho^{PS}_{-1/2\,1/2})-\frac{4}{15}\sqrt{3}\,(\rho^{\Delta D}_{1/2\,-1/2}+\rho^{\Delta D}_{-1/2\,1/2})$$
$$+2\sqrt{3}\,(\rho^{\Delta S}_{3/2\,1/2}-\rho^{\Delta S}_{-3/2\,-1/2})+4(\rho^{DP}_{3/2\,1/2}-\rho^{DP}_{-3/2\,-1/2})$$
$$\left.-2\sqrt{6}\,(\rho^{\Delta S}_{1/2\,-1/2}-\rho^{\Delta S}_{-1/2\,1/2})+4\sqrt{3}\,(\rho^{DP}_{1/2\,-1/2}-\rho^{DP}_{-1/2\,1/2})\right\}, \tag{A.19e}$$

$$a_{21} = \frac{2}{5}\sqrt{10}\,[\rho^{\Delta\Delta}_{3/2\,1/2}-\rho^{\Delta\Delta}_{-1/2\,-3/2}+2(\rho^{DD}_{32/\,1/2}-\rho^{DD}_{-1/2\,-3/2})]$$
$$-\mathrm{Re}\left\{\frac{2}{5}\sqrt{10}\,(\rho^{\Delta P}_{3/2\,1/2}+\rho^{\Delta P}_{-3/2\,-1/2})+\frac{4}{5}\sqrt{5}\,(\rho^{DS}_{3/2\,1/2}+\rho^{DS}_{-3/2\,-1/2})\right.$$
$$\left.-\frac{2}{5}\sqrt{30}\,(\rho^{\Delta P}_{1/2\,-1/2}+\rho^{\Delta P}_{-1/2\,1/2})-\frac{4}{5}\sqrt{15}\,(\rho^{DS}_{1/2\,-1/2}-\rho^{DS}_{-1/2\,1/2})\right\}, \tag{A.19f}$$

$$a_{22} = -\frac{2}{5}\sqrt{10}\,[\rho^{\Delta\Delta}_{3/2\,-1/2}+\rho^{\Delta\Delta}_{1/2\,-3/2}+2(\rho^{DD}_{3/2\,-1/2}+\rho^{DD}_{1/2\,-3/2})]$$
$$-\mathrm{Re}\left\{-\frac{4}{5}\sqrt{10}\,(\rho^{\Delta P}_{3/2\,-1/2}-\rho^{\Delta P}_{-3/2\,1/2})\right.$$
$$\left.-\frac{8}{5}\sqrt{5}\,(\rho^{DS}_{3/2\,-1/2}-\rho^{DS}_{-3/2\,1/2})\right\}, \tag{A.19g}$$

$$a_{31} = \mathrm{Re}\left\{\frac{12}{35}\sqrt{14}\,(\rho^{\Delta D}_{3/2\,1/2}+\rho^{\Delta D}_{-1/2\,-3/2}+\rho^{\Delta D}_{1/2\,3/2}+\rho^{\Delta D}_{-3/2\,-1/2})\right.$$
$$\left.-\frac{6}{35}\sqrt{42}\,(\rho^{\Delta D}_{1/2\,-1/2}+\rho^{\Delta D}_{-1/2\,1/2})\right\}, \tag{A.19h}$$

$$a_{32} = \mathrm{Re}\left\{-\frac{12}{35}\sqrt{35}\,(\rho^{\Delta D}_{3/2\,-1/2}-\rho^{\Delta D}_{1/2\,-3/2}+\rho^{\Delta D}_{-1/2\,3/2}-\rho^{\Delta D}_{-3/2\,1/2})\right\}, \tag{A.19i}$$

$$a_{33} = 0. \tag{A.19j}$$

$$b_{11} = \mathrm{Im}\left\{\frac{4}{5}(\rho^{\Delta D}_{3/2\,1/2} + \rho^{\Delta D}_{-1/2\,-3/2} - \rho^{\Delta D_1}_{1/2\,3/2} - \rho^{\Delta D}_{-3/2\,-1/2}) + \frac{4}{3}\sqrt{6}\,(\rho^{PS}_{1/2\,-1/2} - \rho^{PS}_{-1/2\,1/2}) + \frac{4}{15}\sqrt{3}\,(\rho^{\Delta D}_{1/2\,-1/2} - \rho^{\Delta D}_{-1/2\,1/2}) - 2\sqrt{2}\,(\rho^{\Delta S}_{3/2\,1/2} + \rho^{\Delta S}_{-3/2\,-1/2}) - 4(\rho^{DP}_{3/2\,1/2} + \rho^{DP}_{-3/2\,-1/2}) - 2\sqrt{6}\,(\rho^{\Delta S}_{1/2\,-1/2} + \rho^{\Delta S}_{-1/2\,1/2}) - 4\sqrt{3}\,(\rho^{DP}_{1/2\,-1/2} + \rho^{DP}_{-1/2\,1/2})\right\}, \quad \text{(A.19k)}$$

$$b_{21} = \mathrm{Im}\left\{-\frac{2}{5}\sqrt{10}\,(\rho^{\Delta P}_{3/2\,1/2} - \rho^{\Delta P}_{-3/2\,-1/2}) - \frac{4}{5}\sqrt{5}\,(\rho^{DS}_{3/2\,1/2} - \rho^{DS}_{-3/2\,-1/2}) + \frac{2}{5}\sqrt{30}\,(\rho^{\Delta P}_{1/2\,-1/2} - \rho^{\Delta P}_{-1/2\,1/2}) + \frac{4}{5}\sqrt{15}\,(\rho^{DS}_{1/2\,-1/2} - \rho^{DS}_{-1/2\,1/2})\right\}, \quad \text{(A.19l)}$$

$$b_{22} = \mathrm{Im}\left\{\frac{4}{5}\sqrt{10}\,(\rho^{\Delta P}_{3/2\,-1/2} + \rho^{\Delta P}_{-3/2\,1/2}) + \frac{8}{5}\sqrt{5}\,(\rho^{DS}_{3/2\,-1/2} + \rho^{DS}_{-3/2\,1/2})\right\}, \quad \text{(A.19m)}$$

$$b_{31} = \mathrm{Im}\left\{-\frac{12}{35}\sqrt{14}\,(\rho^{\Delta D}_{3/2\,1/2} + \rho^{\Delta D}_{-1/2\,-3/2} - \rho^{\Delta D}_{1/2\,3/2} - \rho^{\Delta D}_{-3/2\,-1/2}) + \frac{6}{35}\sqrt{42}\,(\rho^{\Delta D}_{1/2\,-1/2} - \rho^{\Delta D}_{-1/2\,1/2})\right\}, \quad \text{(A.19n)}$$

$$b_{32} = \mathrm{Im}\left\{\frac{12}{35}\sqrt{35}\,(\rho^{\Delta D}_{3/2\,-1/2} - \rho^{\Delta D}_{1/2\,-3/2} - \rho^{\Delta D}_{-1/2\,3/2} + \rho^{\Delta D}_{-3/2\,1/2})\right\}, \quad \text{(A.19o)}$$

$$b_{33} = 0. \quad \text{(A.19p)}$$

It remains to express the various density matrix elements in terms of the helicity amplitudes of the respective resonances. This is done by recalling the definition (A.10) of $\rho^{\nu\nu'}_{mm'}$:

$$\rho^{\nu\nu'}_{j_z j_z'} = \tfrac{1}{2} \sum_{s_z = \pm 1/2} (T^{\nu}_{s_z j_z})(T^{\nu'}_{s_z j_z'})^*,$$

where $T^{\nu}_{s_z j_z}$ is the weak production amplitude of the resonance $\mathcal{N}^*_\nu$ in the helicity state j_z including its proper Breit–Wigner amplitude $(\eta^\nu)^*$

$$T^{\nu}_{s_z j_z} = \langle \mathcal{N}^*_\nu(j_z), l \mid \mathscr{H}_W \mid \mathcal{N}(s_z), \nu\rangle (\eta^\nu)^*. \quad \text{(A.20)}$$

According to Eq. (2.11) this is written

$$T^{\nu}_{s_z j_z} = -4GWE\left\{\sqrt{\frac{-q^2}{Q^2}}\,\langle \mathcal{N}^*_\nu, j_z \mid uF_- - vF_+ \mid \mathcal{N}, s_z\rangle + \frac{m_{\mathcal{N}}}{W}\,\langle \mathcal{N}^*_\nu, j_z \mid F_0\sqrt{2uv} \mid \mathcal{N}, s_z\rangle\right\}(\eta^\nu)^*, \quad \text{(A.21)}$$

which may be cast into the form

$$T^{\nu}_{s_z j_z} = \{\alpha(-f^{\nu}_{+|2j_z|})\,\delta_{j_z,s_z-1} - \beta(-f^{\nu}_{-|2j_z|})\,\delta_{j_z,s_z+1} + \delta(f^{\nu}_{0\,\mathrm{sgn}(s_z)})\,\delta_{j_z,s_z}\}(\eta^{\nu})^*. \quad \text{(A.22)}$$

Herein the following abbreviations have been used:

$$\begin{aligned} \alpha &= -4GWE\sqrt{\frac{-q^2}{Q^2}}\,u, \\ \beta &= -4GWE\sqrt{\frac{-q^2}{Q^2}}\,v, \\ \delta &= -4GWE\,\frac{m_{\mathcal{N}}}{W}\sqrt{2uv}. \end{aligned} \quad \text{(A.23)}$$

Incorporating the decay factor $(\eta^{\nu})^*$ into the matrix elements we finally obtain according to Eq. (2.30)

$$T^{\nu}_{s_z j_z} = \{-\alpha(a^{\nu}_{|2j_z|})^*\,\delta_{j_z,s_z-1} + \beta(a^{\nu}_{-|2j_z|})^*\,\delta_{j_z,s_z+1} + \delta(a^{\nu}_{0\,\mathrm{sgn}(s_z)})^*\,\delta_{j_z,s_z}\} \quad \text{(A.24)}$$

and correspondingly

$$(T^{\nu'}_{s_z j_z'})^* = \{-\alpha a^{\nu'}_{|2j_z'|}\,\delta_{j_z',s_z-1} + \beta a^{\nu'}_{-|2j_z'|}\,\delta_{j_z',s_z+1} + \delta a^{\nu'}_{0\,\mathrm{sgn}(s_z)}\,\delta_{j_z',s_z}\}. \quad \text{(A.25)}$$

With the matrix elements T^{ν} now at hand we may easily evaluate every density matrix element of interest. For example,

$$\begin{aligned} \rho^{\Delta D}_{3/2\,3/2} &= \tfrac{1}{2}\sum_{s_z=\pm 1/2}\{-\alpha(a^{\Delta}_{+3})^*\,\delta_{3/2,s_z-1} + \beta(a^{\Delta}_{-3})^*\,\delta_{3/2,s_z+1} + \delta(a^{\Delta}_{0\,\mathrm{sgn}(s_z)})^*\,\delta_{3/2,s_z} \\ &\quad \cdot\{-\alpha a^{D}_{+3}\,\delta_{3/2,s_z-1} + \beta a^{D}_{-3}\,\delta_{3/2,s_z+1} + \delta(a^{D}_{0\,\mathrm{sgn}(s_z)})\,\delta_{3/2,s_z}\} \\ &= \tfrac{1}{2}\beta^2(a^{\Delta}_{-3}(q^2, W))^*\,a^{D}_{-3}(q^2, W) \\ &= \tfrac{1}{2}\beta^2 f^{\Delta}_{-3}(q^2, W) f^{D}_{-3}(q^2, W)(\eta^{\Delta}(W))^*\,\eta^{D}(W) \end{aligned} \quad \text{(A.26)}$$

and all other density matrix elements appearing in Eq. (A.19) are found in the same way.

This completes our discussion of resonance interference patterns in the $\mathcal{N}\pi$-angular distributions. Other cases of interest may be treated accordingly.

ACKNOWLEDGMENTS

We thankfully acknowledge untiring encouragement and advice from Professor Helmut Faissner. We have profited much from conversation and/or correspondence, with Drs. R. M. Barnett, A. J. G. Hey, E. H. Monsay, L. Oliver and F. Ravndal. We are deeply indebted to our experimental colleagues at Aachen who participated in the Aachen–Padua, Gargamelle and BEBC measurements. Special

thanks go to Drs. Martin Pohl from the Gargamelle collaboration and P. Allen from BEBC who met our questions and inquiries concerning the data with never-ending patience and cooperation. We would like to thank Professor R. Rodenberg for reading the final manuscript, and the German Bundesministerium für Forschung und Technologie for financial support.

REFERENCES

1. R. P. FEYNMAN, M. KISLINGER, AND F. RAVNDAL, *Phys. Rev. D* **3** (1971), 2706.
2. G. KNIES, R. G. MOORHOUSE, AND H. OBERLACK, *Phys. Rev. D* **9** (1974), 2680; R. G. MOORHOUSE, *in* "Electromagnetic Interactions of Hadrons" (A. Donnachie and G. Shaw, Ed.), Vol. 1, Plenum, New York/London, 1976, and references quoted therein.
3. F. RAVNDAL, *Nuovo Cimento A* **18** (1973), 385; *Lett. Nuovo Cimento* **3** (1972), 631.
4. R. E. CUTKOSKY *et al.*, *Phys. Rev. D* **20** (1979), 2839.
5. G. HÖHLER *et al.*, "Handbook of Pion–Nucleon-Scattering," Fachinformationszentrum Energie, Physik, Mathematik, Karlsruhe 1979, Physik Daten, Vol. 12-7.
6. S. ADLER, *Ann. Phys. (N.Y.)* **50** (1968), 89; *Phys. Rev. D* **12** (1975), 2644; S. ADLER *et al.*, *Phys. Rev. D* **13** (1976), 1216.
7. P. SCHREINER, F. VON HIPPEL, *Nucl. Phys. B* **58** (1973), 333.
8. L. F. ABBOTT AND R. M. BARNETT, *Phys. Rev. D* **18** (1978), 3214; E. H. MONSAY, *Phys. Rev. D* **18** (1978), 2277.
9. P. ANDREADIS *et al.*, *Ann. Phys. (N.Y.)* **88** (1974), 242; A. LE YAOUANC *et al.*, *Nucl. Phys. B* **125** (1977), 243.
10. T. ABDULLAH AND F. CLOSE, *Phys. Rev. D* **5** (1972), 2332.
11. G. L. FOGLI AND G. NARDULLI, *Nucl. Phys. B* **160** (1979), 116; **165** (1980), 162.
12. C. H. LLEWELLYN SMITH, *Phys. Rep. C* **3** (1972), 264, and further references quoted therein.
13. K. SASAKI, *Nucl. Phys. B* **110** (1976), 434; J. G. KÖRNER, T. KOBAYASHI, AND C. AVILEZ, *Phys. Rev. D* **18** (1978), 3178; V. F. DUSHENKO *et al.*, *Soviet J. Nucl. Phys.* **24** (1976), 344; M. BLAGOJEVIC, preprint Boris Kidric Institute, Beograd, BK1-TP13, July 1979.
14. See, e.g., Particle Data Group, "Review of Particle Properties," April 1980 ed., reprinted from *Rev. Mod. Phys.* **52**, No. 2 (1980), 34.
15. K. GOTTFRIED AND J. D. JACKSON, *Nuovo Cimento* **33** (1964), 309; J. D. JACKSON, Les Houches 1965, p. 327.
16. R. L. WALKER, *Phys. Rev.* **182** (1969), 1729.
17. S. L. ADLER, "Proceedings of the VI Hawaii Topical Conference in Particle Physics, 1975" (P. N. Dobson, S. Pakvasa, V. Z. Peterson, and S. F. Tuan, Eds.), Honolulu 1976.
18. R. P. FEYNMAN, "Photon Hadron Interactions," Benjamin, Reading, Mass., 1972; see also Ref. [1, Appendix] and Ref. [17].
19. P. N. BOGOLIUBOV, *Ann. Inst. Henri Poincaré A* **8** (1968), 162.
20. S. GLASHOW, *Nucl. Phys.* **22** (1961), 579; S. WEINBERG, *Phys. Rev. Lett.* **19** (1967), 1264; A. SALAM, *in* "Elementary Particle Theory" (N. Svartholm, Ed.), p. 367, Almquist & Wiksells, Stockholm, 1968.
21. F. SCIULLI, "Proceedings of the Topical Conference on Neutrino Physics, Oxford, 1978" (A. G. Michette and P. B. Renton, Eds.), p. 405, Oxford, 1978.
22. R. L. WALKER, "Proceedings of the 4th International Symposium on Electron and Photon Interactions at High Energies, Liverpool, 1970" (D. W. Braben and R. E. Rand, Eds.), Daresbury, 1970; see also Ref. [16].
23. W. J. METCALF AND R. L. WALKER, *Nucl. Phys. B* **76** (1974), 253; R. G. MOORHOUSE AND H. OBERLACK, *Phys. Lett. B* **43** (1973), 44; see also Ref. [2].
24. F. RAVNDAL, *Phys. Rev. D* **4** (1971), 1466.
25. M. DEWIT, "Proceedings of the Topical Conference on Neutrino Physics, Oxford, 1978" (A. G. Michette and P. B. Renton, Eds.), p. 75, Oxford, 1978.

26. M. ROLLIER, "Proceedings of the Topical Conference on Neutrino Physics, Oxford, 1978" A. G. Michette and P. B. Renton, Eds.), p. 68, Oxford, 1978.
27. T. EICHTEN *et al.*, *Phys. Lett. B* **46** (1973), 281.
28. J. J. SAKURAI, *Phys. Rev. Lett.* **35** (1975), 1037.
29. G. LEVMAN, "Proceedings of the Topical Conference on Neutrino Physics, Oxford, 1978" (A. G. Michette and P. B. Renton, Eds.), p. 58, Oxford, 1978.
30. S. J. BARISH *et al.*, *Phys. Rev. D* **19** (1979), 2521; J. CAMPBELL *et al.*, *Phys. Rev. Lett.* **30** (1973), 335.
31. J. BELL *et al.*, *Phys. Rev. Lett.* **41** (1978), 1008, 1012.
32. P. ALLEN *et al.*, *Nucl. Phys. B* **176** (1980), 269.
33. M. JAFFRE, Gargamelle Collaboration, private communication.
34. B. W. LEE, *Phys. Lett. B* **40** (1972), 420.
35. G. L. FOGLI, Parity violating effects in the weak $N\pi$ production, Bari preprint, April 1980.
36. P. ALLEN, BEBC Collaboration, private communication.
37. M. POHL, "Proceedings of the Topical Conference on Neutrino Physics, Oxford, 1978" (A. G. Michette and P. B. Renton, Eds.), p. 78, Oxford, 1978; Aachen thesis, 1978, unpublished; W. LERCHE *et al.*, *Phys. Lett. B* **78** (1978), 510.
38. P. SCHREINER, "Proceedings of the 1979 International Symposium on Lepton and Photon Interactions at High Energies" (T. B. W. Kirk and H. D. I. Abarbanel, Ed.), p. 291, Batavia, Ill., 1979.
39. S. J. BARISH *et al.*, *Phys. Rev. Lett.* **33** (1974), 448; P. SCHREINER, "Proceedings of the International Neutrino Conference, Aachen, 1976" (H. Faissner, H. Reithler, and P. Zerwas, Eds.), p. 333, Vieweg, Braunschweig, 1977; M. DERRICK *et al.*, *Phys. Rev. D* **23** (1981), 569.
40. M. DERRICK *et al.*, *Phys. Lett. B* **92** (1980), 363.
41. W. KRENZ *et al.*, *Nucl. Phys. B* **135** (1978), 45.
42. T. HANSL, "Proceedings of the International Neutrino Conference, Aachen, 1976" (H. Faissner, H. Reithler, and P. Zerwas, eds.), p. 278, Vieweg, Braunschweig, 1977; H. FAISSNER *et al.*, *Phys. Lett. B* **68** (1977), 377; H. DE WITT, Aachen–Padova Collaboration, talk presented at the Int. Neutrino Conference, Erice, 1980.
43. W. LEE, "Proceedings of the International Neutrino Conference, Aachen, 1976" (H. Faissner, H. Reithler, and P. Zerwas, Eds.), p. 319, Vieweg, Braunschweig, 1977; W. LEE *et al.*, *Phys. Rev. Lett.* **38** (1977), 202.
44. O. ERRIQUES *et al.*, *Phys. Lett. B* **73** (1978), 350.
45. S. ADLER, *Phys. Rev. Lett.* **33** (1974), 1511; see also Ref. [17]; J. SAKURAI, Lecture Notes in Physics, Vol. 56, p. 258, Springer-Verlag, Berlin/Heidelberg, New York.
46. D. REIN AND L. SEHGAL, to be published; M. POHL, Aachen thesis, 1978, unpublished.
47. S. J. BARISH *et al.*, *Phys. Lett. B* **91** (1980), 161.
48. T. BOLOGNESE *et al.*, *Phys. Lett. B* **81** (1979), 393.